IMPLICATIONS OF BERYLLIUM-10 MEASUREMENTS IN MARINE SEDIMENTS AND FERROMANGANESE NODULES

BY

PANKAJ SHARMA

A THESIS
SUBMITTED FOR DEGREE OF DOCTOR
OF
PHILOSOPHY OF THE
GUJARAT UNIVERSITY
AHMEDABAD

APRIL 1982

PHYSICAL RESEARCH LABORATORY
AHMEDABAD 380009 (INDIA)

CERTIFICATE

I hereby declare that the work presented in this thesis is original and has not formed the basis for the award of any degree or diploma by any University or Institution.

Pankaj Sharma
Pankaj Sharma
(Author)

Certified by :

Prof. B.L.K. Somayajulu
Guiding teacher

April, 1982

To

MY DEAR MOTHER AND FATHER

CONTENTS

STATEMENT

Beryllium-10 is produced by Cosmic Rays (CR) in the earth's atmosphere. It has a simple chemistry in the atmosphere and oceans and gets quickly removed to the deep-sea deposits in times much shorter than its half-life, 1.5×10^6 yrs. Owing to its long half-life, it is the most suitable radioisotope for studying processes involving time scales of a few million years.

This thesis is primarily concerned with the studies of deep-sea sediments and ferromanganese nodules based on measurements of ^{10}Be, U-Th series radionuclides, trace metals and mineral phases. Such studies have been performed and used for understanding

(i) the effect of meltwater on ^{10}Be distribution in the sediments,

(ii) the nature of CR intensity variations,

(iii) the growth rates of the ferromanganese nodules and

(iv) the depositional history of authigenic elements in the ocean.

The CR intensity variation is an important parameter for understanding the propagation and origin of CR. The records of CR history can be derived by studying either extraterrestrial (e.g. moon and/or meteorites) or terrestrial (deep-sea sediments) samples. The advantage of studying deep-sea sediments is that the records preserved

in them are 'sequential' in character, whereas records contained in the extraterrestrial samples are 'integral' over time and space. The distribution of ^{10}Be in a sediment column is a residuum of several complex processes viz. sedimentation, climate, geomagnetic field and CR intensity variations.

The paleochemistry of the oceans can be deciphered by studying the ferromanganese nodules. These nodules are indicators of long-term variations in the oceanic environments since they are known to be authigenically precipitating from sea water.

For the sake of clarity in the presentation, some of the chapters in the thesis have been divided into two parts (1) studies of marine sediments and (2) studies of ferromanganese nodules.

In Chapter I, a brief introduction of CR followed by ^{10}Be production in the earth's atmosphere is given. The deep-sea sediments and ferromanganese nodules are ideal repositories which hold records of past climate, mangnetism, volcanism, oceanic chemistry, influx of extraterrestrial matter and CR intensity variations. The introduction of time framework is the basic need for unravelling these processes and events in a proper chronological fashion. So far, mostly U-Th decay series radionuclides have been used to determine the rates of accumulation of deep-sea deposits.

The measurements of these radioisotopes are restricted only upto about 400,000 yrs. Due to its long half-life, ^{10}Be provides chronology in the range of one to five m.y. The basic assumptions behind dating by radioisotopes are that their input rates are constant and they do not migrate after deposition. The range of validity of these assumptions needs to be established for different isotopes under different environments of deposition. In the marine sediments I have used ^{10}Be to find out the effect of meltwater input on its distribution and to study the CR intensity variations while in ferromanganese nodules it has been used as the chronometer to determine their growth rates and for finding the depositional history of authigenic elements in sea water.

In Chapter II, are given the description of the samples and the various experimental techniques employed viz. chemical, radiochemical purification and counting of ^{10}Be and U-Th series radionuclides, atomic absorption spectrophotometry and the X-ray diffraction methods. ^{10}Be has been measured by beta counting as well as by atom counting methods. A total of two sediment cores and thirteen nodules from world oceans have been analysed in the present investigation. The activities of ^{10}Be are reproducible within the errors of the measurements ($\pm$5-10%). There is an excellent agreement between the ^{10}Be measurements obtained by beta counting and atom

counting methods. It has been shown that for high precision work the beta counting method is still as good as the atom counting method.

The results of the various measurements are presented in Chapter III and discussed in Chapter IV.

1. Marine sediments :

To evaluate the CR intensity variations in the past and the effect of meltwater on ^{10}Be deposition in deep-sea sediments, very precise measurements ($\pm 5\%$) have been made on two sediment cores viz. NOVA III-16 (Central Equatorial Pacific) and INMD-Box 50 (North Atlantic) respectively. These are the most precise measurements reported so far. The variations in ^{10}Be activities in the sediments can be due to (1) changes in the sedimentation rate, (2) meltwater input, (3) geomagnetic field intensity variations, (4) bioturbation and (5) CR intensity variations. The two cores analysed in this investigation have been chosen in such a manner that they have minimal bioturbation, known meltwater input and constant sedimentation rates as evidenced by the studies of U-Th series radionuclides, ^{14}C, magnetic reversals and $\delta^{18}O$. Since the ^{10}Be production rate varies inversely as the square root of geomagnetic dipole moment, the measured ^{10}Be activities have been corrected for the past variations in the geomagnetic field intensity.

The box core INMD-50 is studied to find out the effect of meltwater input on its ^{10}Be concentration. Based on the $\delta^{18}O$ stratigraphy, two segments, one each from the warm and cold periods have been analysed for ^{10}Be. It is found that the magnetic-field-corrected ^{10}Be activity (on a calcium carbonate free basis) changed from 5.24±0.31 during the Holocene warm period to 4.18±0.17 dpm/kg during the earlier cold period. The $\delta^{18}O$ variations show that this core had a 3% meltwater input (which means an increase of 18% in ^{10}Be) during the Holocene warm period. Thus the net ^{10}Be excess is 1.06±0.35 dpm/kg, of which 0.75 dpm/kg (18%) corresponds to meltwater input and the remaining 0.31 dpm/kg represents CR intensity variation (about 7%).

The ^{10}Be data on NOVA III-16 show that CR variations have been less than ±33% over the mean value in the past 1 m.y. The power spectrum analysis of the data using Maximum Power Entropy Method has yielded the periodicities of 500, 300 and 197 kyr. I have also combined the data on NOVA III-16 and that of Inoue and Tanaka (which though less precise, extend upto the past 2 m.y. and their samples are from nearby locations). The combined data indicate CR intensity variations of about ±50% over the mean value. Power spectrum analysis of this combined data yields periodicities ranging from 177 to 1667 kyr out of which the most prominent ones are 484, 300 and 214 kyr. These are about the same as the ones obtained from NOVA III-16 data.

2. Ferromanganese nodules :

The long term-averaged growth rates of three small and ten large nodules have been determined by ^{10}Be and $^{10}Be/^{9}Be$ methods. The rates obtained by these methods are in excellent agreement with each other and with the rates reported in the literature. In eight of the nodules the short-term-averaged growth rates have also been determined by $^{230}Th_{exc}$, $^{230}Th_{exc}/^{232}Th$ and $^{231}Pa_{exc}$ methods and the agreement in most of the cases is very good. However in a few cases there is discordancy which may be due to changes in short term growth rates compared to the long term ones.

The ^{10}Be growth rates, extrapolated-to-surface activities and inventories do not show any trend either as a function of latitude in a given ocean or from ocean to ocean. The nodule inventories of ^{10}Be are only 1-22% compared to their overhead water column inventories. The thicknesses of water column from which the nodules effectively scavenge all the ^{10}Be (as well as ^{230}Th) activity have been calculated to be in the range of 2-900 m.

The ^{9}Be concentrations of ocean water calculated from the measurements of ^{10}Be in seawater and $^{10}Be/^{9}Be$ in the nodule surfaces are in good agreement with the reported oceanic ^{9}Be concentrations implying thereby the ^{9}Be in the nodules (like ^{10}Be) is mostly authigenic.

Having determined the growth rates of the nodules, I have studied their mineralogy and composition to elucidate the oceanic history of some of the elements.

As far as mineralogy is concerned, out of the thirteen nodules studied in the present investigation ten have only δ-MnO_2 while the remaining three have δ-MnO_2, todorokite and birnessite as the principal phases of manganese minerals. In nodules which contain δ-MnO_2 there is no change in mineralogy with depth. Of the other three only in one nodule are all minerals present at all the depths whereas in the remaining two the todorokite and birnessite phases are not present in the deeper sections.

The concentration of fourteen major and minor elements viz. Mn, Fe, Co, Ni, Cu, Zn, Cr, Pb, Be, Mg, Ca, Ba and Al have been measured in different depth sections of the nodules. It is found that Mn, Fe, Co, Ni, Cu, Zn, Pb, Be, Mg, Ca and Sr are almost quantitatively leached by either 10% $NH_2OH.HCl$ or 6M HCl. It thus appears that these elements mostly reside in the authigenic phases of the nodules. On the other hand Cr, Ba and Al are distributed between the authigenic and detrital phases of the nodules since their leaching efficiencies vary from 10 to 100%. The measured concentrations of the elements studied are in good agreement with the average values reported for the nodules from the world oceans. The interelement correlations of the authigenic elements show that Mn is

well correlated with Ni, Cu and Mg while Fe is anti-correlated with Ni and Cu. Ni-Cu, Zn-Ni, Zn-Cu, Mg-Cu, Ni-Mg, Mg-Zn, Sr-Pb and Co-Pb are internally well correlated (correlation coefficients are greater than 0.6 for 64 observations).

The most striking feature of the ferromanganese nodules is their compositional heterogeneity. This has been attributed to the variations in the (1) sources and rate of supply of elements from continents, hydrothermal activities and interstitial pore waters, (2) chemistry of sea water, (3) mineralogy and (4) the activities of bacteria responsible for fixing manganese. Besides these there may be diagenetic changes in the interior of the nodules. Although the nodules show large compositional variability (the concentration of various elements vary by a factor of 50), an attempt has been made to delineate the depositional history of the elements in the ocean by choosing those nodules, in which the mineralogy has not varied with the depth. The ^{10}Be growth rates have been used to convert the depth intervals into the time intervals. The ratios of elemental concentrations in the deeper sections have been normalised to the surface (recent deposition) concentrations and these have been plotted as a function of time separately for Pacific and Atlantic plus Indian Oceans. The data on the Pacific Ocean nodules show larger scatter compared to that of the other two.

In the Pacific ocean during the past 10 m.y. the deposition of Mn, Fe, Co, Ni, Zn, Pb, Be, Mg, Ca and Sr varied by as much as ±50% except for Cu which shows higher deposition (upto a factor of four) compared to the present day value.

In the Indian Ocean, during the past 10 m.y., Mn, Fe, Co, Ni, Pb, Mg, Ca and Sr have deposited 20-60% lower compared to the present day value. Zn and Be show scatter (±50%) while deposition of Cu was high by about 20%.

The scatter in most of the cases is expected if one considers the chemical reactivities of these elements in seawater. Most of these elements have residence times which are of the same order or less than the mixing time of the oceans (10^3-10^4 yrs). The scatter is probably due to regional variations in the conditions responsible for nodule growth.

In Chapter V are presented the important conclusions drawn from the present investigation. These are

1. In properly chosen sediments in excess ^{10}Be due to meltwater input is clearly measurable.

2. During the past 2 m.y. the CR intensity variations have been about ±50% with periodicities of 500, 300 and 200 kyr.

3. The most suitable radionuclide for dating small as well as large nodules is ^{10}Be and the thicknesses of water column from which nodules effectively scavenge their Be and Th isotopes are of the order of 10^1-10^2 m.

4. The elements Mn, Fe, Co, Ni, Cu, Zn, Pb, Be, Mg, Ca and Sr are present in the authigenic phases whereas Al, Cr and Ba are present in both authigenic and detrital phases of the nodules.

5. Manganese nodules have shown large compositional variability in time and space. From the present study it appears that there have not been any global trends in the deposition pattern of authigenic elements during the past about 10 m.y. Local and regional factors are perhaps responsible for their chemical heterogeneity.

LIST OF FIGURES

LIST OF TABLES

ACKNOWLEDGEMENTS

I express my deep sense of gratitude to Prof.B.L.K. Somayajulu for introducing me to the exciting field of oceanography and for guidance during the various stages of this investigation. I have been closely associated with Prof.S.Krishnaswami and I am indebted to him for constant encouragement, invaluable suggestions and criticisms. I thank Prof.D.Lal for his keen interest in my work and encouragement. I learnt many aspects of analytical techniques especially atomic absorption spectrophotometry from my colleague Mr.M.M. Sarin. I am very thankful to him.

I have benefitted from occasional discussions I had with Dr.S.K.Bhattacharya, Prof. N. Bhandari, Prof.K.Gopalan, Prof.M.N.Rao, Dr.G. Subramaniam, Dr. J.N. Goswami, Dr.D.V. Borole,Dr.M.B.Potdar, M/s N.Hussain, M.Baskaran, R.Jha and R. Rengarajan.

I thank Prof. B.L.K. Somayajulu, Dr. S.K. Bhattacharya and Prof.W.S. Moore for critically reading the manuscript and for making important suggestions. My special thanks are due to Sarvashri M.M. Sarin, R. Rengarajan, N. Hussain and M. Baskaran for numerous suggestions which helped me considerably in improving the thesis.

This study would not have been possible without the generous supply of samples by Prof.G.O.S.Arrhenius, Prof. W.H. Berger and Mr. Tom J. Walsh all of the Scripps Institution of Oceanography, U.S.A., Dr.J.K.Cochran of Yale University, the curator of LDGO collections and Prof.A.P. Lisitzin of the Institute of Oceanography, U.S.S.R. I am thankful to all of them for their generosity.

I am also thankful to Profs. K.K.Turekian (Yale University, U.S.A.) and W.Wolfli (Laboratorium fur Kernphysik, Zurich, Switzerland) for ^{10}Be measurements by accelerator, Prof.W.H.Berger (SIO, U.S.A.) for $\delta^{18}O$ data, Drs.D.P. Agrawal and Sheela Kusumgar (P.R.L., Ahmedabad) for ^{14}C measurements.

I gratefully acknowledge the help received from Mr.C.S.R.Murty and Dr.(Mrs.) S.R.Rao both of P.R.L., in the power spectrum analysis.

The inspiration and cheerful accompany given by my friends Ajay, Ambasta , Ashok, Avinash, Chandrasekhar, Dash, Gopa, Harish, Kamlesh, Nautiyal, Rhama, Surendrapal, Swadha, Venkat and Yashpal were of immense value during the work.

Dedicated help given by Mr.J.P. Bhavsar is thankfully acknowledged. Mr.K.V. Haridas has done an excellent job in typing the thesis. My special thanks are also due to Mr.S.K. Bhavasar, Mr.D.R.Ranpura, Mr.N.D. Dave, Mrs.Kokilaben

Bhatt and Mr.M. Mandlik for their efficient, skillful drafting, photography, xeroxing and cyclostyling respectively.

My special thanks are to M/s N.R. Manchanda, A.R.S. Pandian and G.D. Panchal for maintaining and improving the electronics units. I thank Mr.M.P.K. Kurup and Mr. K.K. Sivasankaran for help with glass blowing jobs and Mr.V.G.Shah for X-ray studies.

This work was supported by grants from PL-480 and Department of Science and Technology, Government of India.

This work would never have been possible but for the constant push, love and affection given by my cousins Neeraj and Pawan.

CHAPTER - I

INTRODUCTION

The earth is a unique planet of our solar system which has a huge water mass, the oceans. The ocean floor occupies an area of about 3.6×10^8 km^2, the top few kilometers of which is composed of sediments. In addition, 20% of the ocean floor is covered by authigenic minerals called the ferromanganese nodules. These deep-sea sediments and ferromanganese nodules are considered as ideal repositories for the retrieval of several terrestrial and extraterrestrial events and processes recorded in them. The introduction of time parameter in these studies is the prime need for deciphering the records. One of the most suitable candidates for this purpose is the long-lived cosmogenic radioisotope ^{10}Be (half-life=1.5×10^6 yrs, Yiou and Raisbeck, 1972).

In the marine sediments, I have used ^{10}Be to find out the Cosmic Ray (henceforth designated as CR) intensity variations in the past two million years and to study the effect of meltwater input on ^{10}Be concentration in the deep-sea sediments. While in ferromanganese nodules, which are known to be primarily authigenic deposits, ^{10}Be has been used as a chronometer to deduce their growth rates and for understanding the paleochemistry of fourteen authigenic elements in the oceans during the past ten million years.

In this chapter, I will discuss the production of ^{10}Be by CR followed by its application to the study of marine sediments and of ferromanganese nodules.

I.1 Cosmic rays and production of ^{10}Be

Galactic cosmic rays are particles with a typical power law spectrum of the form :

$$J=kE^{-\gamma} \qquad \text{.....(1)}$$

where J is flux (number of particles per unit area per unit time per sterdian) E is energy in MeV, k is a constant and γ is the spectral index (=1.6 to 2.2). They mainly consist of protons (93%), alpha particles (6%) and a small fraction of heavier nuclei. The average energy of primary cosmic rays is few GeV/nucleon and the integral flux is about 2 protons/$cm^2(4\pi)$ (Pomerantz, 1971). The GCR are isotropic in nature except possibly at very high energy ($>10^{19}$eV). The origin of GCR is still far from clear. However, according to the present view, most of the GCR originate in our galaxy and get accelerated by the interstellar magnetic fields. Hillas (1975) gives a complete review on GCR.

Matter exposed to cosmic radiation undergoes nuclear interactions resulting in characteristic changes in its isotopic composition. A number of stable and radioactive

cosmogenic isotopes have been detected and measured in the terrestrial and extraterrestrial samples (Lal and Peters, 1967).

Measurement of cosmogenic isotopes in the extra-terrestrial (meteorites, interplanetary dust and lunar material) and terrestrial (rain water, glaciers, marine sediments and manganese nodules) samples would enable us to investigate the history of the CR intensity variations, evolution of our solar system and the various geophysical and geochemical processes operative on the earth (Lal, 1963; Lal and Peters, 1967; Forman and Schaeffer, 1979).

The cosmic ray-induced-nuclear transmutations on the earth take place mainly in the atmosphere which is composed of light atomic nuclei (78% N_2 and 21% O_2). A number of radioisotopes with varying half-lives are produced by the interaction of CR with the earth's atmosphere some of which have found applications in studying meterological and oceanographic processes. [See Lal and Peters (1967) for a complete review on the production of radionuclides in earth's atmosphere by CR and its applications in earth sciences]. Out of these isotopes, ^{10}Be has been chosen for the present investigation because of the following reasons :

1. Owing to its long half-life, it is very suitable for studying processes involving time scale of million years viz. the deposition rates of deep-sea sediments and manganese nodules.

2. Its source and sink functions are fairly well known. ^{10}Be is produced by the spallation reactions of CR with the atmospheric nitrogen and oxygen nuclei, the important nuclear reactions are :

$$n(^{16}O,\ 4p3n)^{10}Be,\ p(^{16}O,\ 5p2n)^{10}Be$$

$$n(^{14}N,\ 3p2n)^{10}Be,\ p(^{14}N,\ 4pn)^{10}Be$$

The measured cross sections in oxygen are 1.0 and 2.9 mb for protons of 135 and 550 MeV (Amin et al., 1972a) and in nitrogen 1.5 and 2.6 for 450 and 2950 MeV protons (Reyss et al., 1981). Most of the ^{10}Be production comes from GCR in the energy region 50-500 MeV. Its average production rate is 1.08 atoms cm^{-2} min^{-1} (Amin et al.,1975). Its production is maximum near the poles while fall-out is maximum in the mid latitudes due to the discontinuity in the tropopause (Lal and Peters, 1967 Finkel et al., 1977). After being produced in the earth's atmosphere, it gets attached to aerosol particles and is brought down to the earth via precipitation and is finally incorporated into the marine sediments and ferromanganese nodules in times short compared to its half-life. The residence time of Be isotopes in the ocean has been calculated to be in the range of 100-6000 years (Merrill et al., 1960, Yokoyama et al., 1978; Raisbeck et al., 1979a, 1980; Krishnaswami et al., 1982).

^{10}Be decays to boron-10 by beta emission ($E_{max}\beta^{-}$=0.555 MeV). The production rate of ^{10}Be is small - nevertheless its concentration in the terrestrial samples is sufficient to permit measurements with the method of low-level beta counting, when combined with proper radiochemical techniques (Table I.1). This so called conventional β-counting technique requires fairly large amounts of samples (about few hundred grams) and stable, sensitive and low background detectors to measure its activity. Using this conventional counting technique ^{10}Be was first detected in deep-sea sediments by Arnold (1956) and Goel et al. (1957) and in a ferromanganese nodule by Somayajulu (1967) and in the Greenland ice sheet by McCorkell et al. (1967).

Recently the sensitivity of radioisotope dating is improved by counting atoms themselves rather than their decays (Mullar, 1977). For example in the case of ^{10}Be one decay per hour implies $2x10^{10}$ atoms of ^{10}Be which is really a large number. A system even with an efficiency of 10^{-5} would be able to count it easily. The so called Ultrasensitive Accelerator Mass Spectrometry technique which has revolutionized the whole field of dating, has been successfully applied to measure a number of radio-isotopes viz. ^{129}I, ^{10}Be, ^{26}Al, ^{36}Cl, ^{14}C and ^{32}Si. Comprehensive reviews on this have been given by Gove (1978) and Mast and Mullar (1979). With the development

Table I.1 : Ranges of ^{10}Be concentration and $^{10}Be/^{9}Be$ ratio in terrestrial materials

Samples	^{10}Be (dpm/kg)	$^{10}Be/^{9}Be$ (atom ratio)	References
Rain water	$(13-50)\times10^{-6}$	-	Raisbeck et al.(1979b) Brown et al.(1981)
Ocean water	$(0.5-5)\times10^{-6}$	-	Raisbeck et al.(1979a,1980) Krishnaswami et al.(1982)
Polar Snow	$(17-120)\times10^{-6}$	-	McCorkell et al.(1967) Raisbeck et al.(1978,1981)
Marine sediments	2-7	$(1-6)\times10^{-10}$	Amin et al.(1966,1975) Finkel et al.(1977) Tanaka and Inoue (1979)
Ferro-manganese nodules	6-120	$(0.8-6)\times10^{-9}$	Somayajulu (1967) Bhat et al. (1970) Krishnaswami et al.(1972) Guichard et al.(1978) Ku et al. (1979)
Soils	0.5	-	Brown et al. (1981)

of the mass spectrometric technique, it has now become possible to measure the rather low ^{10}Be concentrations in natural reservoirs which have hitherto been not possible by the conventional decay counting technique. Using this ultrasensitive accelerator mass-spectrometric technique ^{10}Be has been measured in rain waters, ocean waters, antarctic ice and soils (Table I.1).

The measurements of cosmogenic radionuclide ^{10}Be in the marine deposits have got two potential applications, which are discussed in separate sections given below.

I.2 ^{10}Be in marine sediments

The continents are being continuously eroded mainly by rivers and streams. Annually they carry 4×10^{16} litres of water with 2×10^{16} gm of suspended load (Martin and Meybeck, 1979). This transported solids slowly settle on the ocean floor to form sediments. The marine sediments have been broadly classified into three groups (1) red clays (2) calcareous oozes and (3) silicious oozes. Table I.2 lists the various dating methods employed for finding the sedimentation rates of marine sediments (Goldberg and Bruland, 1974;Burton, 1975;Ku, 1976;Turekian and Cochran, 1978). The most common ones are those based on uranium-thorium series radionuclides.

The limitations of the U-Th series methods are that they are applicable only upto 400,000 years. The K-Ar method is applicable to those sediments which have volcanic

Table I.2 : Commonly used methods for dating marine sediments

Method	Half-life (yrs)	Dating range (yrs)	References
Radiometric methods*			
$^{40}K-^{40}Ar$	1.3×10^9	10^5-10^{10}	Dymond (1966)
^{10}Be	1.5×10^6	10^6-10^7	Amin et al. (1966, 1975) Tanaka et al. (1977) Tanaka and Inoue (1979)
$^{234}U/^{238}U$	2.48×10^5	10^5-10^6	Thurber (1963)
^{230}Th	7.52×10^4	10^4-10^5	Volchok and Kulp (1952)
$^{230}Th/^{232}Th$	7.52×10^4	10^4-10^5	Piccioto and Wilgain (1954) Goldberg and Koide (1962)
^{231}Pa	3.43×10^4	10^4-10^5	Sarma (1964) Sackett (1965)
$^{231}Pa/^{230}Th$	6.20×10^4	10^4-10^5	Rosholt et al. (1961)
^{14}C	5.76×10^3	10^3-10^4	Arrhenius et al. (1951)
^{226}Ra	1.62×10^3	10^3-10^4	Koide et al. (1976)
^{32}Si	1.05×10^2	10^2-10^3	Kharkar et al. (1963, 1969)
^{210}Pb	2.22×10^1	10^1-10^2	Koide et al. (1972)
$^{228}Th/^{232}Th$	1.9	1 -10	Koide et al. (1973)
Non-radiometric methods			
Amino-acids racemization	-	10^4-10^6	Bada et al. (1970)
Magnetic-reversal	-	10^3-10^6	Harrison and Funnell (1964) Opdyke (1972)

* using naturally occurring radionuclides

minerals while magnetic reversal method gives age at discrete stages in time. There was a great need to develop a dating method in the range of 1-5 m.y. The idea of dating sediment cores using cosmogenic ^{10}Be was first suggested by Peters (1955). Subsequent measurements by Amin et al. (1966, 1975). and Tanaka et al., (1977) had shown that rates obtained by ^{10}Be method and other methods agreed well.

The variations in ^{10}Be activities in a sediment core arise due to several extraterrestrial and terrestrial processes (Somayajulu, 1977). These are :

i. Changes in the sedimentation rate:

In the sediments, ^{10}Be activities vary inversely with the sedimentation rate. Inoue and Tanaka (1976) have studied a sediment core from the Samoan Island arc in the Pacific Ocean for ^{10}Be. Based on trace element concentrations and the occurrence of glassy fragments at various depths, they attributed the lower ^{10}Be activities to the dilution of the core material with volcanic products. However such changes are localised phenomena.

ii. Changes in the earth's magnetic field :

It is well known that the earth's magnetic field has flipped (from normal to reversed polarity) number of times in the past (Opdyke 1972). Black

(1967) has calculated a change in ^{10}Be production rate by a factor of two during the reversal period. The assumption made in his calculation is that at the polarity reversal the geomagnetic field was zero for times long enough to attain equilibrium as far as ^{10}Be production is concerned. However, experimentally it has been found that the earth's magnetic field reversals lasted for times less than 1000 years (Kawai et al., 1975). Consequently a factor of two increase would be a gross upper limit and that the corresponding ^{10}Be changes should be very small.

Recently Raisbeck et al. (1979c) have analysed ^{10}Be in a core on which magnetic stratigraphy was done. They did not observe any difference between the ^{10}Be activities in the samples below, in between and above the zones of normal and reversed polarity which again indicates that the zero field if present, was of a short duration. Though field reversals may not change the ^{10}Be production, the variations in the geomagnetic field intensity do affect it. The observed activities have to be corrected for these variations.

iii. Meltwater effect :

Snow from Greenland and Antarctica contain 18.6×10^{-6} and 23×10^{-6} dpm/litre respectively of ^{10}Be activity (McCorkell et al., 1967; Raisbeck et al., 1978). The ice sheets formed during glacial periods melt in the interglacial periods (Flint, 1971) adding ^{10}Be rich water to the ocean. Being a reactive element ^{10}Be gets quickly removed to the sediments. Hence the sediments from a region where meltwater had entered should record excess of ^{10}Be corresponding to the interglacial layers compared to the regions deposited during glacial periods.

iv. Bioturbation :

Benthic organisms churn up the surfacial sediment (Goldberg and Koide, 1962; Berger and Heath, 1968; Berger et al., 1977; Nozaki et al., 1977; Peng et al., 1977, 1979; Krishnamurthy et al., 1979). Because of this the top few centimeters of the sediment column gets mixed up by the burrowing organisms. The effect of this is to smear the ^{10}Be variations if any (Krishnaswami and Lal, 1980).

v. CR intensity variations :

The intensity variations as recorded on the earth are of two types. One is due to the modulation effect from earth's magnetic field and the other

is the change in the primary CR intensity. The meteorite data suggests that averaged over certain periods of time, as defined by the half-lives of the isotopes studied (^{53}Mn, ^{10}Be and ^{26}Al), the CR intensity during the past few million years has been essentially the same as that of today within a factor of two (Arnold et al., 1961). However this analysis does not rule out any short term (10^4-10^5 yrs) variations.

The analysis of CR variations by geochemical methods is complicated but it is the only way to obtain a continuous record of the CR variations in the past (Schaeffer, 1975;Forman and Schaeffer, 1979). It was thought worthwhile to study the above mentioned various changes by systematically analysing the sediment cores. Previous workers did not attempt to make continous measurements of ^{10}Be in the sediment core (Arnold, 1956;Goel et al., 1957; Amin et al., 1975). During the course of our investigation, Inoue and Tanaka (1979) attempted to date piston cores by ^{10}Be technique. Their data shows that ^{10}Be variations are within $\pm$30% for the last 2.5 million years, and seem to show a gradual decrease with time, but the uncertainties in their measurements are rather high (upto $\pm$30%). However it is possible to study quantitatively these

variations by making precise measurements ($\pm 5\%$) in well dated sediment cores. Out of the five factors described above the present work was undertaken to investigate the following two effects in detail : changes due to meltwater input and due to CR intensity variations.

I.2 (a) Effect of meltwater on ^{10}Be :

To study this effect one should analyse a core from a region where meltwater input is known to be present. The sedimentation rate should be constant and the bioturbation effects are known. I have analysed one core INMD-Box 50 from the Atlantic ocean. To ascertain the meltwater input, $\delta^{18}O$ measurements were done on the core in collaboration with Prof. W.H. Berger of Scripps Institution of Oceanography, U.S.A.

I.2 (b) CR intensity variations in the past :

In order to find CR intensity variations in the past, one should first estimate quantitatively the contribution from all other factors. Only after applying these corrections one can attribute the changes in ^{10}Be concentrations to the CR intensity variations. It would be ideal to analyse sediment cores from a region where sedimentation rate has remained fairly constant, bioturbation is absent or minimal and the meltwater effect is also negligible. I have

analysed NOVA III-16, for ^{10}Be from Pacific Ocean. Published data by Tanaka and Inoue (1979) have also been made use of for finding CR intensity variations and to substantiate my work.

I.3 ^{10}Be in oceanic ferromanganese nodules :

Ferromanganese nodules were first discovered in 1876 during the Challenger expedition (Murray and Renard, 1891). These mysterious objects cover about 20% of the ocean floor. They are generally associated with sediments of low accumulation rates. Their shapes are commonly spherical, ellipsoidal and slab like. Generally they have a nucleus consisting of shark tooth or fragments of volcanic rocks. The average thickness of manganese crust varies from few millimeters to several centimeters. Typically the nodules contain about 20% manganese and 15% iron with copper, nickel, cobalt and lead ranging from 0.1 to 1%. The principal phases in which manganese is present are found to be todorokite, birnessite and δ-MnO_2 while iron is found to be in the form of geothite. Complete reviews on manganese nodules are given by Mero (1965), Cronan (1976) and Glasby (1977).

The variability in the chemical and physical characteristics of marine ferromanganese deposits suggests that they may have multiple origins (Bonatti et al., 1972). At present four main theories exist concerning the origin of this most abundant mineral on the ocean floor, some of which were proposed at about the time it was discovered (Murray and Renard, 1891). Depending on their origin, deep sea nodules can be broadly classified into three kinds of deposits.

i. Hydrogenous deposits : These deposits are formed by slow inorganic precipitation of manganese and iron from sea water (Goldberg and Arrhenius, 1958). These are characterised by Mn/Fe ratio between 0.5 to 5. They have relatively high trace metal contents.

ii. Hydrothermal deposits : These deposits are formed by precipitation from volcanic hydrothermal solutions (Murray and Renard, 1891; Bonatti and Nayudu, 1965). These are characterized by variable Mn/Fe ratios often with very high Mn or Fe contents and low trace metal contents.

iii. Diagenetic deposits : These deposits are formed in sediments rich in organic matter where manganese gets mobilized due to reducing conditions and reprecipitated near the sediment-water interface

(Lynn and Bonatti, 1965; Manheim, 1965). These deposits are characterized by high Mn/Fe ratios and low trace metal contents.

iv. Biogenic origin : According to this view the manganese nodules are formed through biological rather than inorganic processes (Graham, 1959; Graham and Cooper, 1959; Ehrlich, 1972; Greenslate, 1974). It has been found that nodules contain a number of organisms. These organisms extract trace metals from sea water and agglomerate to form manganese nodules.

I.3 (a) Growth rates :

The growth rates associated with the types of origins mentioned above are expected to be different. The nature of manganese accumulation for the hydrogenous precipitation should be slow and continuous, whereas for hydrothermal origin, may be fast and episodic. The diagenetic deposits will have their manganese accumulated at rates faster than those of the hydrogenous type and they are mostly found in the regions where the deposition rate of organic matter is relatively high (Bonatti et al., 1972).

A determination of the growth rates of these deposits can, in principle, elucidate the nature of their origin. The growth rate of these nodules itself has become a controversial topic in the last

decade or so in marine geochemistry. Several radiometric and non-radiometric methods have been used to determine the growth rates of these nodules (Table I.3). These dating methods are essentially of two types : (i) those that are used to determine growth rates of the crust, like ^{10}Be, U-Th decay series, magnetic reversals etc. and (ii) those that are used to date the cores only e.g. K-Ar, fission tracks etc. The latter methods give lower limits on the growth rates since it is assumed that eversince the core material formed the nodule crust started accreting on it at a uniform rate. A complete review on various methods used for dating manganese nodules is given by Ku (1977). All these methods have consistently yielded growth rates of the order of a few mm/10^6 yrs.

Of the various methods used to date the nodules, the ones that have been most commonly employed are based on the U-Th decay series radionuclides. These methods also have been criticised and doubts have been raised regarding the validity of the assumptions made (Arrhenius, 1967; Lalou and Brichet, 1972; Lalou et al., 1973, 1976). The criticisms are as follows :

i. The radionuclides used as chronometers are not incorporated in the nodule matrix during their growth but are adsorbed on the surfaces of pre-existing nodules. Subsequently the radionuclides diffuse into the nodule and create an exponential decay-with-depth profiles.

Table I.3 : Commonly used dating methods for ferromanganese nodules.

Method	Half-life (yrs)	Dating range (yrs)	References
Radioactive methods			
$^{40}K-^{40}Ar$	1.3×10^{9}	$10^{5}-10^{10}$	Barnes and Dymond(1967)
Fission track	1.0×10^{17}	$1-10^{9}$	Aumento(1969) Anderson and McDougall(1977)
^{10}Be	1.5×10^{6}	$10^{6}-10^{7}$	Somayajulu(1967) Bhat et al. (1970) Turekian et al. (1979)
^{26}Al	7.2×10^{5}	$10^{5}-10^{6}$	Guichard et al.(1978)
$^{234}U/^{238}U$	2.48×10^{5}	$10^{5}-10^{6}$	Barnes (1967) Ku and Broecker (1967)
^{230}Th	7.52×10^{4}	$10^{4}-10^{5}$	Ku and Broecker (1969) Krishnaswami and Cochran (1978)
$^{230}Th/^{232}Th$	7.52×10^{4}	$10^{4}-10^{5}$	Barnes (1967) Barnes and Dymond (1967)
^{231}Pa	3.43×10^{4}	$10^{4}-10^{5}$	Ku and Broecker (1969) Krishnaswami and Cochran (1978)
Non-radiometric methods			
Amino-acid racemization	-	$10^{4}-10^{6}$	Bada (1972)
Magnetic-reversal	-	$10^{5}-10^{6}$	Crecelius et al.(1973)

ii. The relatively short half-lives of ^{230}Th (75,200 yrs) and ^{231}Pa(34,300 yrs) restrict their measurements to the top surface of about 1 mm, a region dominated by surface irregularities in the nodule topography as well as diagenetic alteration (Burns and Burns, 1978). It is argued that the radionuclide depth profiles could result from sampling artifacts in this region. This hypothesis also implies that the nodules are fossil deposits.

Both these hypotheses reject the application of the radionuclide depth profiles in nodules as an indicator of their growth rates and, based on other arguments, suggest that they either form rapidly or are fossil deposits recently exhumed. One approach to resolve this would logically seem to be to measure in the same nodule the depth profiles of radionuclides with half-lives longer than ^{230}Th and ^{231}Pa. ^{10}Be appears to be the most suitable candidate for this because its measurements can be made upto a greater depth (a few centimeters) much beyond the region of surface irregularities thereby reducing the sampling artifacts. Concordancy in the nodule growth rates based on ^{10}Be, ^{230}Th and ^{231}Pa profiles would strongly argue against the diffusion hypothesis (Bhat et al., 1970).

When the present investigation was undertaken in 1977, only three nodules were dated by ^{10}Be method (Depth decay plots based on 2-3 points only). Out of these three, only in two cases a comparison was made with the ^{230}Th method. Hence the data bank and concordancy checks were limited to three nodules and that too only from the Pacific Ocean.

In the present investigation ten large nodules from world oceans have been analysed for ^{10}Be using conventional beta counting technique to establish the ^{10}Be dating method on a world ocean basis. This conventional technique requires large amount of samples (about 100 gms) with constraints of radiochemically pure BeO source and on the stability of the low background beta counting system. In five of these, growth rates have been determined by $^{230}Th_{exc}$ and $^{230}Th_{exc}/^{232}Th$ methods also.

Another argument raised against earlier measurements of ^{10}Be in the nodules is that these large nodules are a typical ones, which are less abundant on the ocean floor compared to the smaller ones. So the ^{10}Be measurements have also been extended to small nodules which are most abundant on the ocean floor. The measurements on three small nodules were carried out using accelerator mass spectrometry in collaboration with Prof.K.K.Turekian of Yale University (Lanford et al., 1980; Thomas et al., 1981; Krishnaswami et al., 1982). Here again growth rates have

been determined by the ^{230}Th and ^{231}Pa methods for comparison.

I.3(b) Depositional history of authigenic elements :

^{10}Be dating of the nodules supplemented by trace metal study should provide useful information about the history of terrestrial and extraterrestrial processes as recorded by these objects and in ascertaining the authigenic deposition rates of the elements in the oceans (Somayajulu et al., 1971; Krishnaswami and Lal, 1972 ; Krishnaswami et al., 1972). Fourteen major and minor elements (Mn, Fe, Co, Ni, Cu, Zn, Cr, Pb, Be, Mg, Ca, Sr, Ba and Al) have been measured at different depths in the thirteen well dated nodules from the world oceans. Mineralogical studies of the nodule material at different depths have also been carried out.

The experimental techniques employed, the results obtained and their discussion are presented in the following chapters.

CHAPTER - II

EXPERIMENTAL TECHNIQUES

The experimental procedures employed in the present investigation involve sampling of sediments and nodules, chemical, radiochemical purification and counting of ^{10}Be, U-Th series radionuclides, X-ray diffraction studies and trace metal measurements. A brief description of the samples studied and the experimental techniques are described below:

II.1 Description of samples :

II.1(a) Sediments :

Two sediment cores have been analysed in the present study, NOVA III-16 comes from the Pacific ocean while INMD-Box 50 is from the Atlantic ocean. The ^{10}Be study was done on all the sections of NOVA III-16 and in few sections of INMD-Box 50. The measurements of U-Th series radionuclides are performed only on the INMD Box-50 core. The relevant details of the sediment cores are given in Table-II.1.

II.1(b) Nodules:

A total of thirteen nodules have been analysed in the present investigation. Eight nodules are from the Pacific ocean, two are from the Atlantic and three from the Indian Ocean. A detailed physical description of these nodules is given in Table-II.2.

Table II.1 : Physical data of the sediment cores

Sediment core	Location Latitude	Longitude	Water depth (m)	Description	Source
NOVA III-16	0° 14'N	179° 8'W	5180	Red clay, Length=155 cm Dia = 12.5 cm, gravity core.	SIO
INMD-Box 50	31° 11'N	43° 14'W	2757	Calcareous, subcores of length=30 cm and dia = 12.5 cm from a box core.	SIO

SIO = Scripps Institution of Oceanography, La Jolla, California, U.S.A.

Table II.2 : Physical data of the manganese nodules

Nodule code	Location Latitude	Longitude	Water depth (m)	Description*	Source
ARIES 39D	34°15'N	143°51'E	1819/1448	Flat, trapezoidal nodule with basaltic material at the bottom, area = 82 cm^2, thickness of Mn crust = 4 cm.	SIO
ANTP 50D	32°42'N	158°15'E	2607/2083	Almost cylindrical with patches of basaltic material at bottom, area = 175 cm^2, thickness = 1 cm.	SIO
ARIES 15D	20°47'N	173°20'E	1285/1271	Triangular, flat nodule with clay type material at the bottom, area = 125 cm^2, thickness =3 cm.	SIO
ARIES 12D	20°45'N	173°26'E	1834/1783	Trapezoidal and almost flat, area = 56 cm^2 with 2.5 cm thick altered basaltic material.	SIO
A47 16(4)	9°2'N	151°11'W	5049	Ellipsoidal relatively smoother top, nucleus of basaltic material, dimension 5.3x3.4x3.4 cm.	YU
TF 5	13°53'S	150°35'W	3623	Spherical nodule of 3.6 cm dia, Area = 40 cm^2.	SIO
ANTP58D	18°57'S	135°48'E	3555/2836	Rectangular flat nodule, area=115 cm^2 thickness = 3 cm, little basaltic material at bottom.	SIO

Contd..

Nodule code	Location Latitude	Longitude	Water depth (m)	Description*	Source
GEOSECS ID	38°38'S	167°55'E	1418/822	Flat, rectangular nodule, area = 151 cm^2, thickness = 2 cm, with clay patches at bottom.	SIO
RC15 D5	48°28'S	55°14'W	2394	Triangular, flat nodule with layered structure, area = 105 cm^2, thickness = 5 cm.	LDGO
RC16 D10	28°25'S	40°45'W	4388	Odd shaped, slab like structure, area = 120 cm^2, thickness = 2 cm with basaltic layer at bottom.	LDGO
RC14 D4F	23°26'S	50°49'E	4052	Approximately rectangular with rounded corners, area = 180 cm^2, thickness = 5 cm.	LDGO
RC14 D4S	23°26'S	50°49'E	4052	Almost spherical nodule of 11 cm dia with no core, area = 360 cm^2.	LDGO
R/V VITIAZ	26°48'S	108°15'E	5258	Spherical nodule of 7.1 cm dia, Area = 158 cm^2.	IO

* In the case of nodules, the side with more clayey/altered basaltic material is considered to be the bottom side.

SIO = Scripps Institution of Oceanography, La Jolla, California, U.S.A.
LDGO = Lamont-Doherty Geological Observatory, New York, U.S.A.
IO = Institute of Oceanology, Moscow, U.S.S.R.
YU = Yale University, New Haven, Connecticut, U.S.A.

II.2 Sampling :

II.2(a) Sediments :

The sediment cores NOVA III-16 and INMD-50 were procured as full cores. NOVA III-16 was sampled by Amin et al. (1975). In the case of INMD-Box 50, the full core in the plastic liner was vertically mounted with the top facing up. A perspex piston of appropriate diameter was slowly pushed from the bottom of the core using a jack. Several thin and thick sections were sliced from the top using a stainless steel knife (Krishnamurthy et al., 1979). All the samples were powdered and dried at 110°C overnight for analysis.

II.2(b) Nodules :

The depth samples from each nodule were collected by chipping with the aid of a clean stainless steel chisel and hammer and/or a dental drill. For ^{10}Be analysis, typically about 2-5 mm thick samples were chipped upto a few cm depth from the top (area = 19-360 cm^2). Sample thickness was directly measured with a vernier callipers as well as ascertained from the area of the nodule utilized for chipping, the weight of the chipped material and assuming a nodule density equal to 2.0 g/cm^3 (Ku, 1977).

The thickness obtained by the two methods was in agreement within ±20%. In the case of RC 14 D4F flat nodule, the top and bottom were not known and seven samples were made from the whole nodule parallel to the surface having the largest area.

For U-Th analyses, sampling was done from a much smaller area (about 10 cm^2). A few millimeter thick piece was removed and depth samples of about 100 micron thickness were obtained by scrapping with a dental drill and about 10 samples were taken from each such piece. In the case of two small nodules, TF-5 and R/V VITIAZ, the entire surface was used for sampling. The third small nodule A47-16(4) was hand-picked from the top of a box core (Krishnaswami and Cochran, 1978) - so its top and bottom sides were known. Thirteen samples (50-100μm) were collected utilizing entire top surface of the nodule (area = 19 cm^2) for U-Th analysis. After the thin sections five thick samples (about a few mm) were chipped off. All the nodule samples were powdered and dried at 110°C.

II.3 Measurement of ^{10}Be :

II.3(a) Leaching of sediments :

The cosmogenic ^{10}Be gets adsorbed on to the clays and precipitates on to the ocean floor. In this form it is expected to be easily leachable from the core

solution of EDTA (ammonium salt), about 10 ml per gram of of the nodule material. While this method was faster since Be could be recovered by TTA extraction avoiding other procedures (Amin et al. 1966), it has some disadvantages if one tries to analyse other cosmogenic activities like ^{26}Al, ^{53}Mn and ^{59}Ni since EDTA complexes of these elements are stable (Fairhall, 1960). Since the aim of the study is to find the depositional history of authigenic elements, it was felt necessary to look for a new leaching agent which could only dissolve the authigenic part leaving the clay and other detrital components unattacked. My choice fell on $NH_2OH.HCl$ which was in fact used by Kharkar et al. (1963) in an attempt to leach the authigenic ^{10}Be in the sediments. While a good amount of Mn was leached out only a very small amount of ^{10}Be came along with it. Even if one assumes that Be goes along with Mn, their result is not surprising since the Mn content of the sediments is only of the order of 1%. Arrhenius (1963) used a 1M solution of $NH_2OH.HCl$ for leaching manganese nodules and found that Mn, Cu, Ni and Sr are almost quantitatively leached out of the nodules by this reducing reagent. All these observations prompted the use of $NH_2OH.HCl$.

About 100-200 g of the sample was boiled thrice for one hour in a 10% aqueous solution of AR grade $NH_2OH.HCl$ (40 ml/g nodule). The residue was washed, dried and weighed.

The leachates were acidified with HCl. Ten percent of the solution was kept aside for trace metal studies and to the remaining 90% solution, stable ^{9}Be carrier equivalent to 86.9 mg BeO was added in the form of beryllium nitrate. To this NH_4OH was added and the precipitate was centrifuged and dissolved in HCl. This procedure was followed in the case of five nodules, ARIES 39D, ANTP 50D, ARIES 15D, ARIES 12D and ANTP 58D (Table II.2). In the case of GEOSECS 1D, RC 15 D5, RC 16 D10, RC 14 D4F and RC 14 D4S, 6M HCl plus few ml of H_2O_2 (20 ml/g nodule) was used for leaching.

Three small nodules have also been analysed by atom counting method. The advantage with this technique is that it requires samples of the order of a fewgrams as compared to about 100 g in the case of the beta counting technique. About 1-10 g nodule material was leached twice with 6M HCl + H_2O_2 mixture at boiling temperature. Ten percent of the solution was separated and to the remaining solution Be carrier equivalent to about 30 mg BeO was added in the form of beryllium nitrate.

II.3(c) <u>Chemical and radiochemical purification</u> :

The procedure adopted is essentially the same as that given by Amin et al.(1966). The following were the main steps :

1. The solution obtained after dissolution of samples, was dried to make silica insoluble.

2. Bulk of the iron was removed by di-isopropyl ether extration.

3. Removal of Mn by $NaBrO_3$ precipitation in hot concentrated nitric acid medium.

4. Removal of Ca, Mg, Ni, Zn etc. by adding NH_4OH in presence of NH_4Cl and filtering the solution.

5. Separation of Be and Al by selective dissolution in 3M NaOH.

6. Separation of Be from Al by Gooch-Haven's method (Gooch and Havens 1896).

7. Further separation of Be from Al, Fe etc. by cation exchange resin in 1.1 M HCl medium. A glass column containing 60 ml of Dowex-50,200-400 mesh was used (dia = 2.0 cm, length = 25 cm, flow rate one column volume per hour). The same resin was used repeatedly after regeneration with 6M HCl. About 15 ml of 1.1 M HCl solution containing Be was loaded on the column which was followed by elution with 1.1 M HCl. The first three column volumes were rejected and the 4th to 7th column volumes which contain Be were collected.

8. U and Th were removed on anion exchange resin (Dowex-1, 100-200 mesh) in 9M HCl and 8M HNO_3 medium respectively.

9. Be was precipitated by NH_4OH(PH=6.5) in presence of 500 mg of sodium salt of EDTA and was extracted by TTA.

10. Finally Be was precipitated as hydroxide in presence of 10-20 mg of EDTA. The $Be(OH)_2$ precipitate was filtered and ignited at 950°C in the furnace for about one hour to obtain BeO.

11. The pure BeO was powdered in an agate mortar and deposited onto a perspex holder (area = 4.08 cm^2) with a few drops of methanol.

For atom counting technique, the Be fraction obtained after cation exchange column was precipitated in presence of 500 mg of EDTA (sodium salt) and precipitate was ignited at 950°C. The chemically pure BeO was sent to Yale University for the ^{10}Be measurement. The chemical efficiencies of samples processed for atom counting technique ranged 60-90% for small nodules while it was 40-80% for sediments and 30-90% for large nodules by beta counting method. Histograms of the efficiences in the different cases are shown in Fig.II.1. A number of times the chemical efficiencies of the samples were checked by AAS measurements, these values were in a good agreement within ±10% with that obtained by gravimetric methods.

Fig.II.1 : Histograms of Be chemical efficiencies (a) for sediment samples used for beta counting, (b) for nodule samples used for beta counting and (c) nodule samples used for atom counting.

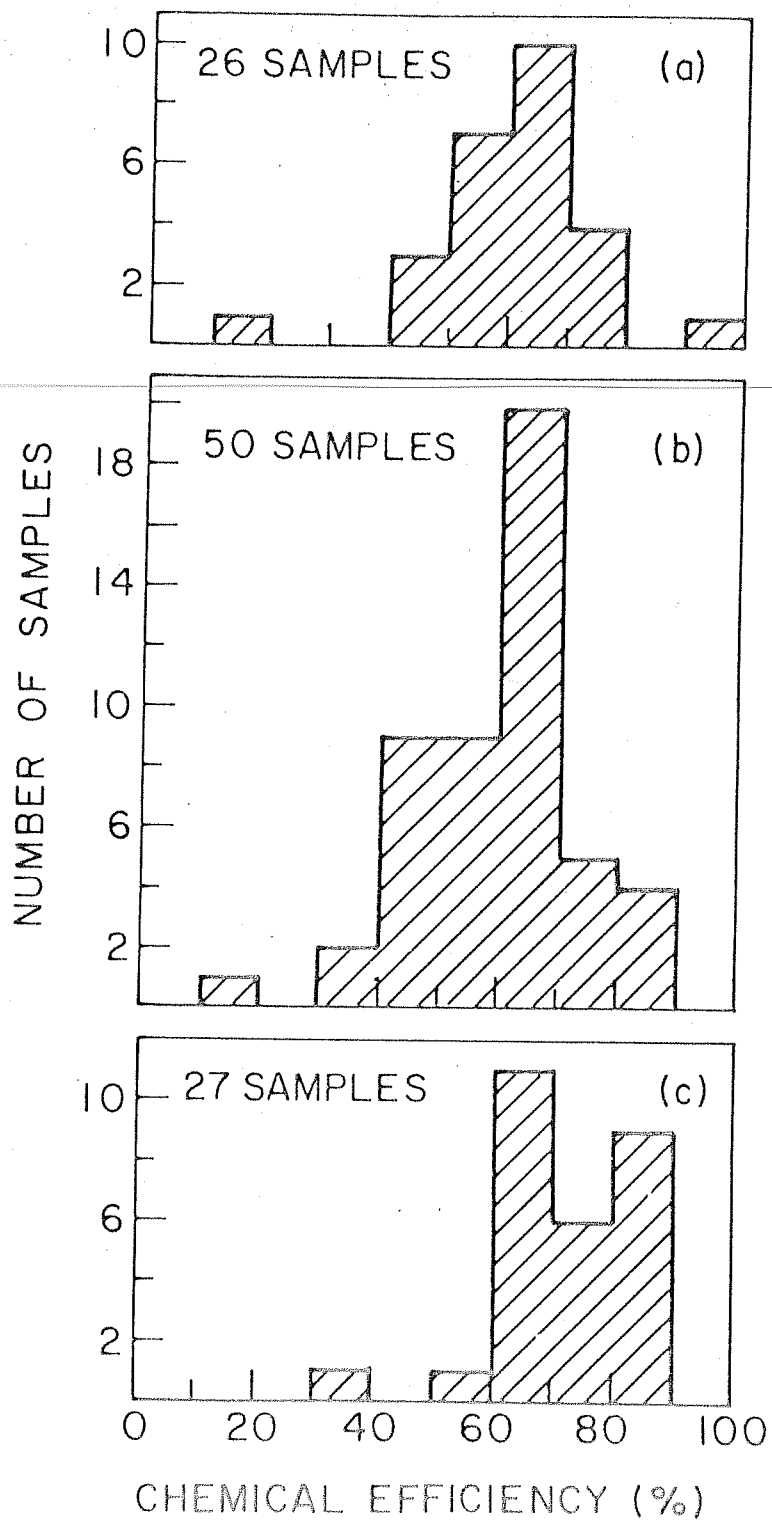
26 SAMPLES
(a)
50 SAMPLES
(b)
27 SAMPLES
(c)
NUMBER OF SAMPLES
CHEMICAL EFFICIENCY (%)
0
20
40
60
80
100
2
6
10
14
18

II.3(d) Beta counting :

^{10}Be decays by beta emission (Lederer et al., 1967),

$$^{10}_{4}Be \xrightarrow[T_{1/2} = 1.5\times10^{6}\ \text{yrs}]{E_{max}\ \beta^{-} = 0.555\ \text{MeV}} {}^{10}_{5}B$$

Samples were counted in a 2π rectangular gas flow type beta counter (Lal and Schink, 1960) using 'Q' gas (98.7% helium and 1.3% isobutane) as counting gas. Typical background of the counter was 7.3 ± 0.3 cph (counts per hour) with a counting efficiency of 32.3 ± 0.8% for ^{40}K betas.

During the later stages, the counting efficiency was improved to 47% by using a thin Cu holder (area = 2.5 cm^2) supported by a perspex holder.

In most of the cases, the sample activity ranged from 10-25 cph. However in a few cases, e.g. INMD-Box 50 samples, the activity encountered was low, about 5 cph. Therefore a second counter was made which had very low background (about 1 cph) and a detection efficiency of about 45%.

An exploded view of the counter assembly is given in Fig.II.2 and the associated electronics in Fig.II.3. The design of this system was similar to that of Bhandari (1969). The system consists of a 2π rectangular gas flow perspex counter operating inside the well of a NaI(Tl) crystal. ('Q' gas was used as counting gas). The characteristics of the system are given in Table II.3.

II.3(e) Atom counting :

The $^{10}Be/^{9}Be$ ratios of some of the samples were measured using MP Tandem Accelerator at Yale University, U.S.A. (Lanford et al., 1980; Thomas et al., 1981; Krishnaswami et al., 1982) and later-on a few measurements were made at the Institut fur Kernphysik, at Zurich, Switzerland (Suter et al., 1981; Sharma et al., 1982).

At Yale, the ^{10}Be concentration in BeO samples were determined by comparing the $^{10}Be/^{9}Be$ ratios in the samples with that of standards. A block diagram of the system used for accelerator counting is shown in Fig.II.4. In the present work, typically 1-2 mg BeO was used for each measurement which yielded a few hundred nA of BeO^{-} beam at the source. The ^{10}Be counts (about few hundreds) were integrated for 400 seconds.

Fig.II.2 : Exploded view of the $\beta-\gamma$ anticoincidence system. Constructional details of the beta counter are also given. Size of the shield 10 cm Pb+ 1 cm Fe) is 31x60x34 cm.

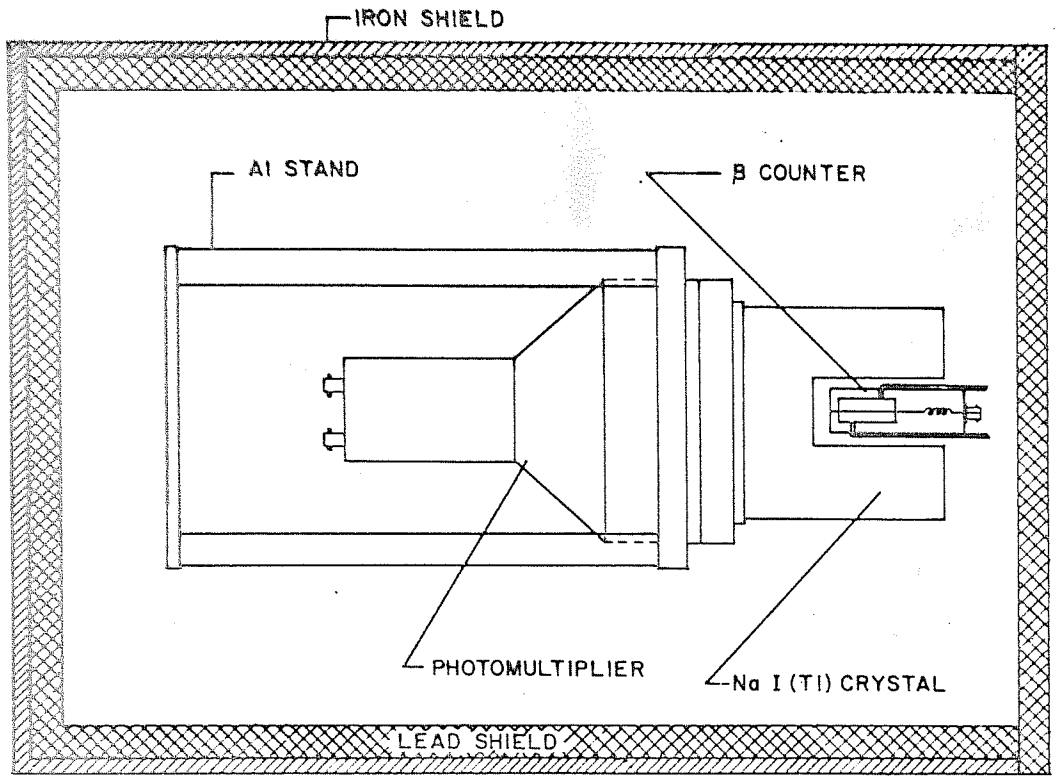
IRON SHIELD
Al STAND
β COUNTER
PHOTOMULTIPLIER
Na I (Tl) CRYSTAL
LEAD SHIELD

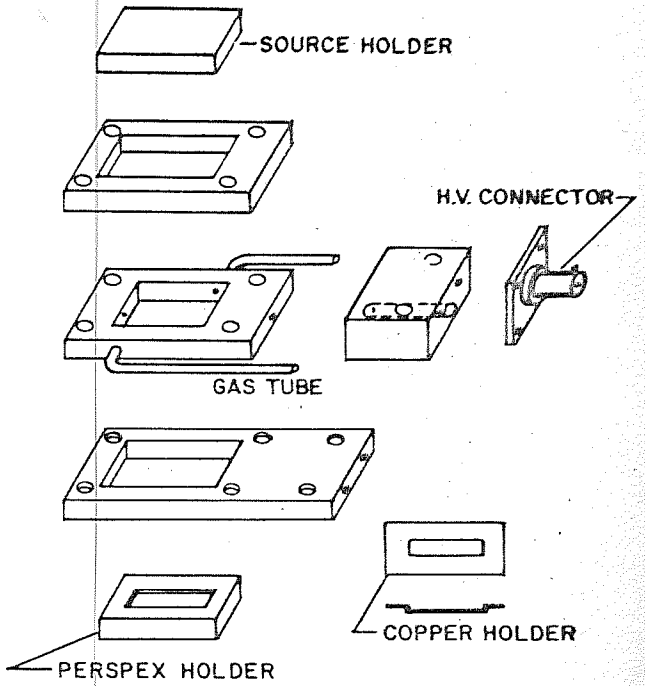
SOURCE HOLDER
H.V. CONNECTOR
GAS TUBE
COPPER HOLDER
PERSPEX HOLDER

Fig.II.3 : Block diagram of the electronics used for the β-γ anticoincidence system.

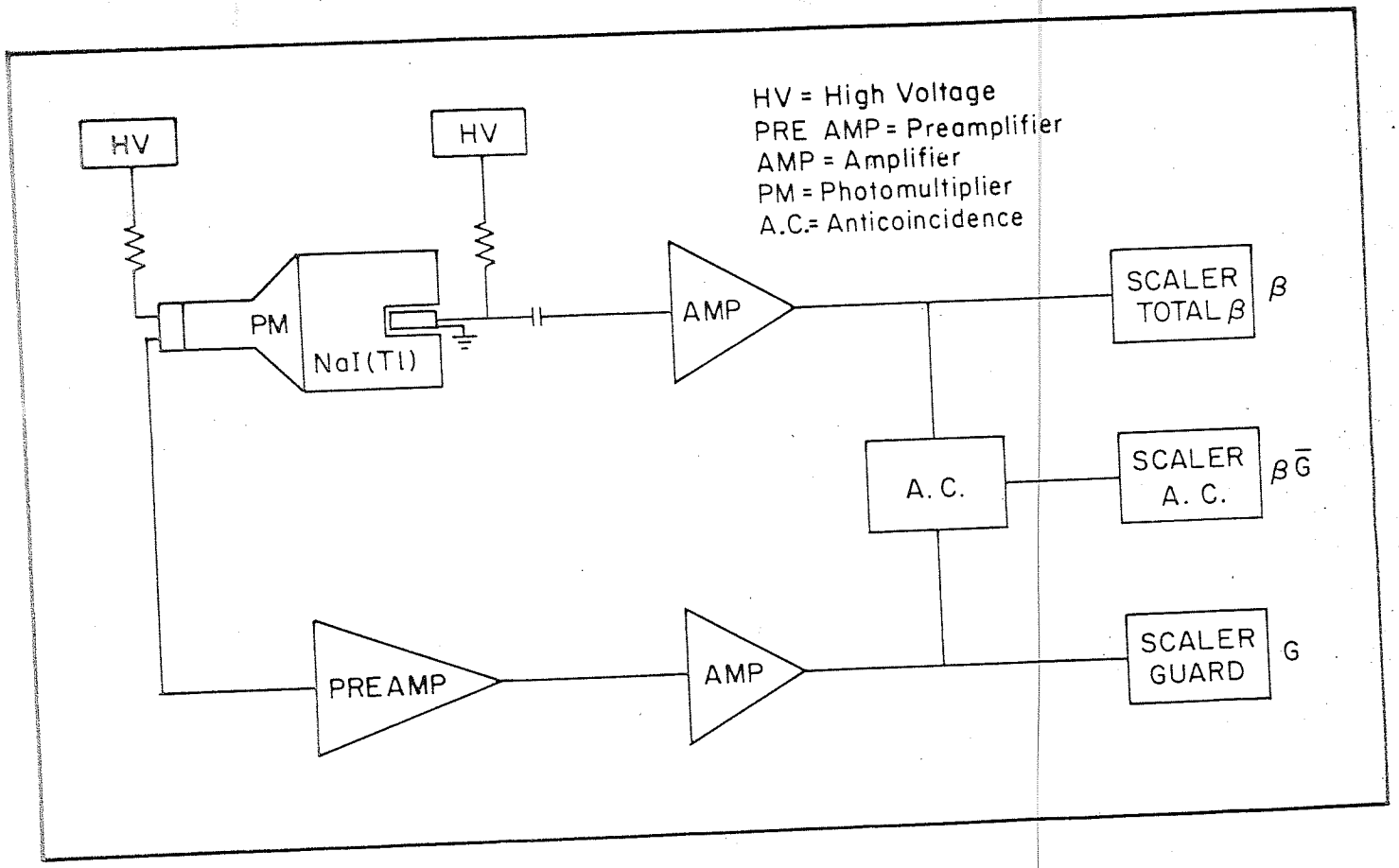
HV = High Voltage
PRE AMP = Preamplifier
AMP = Amplifier
PM = Photomultiplier
A.C.= Anticoincidence
HV
HV
PM
NaI(Tl)
AMP
SCALER TOTAL β
β
A. C.
SCALER A. C.
β G̅
PREAMP
AMP
SCALER GUARD
G

Table II.3 : Characteristics of the β-γ anticoincidence system.

1.	NaI crystal size (dia x thickness)	13x12 cm
2.	Well dimensions (dia x depth)	3.8x7.6 cm
3.	Active area of β counter	5.0 cm^2
4.	Source area	3.2 cm^2
5.	Starting voltage of β counter	1100 volts
6.	Operating voltage of β counter	1172 volts
7.	Plateau	About 300 volts
8.	Material of sample holder	Copper
9.	Background of the β counter	1.2 cph
10.	Counting efficiency for ^{40}K betas	44%
11.	Figure of merit ($\frac{S^2}{B}$)	1690
12.	Stability	Stable over a period of three years.

Fig.II.4 : Schematic of the Yale MP Tandem accelerator set up for atom counting.

YALE MP TANDEM ISOTOPE ANALYSIS SYSTEM

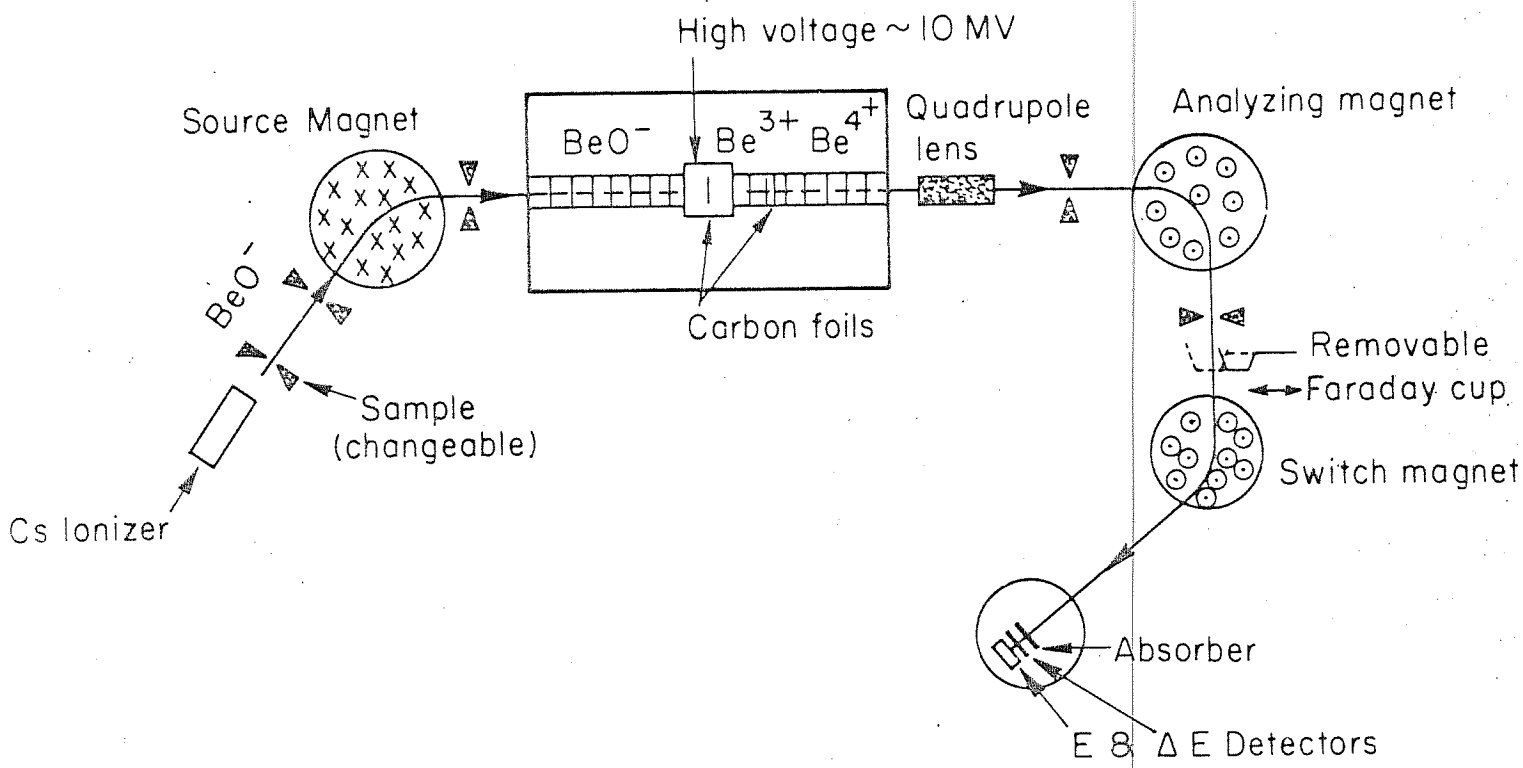

The $^{10}Be/^{9}Be$ standard used in this work was made by dissolving BeO samples extracted from 135 MeV proton irradiated water samples (sample A+B, Amin et al., 1972a). The BeO dissolved had a specific activity of $(6.58 \pm 0.33) \times 10^{-2}$ dpm/mg BeO. The BeO was dissolved in HF, H_2SO_4 and suitably diluted with ^{9}Be carrier to yield a working standard with a $^{10}Be/^{9}Be$ atom ratio of about 10^{-10}.

Along with the samples, several reagent blanks were also run to assay ^{10}Be contamination levels.

II.3(f) Purity checks :

In case of ^{10}Be measurements by beta counting, all the samples were counted at regular intervals for about a month until the beta activity reached a constant level. Immediately after deposition of the sample in the holder there was usually short lived activity which decayed within a few weeks. To make sure that the measured activity was due to ^{10}Be, absorption measurements were performed using mylar (polyethylene tetraphthalate, manufactured by Dupont, U.S.A.) of different thicknesses (Fig.II.5). The half-thickness ($t_{1/2}$) of the beta radiation (which is indicative of the beta energy) for all the samples ranged from 17.5 to 25.0 mg cm^{-2} compared to 21.5 mg cm^{-2} measured for synthetic ^{10}Be source

Fig.II.5 : Plots of net counting rate versus absorber thickness for synthetic ^{10}Be and three samples. Half thickness (mg cm^{-2}) of beta radiation in all the cases are also indicated.

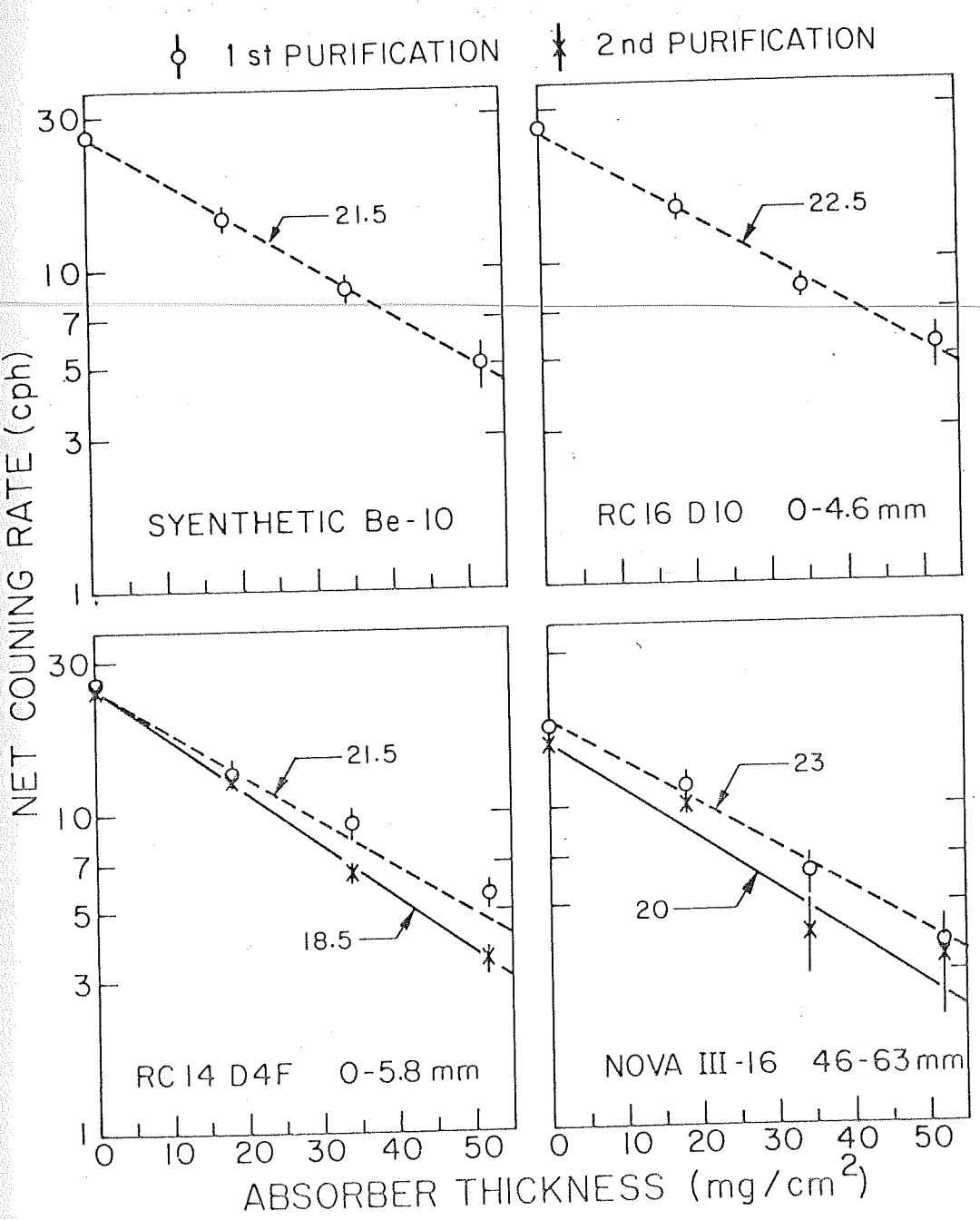
1 st PURIFICATION
2 nd PURIFICATION
NET COUNING RATE (cph)
30
10
7
5
3
1
21.5
SYENTHETIC Be-10
22.5
RC 16 D10 0-4.6 mm
21.5
18.5
RC 14 D4F 0-5.8 mm
23
20
NOVA III-16 46-63 mm
0 10 20 30 40 50
ABSORBER THICKNESS (mg/cm2)

(Amin et al., 1972a). Samples which gave $t_{1/2}$ values within ±25% were accepted for final counting, otherwise they were repurified by cation exchange column and/or TTA extraction. Some of the samples were repurified and recounted to reproduce the activity. In all the cases samples were finally counted few months after their deposition. The sediment samples were continuously counted for 7 to 15 days (to collect 2000-5000 counts to minimize the counting error) while nodule samples were counted for about 3 days. The background and efficiency of the counter were monitored regularly.

II.4 ^{210}Pb, ^{226}Ra, $^{232,230,227}Th$ and $^{238,234}U$ measurements :

In the case of sediments, about 2-10 g of the sample was leached with dilute HCl and the residue was dissolved by $HF+HClO_4$ treatment. Both the solutions were combined and ^{232}U, ^{234}Th tracers and stable Pb carrier were added. The solution was transferred to a radon flask and flushed with helium and kept for ^{222}Rn growth for two weeks. The radium concentrations were determined by ^{222}Rn emanation method (Broecker, 1965; Bhat et al.,1974). From the solution left after ^{222}Rn determination, iron was precipitated with NH_4OH in presence of NH_4Cl (pH=7-8) and the $Fe(OH)_3$ precipitate was

dissolved in HCl. From this solution U, Th and Pb were separated according to the procedures given by Bhat et al. (1969) and Krishnaswami and Sarin (1976).

In the case of nodules, about 50-100 mg material was digested in 8M HNO_3 (containing a few drops of H_2O_2) in the presence of ^{234}Th and ^{232}U tracers. The solution was taken to near-dryness and brought into 8M HNO_3 solution. Radiochemically pure U and Th (Bhat et al., 1970; Krishnaswami and Cochran, 1978) were electrodeposited on to platinum planchets. ^{227}Th was taken as an index of ^{231}Pa. Since the half-life of ^{227}Th is only 18.6 days, all the thorium sources for ^{231}Pa measurements were counted within 2-3 days of their deposition (Moore and Somayajulu, 1974).

For the estimation of chemical efficiencies of Th, the Th plates were beta counted in a 2π gas-flow counter (Bkg=2.5$\pm$0.04 cpm, counting efficiency = 66%). The alpha counting of U-Th sources was done using an Ortec surface barrier detector (area = 450 mm^2; depletion depth = 200 microns, counting efficiency = 29.0$\pm$0.5% for 4.0 MeV of ^{232}Th alphas) coupled to a Canberra amplifier

system (Canberra Industries, Inc., Connecticut, U.S.A.) followed by a 4096 channels pulse height analyser (ND100, Nuclear Data, Illinois, U.S.A.).

II.5 ^{14}C measurements :

The ^{14}C measurements were done on samples from INMD-Box 50 core in the PRL Radiocarbon laboratory (Agrawal et al., 1965).

II.6 Mineralogy of nodules by X-ray diffraction technique :

This study was done only on the bulk samples of manganese nodules. The samples were powedered to 5-10 μm size in an agate mortar. About 100 mg of the sample was deposited on a glass slide and scanned in the X-ray diffraction unit (PW1730 Phillips, Holland) using 35 kV as anode voltage and 25 mA current. Monochromatic FeKα line (wavelength = 1.94Å) with Mn filter was used.

The three main manganese minerals (Burns and Burns, 1977) reported are (1) birnessite (7Å manganite) with a principal X-ray reflection at 15.5° (2θ), corresponding to a d spacing of 7Å, (2) todorokite (10Å manganite) with principal reflection at 11.5° (2θ) and a second order reflection at 23.5° (2θ), corresponding to d spacings of 9.8 and 4.9Å respectively and (3) δ-MnO_2, with principal

reflections at 46.5^{o} and $85.5^{o}(2\theta)$, corresponding to d spacings of 2.44 and 1.42Å respectively. The samples were scanned in the range $2\theta=5^{o}$ to 30°, 43° to 50°, and 83° to 90° (Figs.II.6 and II.7) where most of the peaks from these three minerals are expected.

II.7 Measurement of trace metals in nodules :

The concentrations of fourteen elements, Mn, Fe, Co, Ni, Cu, Zn, Cr, Pb, Be, Mg, Ca, Sr, Ba and Al were measured in the leachates ($NH_2OH.HCl$ or 6M HCl) of 64 sections of thirteen nodules using Atomic Absorption Spectrophotometer Model 305A (Perkin Elmer, U.S.A.). In the case of 29 samples, the residues left after leaching were also analysed for trace metals. In 25 cases the residues were totally dissolved by $HF+HClO_4$ treatments. For the other four, the residues were leached with 6M HCl and the residues left after the leaching were brought into total solution-in these cases both the fractions were studied. Table II.4 describes the details of the nature of the flame, the linearity range, dilution factor, wavelength used etc. In order to suppress the ionization interference of Mg, Sr, Co, Ba and Al all solutions and standards were made in presence of 2000 µg/ml of K as a releasing agent.

Fig.II.6 : X-ray diffractograms for two sections of ARIES 12D. δ-MnO_2(D) is the only mineral phase present in both the sections.

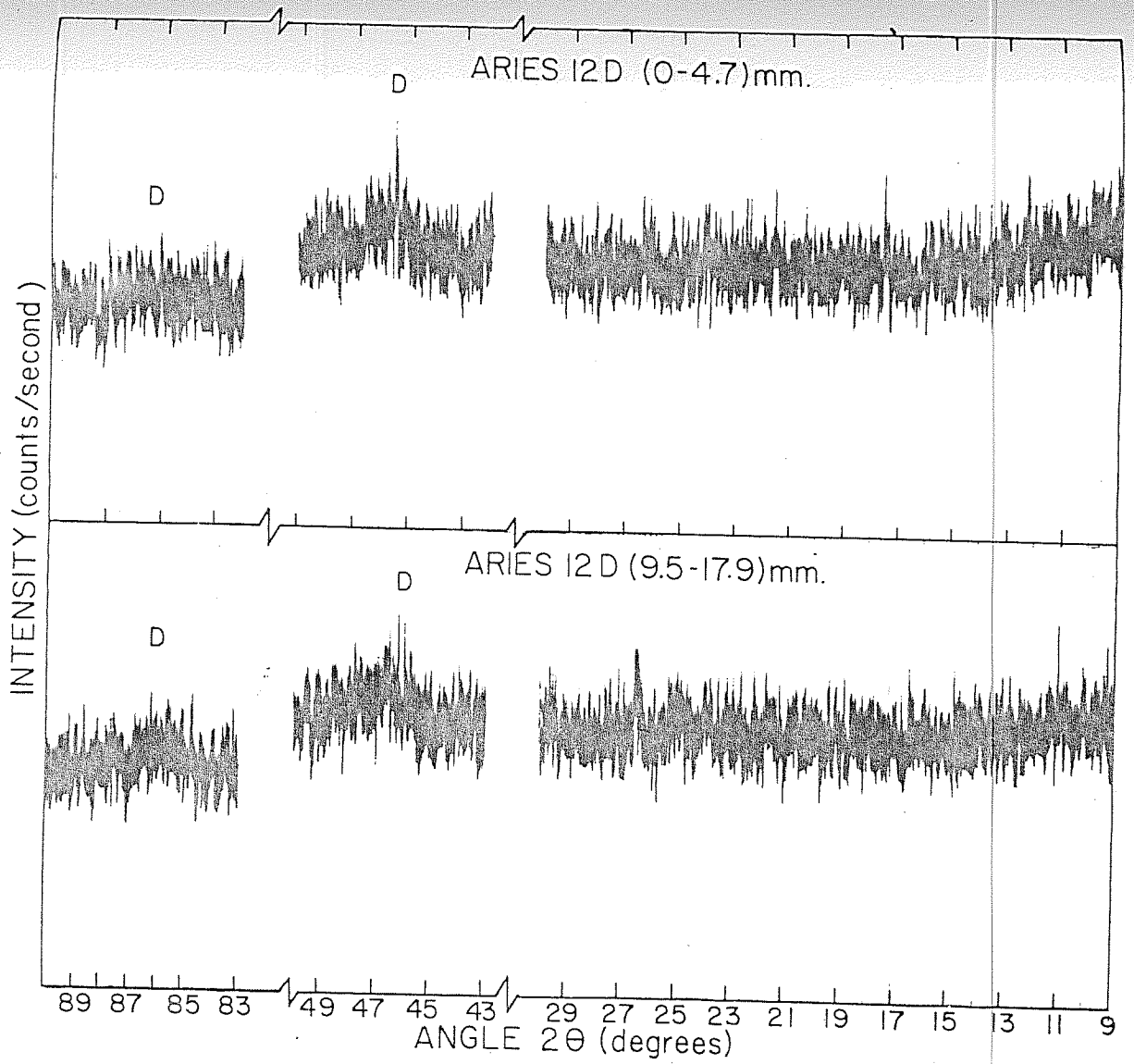
ARIES 12 D (0-4.7) mm.
D
D
ARIES 12 D (9.5-17.9) mm.
D
D
INTENSITY (counts/second)
89 87 85 83
49 47 45 43
29 27 25 23 21 19 17 15 13 11 9
ANGLE 2θ (degrees)

Fig.II.7 : X-ray diffractograms for two sections of nodule A47-16(4). Three manganese minerals todorokite(T), birnessite(B) and δ-MnO_2(D) are present in both the samples.

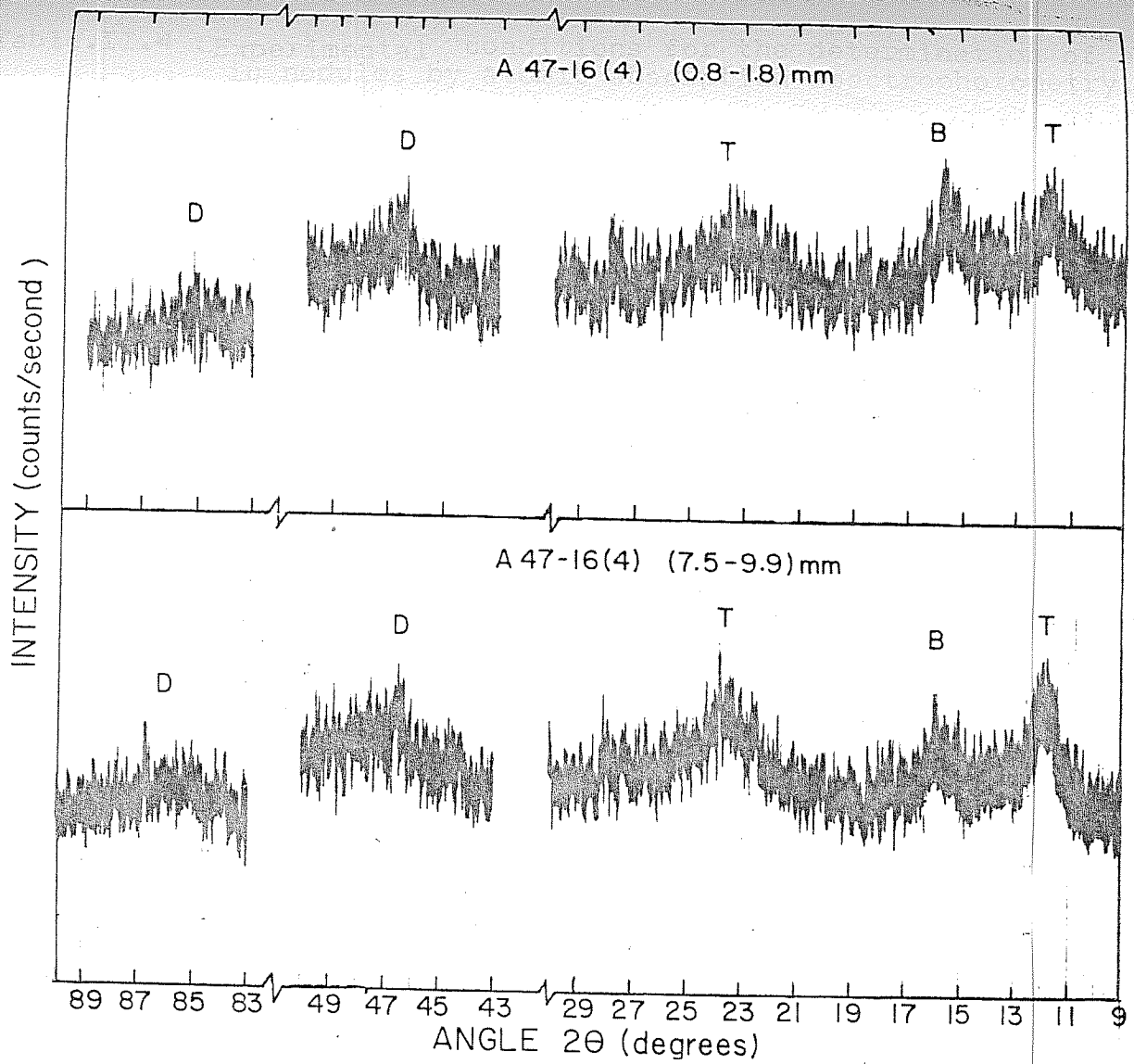
A 47-16(4) (0.8-1.8) mm
D
D
T
B
T
A 47-16(4) (7.5-9.9) mm
D
D
T
B
T
INTENSITY (counts/second)
89 87 85 83 49 47 45 43 29 27 25 23 21 19 17 15 13 11 9
ANGLE 2θ (degrees)

Table.II.4 : Experimental conditions for the determination of elements in nodules by atomic absorption spectrophotometry.

Element	Wave-length (Å)	Slit width (Å)	Dilution factor	Flame	Working range (μg/ml)	Remarks
Mn	4030.8	2	1000	Air-C_2H_2	5 - 20	-
Fe	3737.1	2	100	Air-C_2H_2	20 - 100	-
Co	2407.2	2	100	Air-C_2H_2	1 - 5	Using background corrector
Ni	2320.0	2	100	Air-C_2H_2	1 - 5	Using background corrector
Cu	3247.5	2	100	Air-C_2H_2	1 - 5	-
Zn	2138.6	7	100	Air-C_2H_2	0.1 - 1.0	-
Cr	3578.7	7	*	Air-C_2H_2	1 - 5	Fuel rich flame
Pb	2883.1	7	5	Air-C_2H_2	1 - 5	-
Be	2348.6	7	1000	**	1 - 3ng/ml	Using background corrector
Mg	2852.1	7	100	N_2O-C_2H_2	1 - 10	Turning the burner head to 30°
Ca	4226.7	14	100	N_2O-C_2H_2	1 - 20	Turning the burner head to 30°
Sr	4607.3	4	100	N_2O-C_2H_2	1 - 5	-
Ba	5535.5	2	5	N_2O-O_2H_2	1 - 5	-
Al	3092.8	7	5	N_2O-C_2H_2	20 - 50	Fuel rich flame

* 10 ml of the leaches were dried and made to 5 ml with deionized water
** By flameless atomic absorption spectroscopy

The beryllium concentrations were measured in the samples by flameless atomic absorption spectro-photometry using a HGA 500 graphite furnace coupled to a Atomic Absorption Spectrophotometer. These measurements were done by the method of addition. Ten to twenty µl of the solutions were made to 10 ml in 1M HCl matrix with and without ^{9}Be spike (2 ng/ml). Fifty µl of these solutions were injected into the uncoated graphite tube with an Eppendorf pipette. The solution was dried at 110°C for 35 sec., charred at 800°C for 25 sec. and atomized at 2650°C for 4 sec. Deuterium arc was used as background corrector for non-atomic absorption processes.

Along with the samples, USGS reference rocks, standards W-1 and G-2 and several reagent blanks were also measured.

CHAPTER - III

RESULTS

The method of calculation of the activities of ^{10}Be and of U-Th series radionuclides are described and the results of these are presented in this Chapter along with the X-ray diffraction data and trace metal concentrations of manganese nodules.

III.1. ^{10}Be measurements in sediments and manganese nodules :

These are made using two different techniques and hence the results obtained by the two techniques are presented separately.

III.1(a) Beta counting method :

The activity of ^{10}Be (in units of 'distintegrations per minute per kilogram of the bulk sample') is calculated using the following equation :

$$^{10}Be \text{ activity(dpm/kg)} = \frac{C_o \cdot F_{Ea} \cdot F_{Sa} \cdot 1000}{60 \cdot E_{Co} \cdot E_{Ch} \cdot W.K.} \quad \ldots\ldots\ldots\ldots\ldots(1)$$

where

C_o = Net counting rate of the sample (cph)

F_{Ea} = External absorption factor

F_{Sa} = Self-absorption factor

E_{Co} = Counting efficiency

E_{Ch} = Chemical efficiency

W = Weight of the sample taken for analysis (g)

K = Fraction of the leach used for ^{10}Be analysis

F_{Ea} is calculated using the relation

$$F_{Ea} = e^{\mu t} \qquad \text{.....(2)}$$

where

μ = Absorption coefficient of ^{10}Be beta radiation in mylar ($=0.03466\ cm^2\ mg^{-1}$, Amin, 1970)

t = Thickness of the mylar used for covering the source ($=0.9\ mg\ cm^{-2}$)

F_{Sa} is calculated using the formula

$$F_{Sa} = \frac{\mu t}{1-e^{-\mu t}} \qquad \text{.....(3)}$$

Where

μ = Absorption coefficient of ^{10}Be beta radiation in BeO($=0.0356\ cm^2\ mg^{-1}$, Amin, 1970)

t = Thickness of the source ($mg\ cm^{-2}$)

There was a slight difference in the procedure adopted for calculating the ^{10}Be activities in sediments and nodules although the basic equation (1) employed remained the same.

In the case of NOVA III-16 sediment samples, to determine the net ^{10}Be counting rate of a sample, the gross counting rate had been corrected for blank counting rate. The counting rates of the blanks processed during the course of investigation as well as that of two residues (after HCl leach) varied from 1.2-2.7 cph (Table III.1) above the counter background and so a mean value of 2.2 cph had been used. The The net counting rates and the calculated ^{10}Be activities of the various sections of NOVA-III-16 are presented in Table III.2. The overall errors given (3.4-5.8%) are cumulative of (1) counting statistics error (2.6-5.4%), (2) chemical efficiency error (1.8%) and (3) counting efficiency error (1.3%).

The two samples of INMD-Box 50 core were counted in a low-level β-γ anticoincidence system described in the section II.3(d). A reagent blank was run along with the samples and counted to a precision of less than 3%. The gross counting rate (3.16 ± 0.09 cph) of the blank is then subtracted from that of the samples (after appropriate chemical efficiency correction) to obtain the net ^{10}Be signals (cph) in the samples. From the net cph, the ^{10}Be

Table III.1 : ^{10}Be data on residues and blanks

S.No.	Sample	Depth interval	Residue weight (g)	Net beta rate (cph)	^{10}Be* (dpm)
1.	ARIES 39D	0 - 6.9(mm)	17.9	1.8 ± 0.5	0.19 ± 0.05
2.	ANTP 50D	0 - 5.5 ''	33.7	2.6 ± 0.5	0.27 ± 0.05
3.	ANTP 58D	0 - 4.8 ''	23.2	2.9 ± 0.9	0.27 ± 0.10
4.	ARIES 15D	0 - 3.8 ''	9.5	1.2 ± 0.5	0.25 ± 0.10
5.	RC14 D4S	0 - 1.0 ''	11.0	5.1 ± 0.5	0.39 ± 0.04
6.	RC14 D4S	8.3- 9.2 ''	66.1	3.0 ± 0.5	0.33 ± 0.06
7.	NOVA III-16	32 - 48(cm)	102.8	1.2 ± 0.3	ND
8.	80-G-3	10 - 40 ''	80.8	1.4 ± 0.2	ND
9.	Reagent Blank+ (5 separate analyses)	-	-	1.3 ± 0.5 to 2.7 ± 0.4 (2.2 ± 0.05)**	0.14 ± 0.05 to 0.27 ± 0.04 (0.22 ± 0.05)**
10.	Reagent Blank++ (2 separate analyses)	-	-	1.64±0.23 and 1.74±0.26	0.110±0.017 and 0.114±0.016 (0.112±0.017)**

ND = Not Detectable

* Calculated assuming the net beta activity is wholly due to ^{10}Be.

** Number in paranthesis indicates the mean value of the separate measurements.

\+ Used counter having Bkg = 7.3 ± 0.3 cph (old system)

++ Used counter having Bkg = 1.25 ± 0.25 cph (new system)

Table III.2 : ^{10}Be measurements in sediment cores*

Sediment Core	Depth interval (cm)	^{10}Be net counting rate (cph)	^{10}Be concentration (dpm/kg)
	0 - 10	9.70 ± 0.37	6.54 ± 0.37
	20 - 32	26.26 ± 0.37	5.79 ± 0.21
	32 - 48	29.31 ± 0.42	7.11 ± 0.25
	48 - 63	12.33 ± 0.37	6.77 ± 0.32
	63 - 77	23.13 ± 0.32	6.00 ± 0.23
NOVA III-16	77 - 88	23.00 ± 0.33	7.63 ± 0.31
	88 - 99	25.18 ± 0.39	7.18 ± 0.28
	99 -120	18.22 ± 0.33	8.22 ± 0.48
	120 -135	21.77 ± 0.34	7.28 ± 0.32
	135 -155	21.58 ± 0.36	9.88 ± 0.46
	4 - 15	2.72 ± 0.08	4.56 ± 0.27+
INMD-BOX 50	20 - 30	6.02 ± 0.17	4.18 ± 0.17+

* Measured by beta counting

\+ On $CaCO_3$ free basis. The $CaCO_3$ contents of samples 4-15 and 20-30 cm were 92.8 and 80.6% respectively.

activities are calculated using equation (1). Since the core is calcareous, the ^{10}Be activities are calculated on a $CaCO_3$ free basis and are given in Table III.2. The total errors in the ^{10}Be activities (4-6%) are inclusive of (1) 3-5% error in counting statistics, (2) 2% error in the chemical efficiency, (3) 0.5% error in the counting efficiency and (4) 2% error in the $CaCO_3$ determination.

In the case of nodules, the net ^{10}Be count rate (after background subtraction) of the sample was used to calculate ^{10}Be activity in the amount of sample taken for analysis. A blank correction for this was applied in the following manner. - five reagent blanks analysed along with the nodule samples, yielded ^{10}Be activities ranging from 0.14-0.27 dpm (Table III.1). The mean value 0.22 ± 0.05 dpm was subtracted from the dpm values of the samples calculated above. This net ^{10}Be activity in the sample was used to obtain the ^{10}Be activity (dpm/kg) and specific activity (dpm/mg Be) given in Table III.3. It should be added here that a total of six residues (after either $NH_2OH.HCl$ or 6M $HCl+H_2O_2$ leaching) of the nodule samples were also analysed for ^{10}Be and their activities (in units of dpm in total residue) ranged from 0.19 to 0.33 dpm (Table III.1). The overall errors on the ^{10}Be activities presented in Table III.1 and III.3 are inclusive of counting statistics (2.9-11.9%), counting efficiency (2-3.7%) and chemical efficiencey (1.2-2.5%). The $^{10}Be/^{9}Be$ measurements include an additional 10% error in the ^{9}Be determination.

Table III.3 : ^{10}Be measurements in large nodules*

Nodule code	Sample depth (mm)	^{10}Be net counting rate(cph)	$^{9}Be^{+}$ (ppm)	^{10}Be concentration (dpm/kg)	^{10}Be specific activity (dpm/mg ^{9}Be)
1	2	3	4	5	6
ARIES 39D	0 - 6.9	9.4 ± 0.5	2.2	6.6 ± 0.8	3.0 ± 0.5
	6.9 -12.3	1.9 ± 0.5	NM	-**	-
ANTP 50D	0 - 5.5	26.0 ± 0.7	3.3	17.1 ± 1.1	5.2 ± 0.6
	5.5 -10.6	16.2 ± 0.8	3.3	12.8 ± 0.9	3.9 ± 0.5
ARIES 15D	0 - 3.8	16.5 ± 0.9	2.9	20.7 ± 1.7	7.1 ± 0.9
	3.8 - 6.8	7.5 ± 0.7	3.0	10.0 ± 1.5	3.3 ± 0.6
	6.8 - 9.7	3.1 ± 0.6	2.5	6.8 ± 2.3	2.7 ± 1.0
	9.7 -17.9	5.4 ± 0.9	4.1	2.5 ± 0.7	0.61± 0.18
	17.9 -27.0	2.9 ± 0.7	4.0	0.83± 0.5	0.21± 0.13
ARIES 12D	0 - 4.7	9.4 ± 0.5	5.0	16.2 ± 1.8	3.2 ± 0.5
	4.7 - 9.5	6.7 ± 0.7	3.5	8.5 ± 1.6	2.4 ± 0.5
	9.5 -17.9	7.5 ± 0.7	3.8	3.1 ± 0.5	0.82± 0.16
ANTP 58D	0 - 4.8	20.5 ± 0.7	3.9	27.1 ± 1.4	7.0 ± 0.8
	4.8 -12.8	16.7 ± 0.7	4.9	11.9 ± 0.8	2.4 ± 0.3
	21.0 -27.8	10.3 ± 0.9	4.9	10.3 ± 1.2	2.1 ± 0.3

1	2	3	4	5	6
	0 - 3.2	17.9 ± 0.6	4.0	17.7 ± 1.4	4.4 ± 0.6
	3.2 - 6.9	6.2 ± 0.5	5.1	3.7 ± 0.9	0.73± 0.19
GEOSECS 1D	6.9 -12.5	2.9 ± 0.6	NM	0.39± 0.62	-
	12.5 -16.4	3.5 ± 0.4	NM	0.82±0.62	-
	0 - 6.6	7.0 ± 0.5	9.3	2.8 ± 0.7	0.30± 0.08
	6.6 -16.2	2.4 ± 0.4	NM	0.19± 0.34	-
RC15 D5	16.2 -22.6	1.6 ± 0.4	NM	-**	-
	22.6 -28.6	2.2 ± 0.5	NM	-**	-
	36.9 -40.9	2.4 ± 0.4	NM	0.20± 0.59	-
	0 - 4.6	22.3 ± 0.7	5.7	17.2 ± 1.3	3.0 ± 0.4
RC16 D10	4.6 -10.6	7.5 ± 0.4	5.9	3.0 ± 0.6	0.51± 0.11
	10.6 -15.0	1.4 ± 0.5	NM	1.2 ± 1.5	-
	0 - 5.8	23.5 ± 0.7	4.0	13.7 ± 0.8	3.4 ± 0.4
	5.8 -12.0	12.4 ± 0.6	7.3	4.2 ± 0.5	0.58± 0.09
	12.0 -17.4	5.2 ± 0.5	12.1	0.82± 0.34	0.07± 0.03
RC14 D4F	17.4 -27.4	5.1 ± 0.7	7.2	0.66± 0.27	0.09± 0.04
	27.5 -34.5	6.6 ± 0.5	10.0	1.4 ± 0.3	0.14± 0.03
	34.5 -45.9	12.2 ± 0.11	10.9	3.1 ± 0.3	0.28± 0.04
	45.9 -54.1	22.5 ± 0.7	3.2	7.8 ± 0.5	2.4 ± 0.04

1	2	3	4	5	6
	0 - 1.0	19.4 ± 0.7	5.8	19.8 ± 1.4	3.4 ± 0.4
	1.0 - 2.6	15.1 ± 0.6	3.7	11.6 ± 1.2	3.1 ± 0.5
RC14 D4S	2.6 - 8.3	8.6 ± 0.5	4.8	2.3 ± 0.3	0.48± 0.08
	8.3 - 9.2	6.0 ± 0.5	4.0	1.1 ± 0.3	0.28± 0.08
	9.2 -57.4	1.7 ± 0.5	4.0	-	-

NM = Not measured

* Using beta counting technique

\+ Measured by flameless atomic absorption spectrophotometry. Precision of analysis is ± 10% .

** No net ^{10}Be activity after blank correction

III.1(b) Atom counting method :

The ^{10}Be concentrations (atoms/g) and $^{10}Be/^{9}Be$ ratios (^{10}Be atoms/ μg) in the three nodules are given in Table III.4. The concentrations of the reagent blanks were negligible, typically 1-2 counts/400 seconds compared to several hundred counts of ^{10}Be/400 seconds in the nodule samples. An error of 10% has been assigned to all the samples while samples of R/V VITIAZ have been assigned an error of ±20% based on several repeat measurements of $^{10}Be/^{9}Be$ standard over a period of about 2 years (Krishnaswami et al., 1982).

II.2 ^{210}Pb and ^{226}Ra measurements :

The concentrations of ^{210}Pb and ^{226}Ra are calculated by standard procedures (Krishnaswami et al., 1971; Bhat et al., 1974). The results of these measurements in the nine sections of INMD-Box 50 core are presented in Table III.5. The overall errors in the ^{210}Pb measurements are less than 5% whereas in the case of ^{226}Ra they are less than 2% . The activity levels of reagent blanks for ^{210}Pb and ^{226}Ra were negligibly small compared to the samples.

Table III.4 : ^{10}Be measurements in small nodules*

	Depth interval (mm)	^{9}Be+ (ppm)	^{10}Be concentration 10^{10} atoms/g	dpm/kg	$^{10}Be/^{9}Be$ (10^{9} atoms/µg ^{9}Be)
A47-16(4)	0 - 0.8	2.5	1.9 ± 0.38	16.7 ± 3.3	7.60 ± 1.7
	0.8 - 1.8	3.1	2.1 ± 0.42	18.5 ± 3.7	6.77 ± 1.6
	1.8 - 3.2	4.6	1.4 ± 0.28	12.3 ± 2.5	3.04 ± 0.70
	3.2 - 5.7	2.4	0.97± 0.19	8.54± 1.7	4.04 ± 0.93
	5.7 - 7.5	2.4	0.49± 0.1	4.31± 0.86	2.04 ± 0.47
TF 5	0.5 - 1.4	7.8	3.2 ± 0.6	28.2 ± 5.6	4.10 ± 0.94
	1.4 - 3.3	6.4	1.5 ± 0.3	13.2 ± 2.6	2.34 ± 0.53
	3.3 - 5.5	4.0	0.51± 0.1	4.49± 0.9	1.28 ± 0.3
	5.5 - 8.7	7.9	0.19± 0.04	1.67± 0.33	0.241± 0.06
	8.7 -17.3	24.5	0.18± 0.04	1.58± 0.32	0.074± 0.02
R/V VITIAZ	0 - 0.4	4.2	2.5 ± 0.3	22.0 ± 2.6	5.95 ± 0.93
	0.4 - 2.0	7.8	2.3 ± 1.0	20.2 ± 8.8	2.95 ± 1.3
	2.0 - 6.5	6.7	1.1 ± 0.5	9.68± 4.4	1.64 ± 0.76
	6.5 - 8.2	4.3	0.37± 0.16	3.26± 1.4	0.860± 0.38
	8.2 - 9.6	-	0.47± 0.10	4.14± 0.88	-
	9.6 -11.0	4.0	0.27± 0.05	2.38± 0.50	0.675± 0.16
	11.0 -12.6	3.8	0.24± 0.05	2.11± 0.42	0.632± 0.15
	12.6 -14.8	3.1	0.17± 1.50	1.50± 0.30	0.548± 0.13

* Measured by atom counting method.

\+ Measured by flameless atomic absorption spectrophotometry. Precision of analysis is ±10% .

Table III.5 : ^{210}Pb and ^{226}Ra concentrations in sediment core INMD-BOX 50

Sample depth (cm)	$CaCO_3$ (%)	Concentration (dpm/g) ^{210}Pb	^{226}Ra	$^{210}Pb^*_{excess}$
0-0.7	92.0	5.5 ± 0.3	3.5 ± 0.1	2.0 ± 0.3
0.7 - 1.2	90.9	6.3 ± 0.3	3.8 ± 0.1	2.5 ± 0.3
1.2 - 2.0	90.6	4.5 ± 0.2	3.8 ± 0.1	0.7 ± 0.2
2.0 - 2.6	89.6	6.9 ± 0.4	3.0 ± 0.1	3.9 ± 0.4
2.6 - 3.5	91.0	6.0 ± 0.3	4.2 ± 0.1	1.8 ± 0.3
3.5 - 4.0	91.2	6.1 ± 0.3	4.2 ± 0.1	1.9 ± 0.3
4.0 - 5.0	86.8	4.2 ± 0.2	4.4 ± 0.1	-0.2 ± 0.2
6.0 - 8.0	91.7	5.1 ± 0.3	6.0 ± 0.1	-0.9 ± 0.3
10.0 -12.5	91.1	4.7 ± 0.2	5.8 ± 0.1	-1.1 ± 0.3

$$* \; ^{210}Pb_{excess} = ^{210}Pb - ^{226}Ra \text{(all in dpm/g)}$$

III.3 U-Th measurements :

The concentrations of ^{238}U(ppm), ^{230}Th(dpm/g) and ^{232}Th(ppm) were measured in the seven sections of INMD-Box 50 sediment core and seventy five sections of eight nodules by standard procedures (Amin, 1970; Krishnaswami and Cochran, 1978) and results are presented in Tables III.6 and III.7. The ^{227}Th(dpm/g) was measured only in the fifteen sections of three nodules (Table III.8). The measured ^{227}Th concentrations in the nodules have been used as an index of the concentrations of its grand parent ^{231}Pa, assuming that the decay chain $^{231}Pa \longrightarrow {}^{227}Ac \longrightarrow {}^{227}Th$ behaves as a closed system (Moore and Somayajulu,1974).

The total errors in the reported measurements are in the range of 1.9-10.8% for Th isotopes, and 4.2-15.3% for U.

Here also the activity levels of reagent blanks were negligibly small. The ^{238}U concentrations were measured only in a few sections of each nodule and an average value of these have been used for calculating $^{230}Th_{exc}$ and $^{227}Th_{exc}$.

III.4 ^{14}C measurements in INMD-Box 50 :

The ^{14}C ages of three sections of INMD-Box 50 are given in the foot note of Table III.6.

Table III.6 : ^{238}U, $^{232,230}Th$ and ^{14}C* measurements in box core INMD-50

Sample depth (cm)	$CaCO_3$ (%)	^{238}U+ (dpm/g)	^{232}Th+ (ppm)	$^{230}Th_{excess}$** (dpm/g)	$^{230}Th_{excess}$**/^{232}Th (Activity Ratio)
0-0.7	92.0	-	19.0 ± 1.0	8.58 ± 0.28++	22.58 ± 1.41++
2.6 - 3.5	91.0	-	18.7 ± 1.3	10.12 ± 0.34++	24.10 ± 1.90++
6.0 - 8.0	91.7	2.3 ± 0.2	19.8 ± 1.0	11.57 ± 0.30	28.22 ± 1.57
10.0 -12.5	91.1	2.1 ± 0.1	21.6 ± 0.9	9.57 ± 0.18	19.93 ± 0.92
15.0 -17.5	82.1	1.7 ± 0.1	18.5 ± 0.5	8.03 ± 0.20	9.67 ± 0.34
20.0 - 24.0	83.9	1.7 ± 0.1	15.9 ± 0.5	6.39 ± 0.16	9.98 ± 0.40
24.0 - 29.4	85.5	1.7 ± 0.1	15.7 ± 0.6	6.00 ± 0.15	10.50 ± 0.46

* The ^{14}C ages of 8-10, 17.5-20 and 24-29.4 cm sections are 7700 ± 160, 17410^{+740}_{-680} and $24,810^{+1610}_{-1350}$ years respectively.

\+ On $CaCO_3$ free basis

** $^{230}Th_{excess} = {}^{230}Th_{Total} - {}^{238}U$(all in units of dpm/g)

++ Calculated using $^{238}U = 0.19 \pm 0.02$(dpm/g)

Table III.7 : ^{232}Th, ^{230}Th and ^{238}U in manganese nodules

Nodule	Sample depth (mm)	^{232}Th (ppm)	$^{230}Th^{*}_{exc}$ (dpm/g)	$^{230}Th^{*}_{exc}/^{232}Th$ (A.R)	^{238}U (ppm)
1	2	3	4	5	6
	0-0.073	38.4 ± 3.6	848 ± 26	88.3 ± 8.7	NM
	0.073-0.107	38.8 ± 3.6	620 ± 22	65.2 ± 6.5	6.1 ± 0.6
	0.107-0.162	28.0 ± 2.4	499 ± 16	71.3 ± 6.5	NM
	0.162-0.244	33.6 ± 2.8	460 ± 16	54.8 ± 4.9	6.4 ± 0.4
	0.244-0.256	35.2 ± 2.8	462 ± 14	52.5 ± 4.5	NM
	0.256-0.306	33.6 ± 3.6	414 ± 14	49.3 ± 5.5	NM
	0.306-0.358	28.4 ± 2.8	393 ± 13	55.4 ± 5.8	NM
A47 16(4)	0.358-0.430	30.0 ± 3.2	373 ± 13	49.7 ± 5.6	NM
	0.430-0.482	33.2 ± 2.4	337 ± 8	40.6 ± 3.1	NM
	0.482-0.554	32.0 ± 3.2	312 ± 12	39.0 ± 4.2	NM
	0.554-0.637	29.6 ± 3.2	222 ± 7	30.0 ± 3.4	NM
	0.637-0.701	31.6 ± 2.4	197 ± 6	24.9 ± 2.0	NM
	0.701-0.756	47.2 ± 4.0	229 ± 9	19.4 ± 1.8	NM
	0.756-1.76	28.8 ± 2.0	74.8 ± 3.3	10.4 ± 0.9	NM
	3.15 -5.7	35.2 ± 2.8	34.4 ± 2.1	3.9 ± 0.4	4.0 ± 0.4

1	2	3	4	5	6
	0-0.025	23.2 ± 2.4	669 ± 14	115 ± 12	10.7 ± 1.6
	0.025-0.054	27.2 ± 2.0	551 ± 12	81.0± 6.2	10.8 ± 0.9
	0.054-0.098	21.6 ± 1.6	377 ± 8	69.8± 5.4	NM
	0.098-0.172	25.2 ± 2.0	355 ± 8	53.2± 4.4	NM
	0.172-0.249	22.0 ± 1.2	183 ± 4	33.3± 2.0	NM
TF 5	0.249-0.297	24.4 ± 1.6	114 ± 3	18.7± 1.3	14.1 ± 1.2
	0.297-0.348	23.6 ± 1.2	79.0± 2.4	13.4± 0.7	NM
	0.348-0.396	24.8 ± 1.2	37.5± 1.3	6.0± 0.4	NM
	0.396-0.436	23.6 ± 1.6	26.0± 1.5	4.4± 0.4	NM
	0.436-0.475	21.2 ± 1.2	12.7± 1.1	2.4± 0.3	13.5 ± 1.3
	0.475-0.512	22.8 ± 2.4	9.2± 1.3	1.6± 0.3	NM
	0.512-1.29	15.6 ± 1.2	1.3± 1.1	0.33± 0.29	9.5 ± 0.8
	0-0.122	16.8 ± 2.4	63.2± 3.6	15.0± 2.3	15.5 ± 1.9
	0.122-0.248	25.6 ± 2.0	17.2± 1.9	2.7± 0.4	NM
GEOSECS	0.248-0.432	21.2 ± 1.6	4.4± 1.7	0.83± 0.33	NM
1D	0.432-0.719	22.4 ± 1.6	3.6± 1.6	0.64± 0.29	NM

1	2	3	4	5	6
	0-0.125	54.0 ± 2.8	9.9 ± 1.6	0.73 ± 0.12	12.3 ± 1.5
RC 15 D5	0.125-0.250	57.2 ± 4.0	2.9 ± 1.3	0.20 ± 0.09	NM
	0.250-0.345	45.2 ± 2.8	1.7 ± 1.3	0.15 ± 0.11	NM
	0-0.063	53.2 ± 4.4	222 ± 9	16.7 ± 1.5	16.3 ± 1.2
	0.063-0.123	48.4 ± 2.8	88.8 ± 3.4	7.3 ± 0.5	NM
	0.123-0.189	38.4 ± 2.8	31.9 ± 2.1	3.3 ± 0.3	18.7 ± 1.3
	0.189-0.263	36.4 ± 2.8	24.5 ± 1.9	2.7 ± 0.3	NM
	0.263-0.355	44.0 ± 2.4	25.1 ± 1.8	2.3 ± 0.2	NM
	0.355-0.462	44.0 ± 2.4	16.6 ± 1.6	1.5 ± 0.2	NM
RC16 D10	0.462-0.596	37.2 ± 2.0	13.5 ± 1.5	1.5 ± 0.2	NM
	0.596-0.711	36.0 ± 2.4	10.1 ± 1.2	1.1 ± 0.1	NM
	0.711-0.822	44.0 ± 3.2	9.0 ± 1.6	0.82 ± 0.16	20.0 ± 1.7
	0.822-0.898	47.6 ± 2.8	11.5 ± 1.6	1.0 ± 0.2	NM
	0.898-0.984	42.8 ± 2.0	9.6 ± 1.3	0.90 ± 0.10	NM

1	2	3	4	5	6
	0-0.054	50.0 ± 3.2	212 ± 7	17.0 ± 1.2	NM
	0.054-0.090	39.2 ± 3.2	153 ± 6	15.6 ± 1.4	NM
	0.090-0.150	36.4 ± 2.8	104 ± 5	11.4 ± 1.0	13.1 ± 0.9
	0.150-0.231	36.8 ± 2.8	55.8 ± 2.9	6.1 ± 0.6	NM
RC14 D4F	0.231-0.286	35.6 ± 2.4	37.9 ± 2.5	4.3 ± 0.4	NM
	0.286-0.333	30.0 ± 2.0	27.2 ± 1.7	3.6 ± 0.3	16.1 ± 1.5
	0.333-0.400	24.0 ± 1.2	10.3 ± 1.7	1.7 ± 0.3	NM
	0.400-0.462	30.0 ± 2.0	11.8 ± 1.9	1.6 ± 0.3	NM
	0.462-0.546	31.6 ± 1.6	9.3 ± 1.7	1.2 ± 0.2	18.0 ± 2.3
	0-0.080	54.8 ± 2.8	43.5 ± 2.1	3.2 ± 0.2	NM
	0.080-0.163	65.6 ± 3.6	37.3 ± 2.1	2.3 ± 0.2	NM
	0.163-0.240	68.0 ± 4.0	28.7 ± 2.0	1.7 ± 0.2	11.5 ± 1.5
	0.240-0.307	69.6 ± 4.0	24.6 ± 1.9	1.4 ± 0.1	NM
RC14 D4S	0.306-0.406	56.0 ± 2.8	15.4 ± 1.6	1.1 ± 0.1	NM
	0.406-0.478	54.0 ± 3.2	14.6 ± 1.6	1.1 ± 0.1	NM
	0.478-0.604	58.0 ± 3.6	7.5 ± 1.5	0.52 ± 0.10	NM
	0.604-0.692	58.8 ± 2.8	9.5 ± 1.4	0.65 ± 0.11	13.1 ± 1.5

1	2	3	4	5	6
	0-0.024	240 ± 11	135 ± 31	22.4 ± 1.1	14.8 ± 2.3
	0.024-0.043	161 ± 6	872 ± 18	21.6 ± 0.9	NM
	0.043-0.069	126 ± 5	673 ± 15	21.4 ± 1.0	NM
	0.069-0.087	123 ± 4	415 ± 9	13.5 ± 0.5	NM
	0.087-0.105	140 ± 6	447 ± 11	12.8 ± 0.6	10.9 ± 1.3
R/V VITIAZ	0.105-0.133	91.2 ± 3.6	266 ± 6	11.7 ± 0.5	NM
	0.133-0.146	91.6 ± 4.4	179 ± 5	7.8 ± 0.4	10.7 ± 2.1
	0.146-0.182	157 ± 7	276 ± 9	7.0 ± 0.4	NM
	0.182-0.225	122 ± 4	168 ± 4	5.5 ± 0.2	13.2 ± 2.0
	0.225-0.269	139 ± 6	142 ± 5	4.0 ± 0.2	NM
	0.269-0.372	142 ± 6	74.7 ± 3.2	2.1 ± 0.1	NM
	0.372-19	135 ± 5	4.1 ± 1.7	0.12 ± 0.05	NM

A.R. = Activity Ratio

$*^{230}Th_{exc} = {}^{230}Th_{total} - {}^{238}U$ (all in dpm/g)

Table III.8 : $^{227}Th_{exc}$($^{231}Pa_{exc}$) in nodules

Nodule	Depth interval(mm)	$^{227}Th^{*}_{exc}$ (dpm/g)
	0.107 - 0.162	50.3 ± 3.1
	0.162 - 0.224	37.3 ± 2.7
A47-16(4)	0.256 - 0.306	28.8 ± 3.2
	0.306 - 0.358	27.0 ± 2.5
	0.358 - 0.430	22.4 ± 2.6
	0 - 0.025	43.9 ± 3.0
	0.025 - 0.054	37.7 ± 2.4
TF 5	0.054 - 0.098	20.0 ± 1.2
	0.098 - 0.172	12.4 ± 1.5
	0.172 - 0.249	6.8 ± 0.7
	0 - 0.024	93.9 ± 4.7
	0.024 - 0.043	49.4 ± 2.4
R/V VITIAZ	0.043 - 0.069	32.0 ± 1.8
	0.069 - 0.087	13.6 ± 1.2
	0.087 - 0.105	20.8 ± 1.8

Average ^{238}U concentrations of the nodules A47-16(4), TF 5 and R/V VITIAZ are 4.1 ± 0.7, 8.8 ± 1.0 and 9.3 ± 1.5 dpm/g respectively.

* $^{227}Th_{exc} = {}^{227}Th_{total} - \frac{^{238}U}{21.96}$ (All in units of dpm/g)

III.5 Mineralogy of manganese nodules :

The minerals present in the various sections of the manganese nodule samples were studied using the X-ray diffraction technique and are given in Table III.9.

III.6 Trace metal concentrations in manganese nodules :

The measurements of fourteen major and minor elements, Mn, Fe, Co, Ni, Cu, Zn, Cr, Pb, Be, Mg, Ca, Sr, Ba and Al in $NH_2OH.HCl$ or HCl leaches and in the insoluble residues of the nodules are given in the Appendix.

The measured concentrations of the elements in two USGS rocks are given Table III.10. The concentrations of various elements in W-1 and G-2 are within ±3.5% for major elements (Mg, Al, Ca and Fe) and within ±6% for minor elements (Mn,Cu,Ni,Cr,Co, Pb,Ba, Sr and Zn) of those reported in the literature (Flanagan, 1973; Sarin et al., 1979) except for Be which agrees within ±10%. The coefficient of variation in W-1 is 2.3% for Mg, 2.6% for Al, 2.2% for Ca, 2.1% for Fe, 3.4% for Mn, 4.9% for Cu, 8.0% for Ni, 2.0% for Cr, 6.4% for Co, 1.0% for Ba, 8.7% for Sr, 4.3% for Zn and in G-2 4.8% for Mg,

Table III.9 : X-ray diffraction study of nodules

Nodule 1	Depth interval (mm) 2	Minerals present 3
ARIES 39D	0-69	todorokite, birnessite, δ-MnO_2
	12.3-15.9	δ-MnO_2
ANTP 50D	0-5.5	δ-MnO_2
ARIES 15D	0-3.8	δ-MnO_2
	6.8-9.7	δ-MnO_2
	17.9-27.0	δ-MnO_2
ARIES 12D	0-4.7	δ-MnO_2
	9.5-17.9	δ-MnO_2
A47 16(4)	0.8-1.8	todorokite, birnessite, δ-MnO_2
	7.5-9.9	todorokite, birnessite, δ-MnO_2
ANTP 58D	0-4.8	δ-MnO_2
	12.8-21.0	δ-MnO_2
TF 5	0-0.5	δ-MnO_2
	8.7-17.3	δ-MnO_2
GEOSECS 1D	0-3.2	δ-MnO_2
	6.9-12.5	δ-MnO_2

1	2	3
RC16 D10	0-4.6	δ -MnO_2
	10.6-15.0	δ -MnO_2
RC15 D5	0-6.6	δ -MnO_2
	16.2-22.6	δ -MnO_2
	28.6-36.9	δ -MnO_2
RC14 D4S	0-1.0	δ -MnO_2
	2.6-8.3	δ -MnO_2
	9.2-57.3	δ -MnO_2
RC14 D4F	0-5.8	δ -MnO_2
	5.8-12.0	δ -MnO_2
	12.0-17.4	δ -MnO_2
	17.4-27.4	δ -MnO_2
	27.4-34.5	δ -MnO_2
	34.5-45.9	δ -MnO_2
	45.9-54.1	todorokite, birnessite, δ -MnO_2
R/V VITIAZ	0.4-2.0	δ -MnO_2
	8.2-9.6	δ -MnO_2
	12.6-14.8	δ -MnO_2

Table III.10 : Trace metal measurements in USGS reference rocks

Element	W-1 measured*	W-1 reported+	G-2 measured**	G-2 reported+
Mg %	3.89	3.99	0.45	0.46
Al ''	7.94	7.94	8.00	8.15
Ca ''	7.56	7.83	1.39	1.39
Fe ''	7.74	7.76	1.84	1.85
Mn ppm	1316	1316	-	260.0
Cu ''	112.9	110.0	-	12.0
Ni ''	75.6	76.0	-	5.1
Cr ''	118.0	114.0	-	7.0
Co ''	47.5	47.0	-	5.5
Pb ''	-	7.8	29.3	31.2
Ba ''	167.7	160.0	1867	1870
Sr ''	192.1	190.0	450.2	479.0
Zn ''	91.3	86.0	89.3	85.0
Be ''	-	-	3.0	2.6

* Average of five separate measurements

\+ Flanagan (1973)

** Average of two separate measurements

0.4% for Al, 4.1% for Ca, 1.5% for Fe, 5.4% for Ba, 4.5% for Sr and 1.1% for Zn.

The concentrations of elements in the reagent blanks were negligibly small compared to the sample values and hence no corrections were applied.

CHAPTER - IV

DISCUSSION

The results of measurements of ^{10}Be, U-Th series radionuclides in sediment cores and manganese nodules, trace metals and X-ray diffraction studies in nodules presented in the Chapter-III are discussed here.

The ^{10}Be results have important bearing on the understanding of the effect of meltwater addition to the ocean during interglacial periods, the CR intensity variations and on the genesis of ferromanganese nodules. For the sake of clarity the results on marine sediments and ferromanganese nodules are discussed separately. Before the data is discussed, it is pertinent to discuss the reliability and reproducibility of the ^{10}Be data and the results of intercomparison between the two methods employed for ^{10}Be measurements.

IV.1 Reliability and reproducibility of ^{10}Be measurements :

The net ^{10}Be counting rates and activities in the samples ranged from 1.4 to 29.3 cph and from negligible to 27.1 dpm/kg respectively (Tables III.2, III.3 and III.4). The net ^{10}Be counting rates of the seven reagent blanks and seven residues (after 6M HCl or $NH_2OH.HCl$ leach) of sediments and nodules ranged from 1.2 to 3.1 cph, except for one sample, RC 14 D4S (0-1 mm) which gave 5.1 cph (Table III.1).

In all the cases the ^{10}Be activity in the residues ranged from negligible to 3% of the activities found in the corresponding leachates proving thereby that $NH_2OH.HCl$ and 6M HCl almost quantitatively dissolve ^{10}Be in nodules. The data in Table III.1 also show that the contamination from the reagents used in this study is negligibly small.

As mentioned in the section II.3(f), the purities of the ^{10}Be samples were checked by half-thickness ($t_{1/2}$) measurements. Samples which did not give $t_{1/2}$ values within $\pm$25% of the value obtained for synthetic ^{10}Be source were repurified until they gave correct $t_{1/2}$ value. In three cases in addition to half-thickness measurements the samples were repurified and ^{10}Be activities were reproducible within $\pm$(5-10)%.

IV.2 Intercomparison of ^{10}Be measurements by beta and atom counting techniques :

Most of the ^{10}Be measurements were made using the decay counting method, while about one-fourth were measured by atom counting method. To have a check on the reproducibility by both the methods, one sediment sample and three sections of a nodule have been investigated. After the final beta assay, the BeO samples were sent to Prof.Wolfli's group (Eidgenossische Technische Hochschule, Zurich, Switzerland) where they

Table IV.1 : Intercomparison of ^{10}Be measurements made by decay and atom counting techniques

S.No	Sample (Depth	^{10}Be(atoms/g)*	
		Decay counting (Ahmedabad)	Atom counting (Zurich)
1	NOVA III-16		
	(32-48 cm)	$(7.22 \pm 0.31)\times10^{9}$	$(6.3 \pm 1.0)\times10^{9}$
	ANTP 58 D		
2	0 - 4.8 mm	$(3.1 \pm 0.2)\times10^{10}$	$(2.4 \pm 0.4)\times10^{10}$
3	4.8-12.8 mm	$(1.4 \pm 0.1)\times10^{10}$	$(1.3 \pm 0.2)\times10^{10}$
4	21-27.8 mm	$(1.2 \pm 0.1)\times10^{10}$	$(1.2 \pm 0.2)\times10^{10}$

Sample 1 is a deep sea clay from the Pacific whereas samples 2-4 are from manganese nodule, also from the Pacific (See Tables II.1 and II.2 for details).

* Errors quoted for the decay counting data are inclusive of 1 σ counting statistics and errors associated with chemical and counting efficiencies. In the case of atom counting the maximum uncertainty ($\pm$15%) is associated with ^{10}Be standard which is indicated (accuracy of the sample run is about 2-3%).

measured ^{10}Be by accelerator mass spectrometry. The results of intercomparison are given in Table IV.1 (Sharma et al., 1982a). In three out of four cases the agreement is excellent. Even in the fourth one the results are in agreement within 2 sigma (standard deviation).

This comparison also indicates that given sufficient amount of sample the beta counting technique can still be used to determine the concentration of ^{10}Be very precisely.

IV.3 Marine sediments' studies :

The effect of meltwater on the ^{10}Be concentrations of marine sediments and CR intensity variations are the two parameters which have been studied in detail. As has been discussed in Section I.2, both CR intensity and meltwater effects can be studied from ^{10}Be variations provided one finds a core which has (1) a constant sedimentation rate over its entire length as obtained by independent methods, (2) bioturbation effects in the core either minimal or absent and (3) the continuous variation of magnetic field intensity in the past and its effect on ^{10}Be production in the atmosphere known. It should be noted that both these effects cannot be simultaneously studied on the same core.

One has to make a choice so as to get cores from regions of known meltwater input and regions where the meltwater input is negligible. Such a choice has been made. I have used INMD-Box 50 core from North Atlantic for observing the meltwater-input effect on ^{10}Be and NOVA III-16 from Central Equatorial Pacific for the study of CR intensity-variations. To study these two effects quantitatively, one has to correct for the factors which are responsible for ^{10}Be variations. These factors have been taken into consideration. The most important of these correction factors is the change in ^{10}Be production due to geomagnetic field intensity variations, which is discussed below :

In order to establish the effect of a change in the earth's magnetic field intensity on ^{10}Be production, I have followed the procedure of Ramaty (1965) who calculated the effect of magnetic intensity variation on ^{14}C production. It has been found that ^{10}Be production rate varies inversely as the square root of geomagnetic dipole moment. The relevant equation is

$$\frac{P}{P_o} = \left[\frac{M_o}{M}\right]^{0.5} \qquad \text{.....(1)}$$

where P and P_o are ^{10}Be production rates corresponding to the magnetic dipole moments M and M_o respectively (subscript o denotes the average value for the past

2 m.y.). Hence the measured ^{10}Be activities can be corrected for magnetic field variations. The calculation reduces to finding out P/P_o values during different time periods in the past. The measured ^{10}Be decay corrected activities A_d, have to be divided by P/P_o to obtain magnetic field corrected ^{10}Be activities A_{dm}. The P/P_o can be calculated provided earth's past magnetic field intensity is known. Fortunately data on the variations of the earth's magnetic field intensity for the past 2 m.y. are available (Kawal et al., 1975; Wollin et al., 1978). The geomagnetic field intensity H has been used in place of M in the calculations since M is proportional to H and the proportionality constant does not vary with time.

To evaluate the effect of meltwater on ^{10}Be deposition and the CR intensity variations in the past, very precise ^{10}Be measurements ($\pm 5\%$) have been made on two sediment cores viz. INMD-Box 50 and NOVA III-16 (Table III.2; Sharma et al., 1982b; Somayajulu et al., 1982). It should be noted here that these are the most precise ^{10}Be measurements reported so far. Results on these cores are discussed below separately.

IV.3(a) Effect of meltwater input :

As mentioned in the section I.2(a), in order to evaluate the effect of meltwater on ^{10}Be, one should analyse a sediment core from a region where meltwater

input is known. In addition the core should have minimal bioturbation and constant sedimentation rates. The calcareous box core INMD-50 from North Atlantic ocean has been analysed for $\delta^{18}O$ (to evaluate melt-water-input) , U-Th series radionuclides (for finding bioturbation depth), ^{14}C (to determine accumulation rate) and ^{10}Be. The results of these studies presented in Chapter III.

IV.3(a)(i) ^{18}O stratigraphy :

The results of $\delta^{18}O$ measurements are graphically shown in Fig.IV.1 (Somayajulu et al., 1982). These measurements were performed on the planktonic foraminifer Globigerinoides rubber (pink variety). The $\delta^{18}O$ increases from $-1.2\ ^{o}/_{oo}$ to $+0.86\ ^{o}/_{oo}$. The total range of the $\delta^{18}O$ signal is near $2^{o}/_{oo}$. About $1.2\ ^{o}/_{oo}$ may be ascribed to a meltwater effect (Berger and Gardner, 1975).

IV.3(a)(ii) Mixed layer thickness :

Two methods are employed for determining the bioturbation depth in the core (1) The $^{210}Pb_{exc}$ and (2) U-Th isotopes.

Table III.5 gives the $CaCO_3$% and ^{210}Pb, ^{226}Ra and $^{210}Pb_{exc}$ activities. The $^{210}Pb_{exc}$ varies from 0 to 3.9 dpm/g. The $^{210}Pb_{exc}$ values are expected to decrease uniformly with depth in the core through

Fig.IV.1 : ^{18}O and ^{14}C stratigraphies of the box core INMD-50. The shaded areas indicate the segments of samples analysed for ^{10}Be. The numbers shown are the magnetic-field-corrected ^{10}Be activities in units of dpm/kg on a $CaCO_3$ free basis.

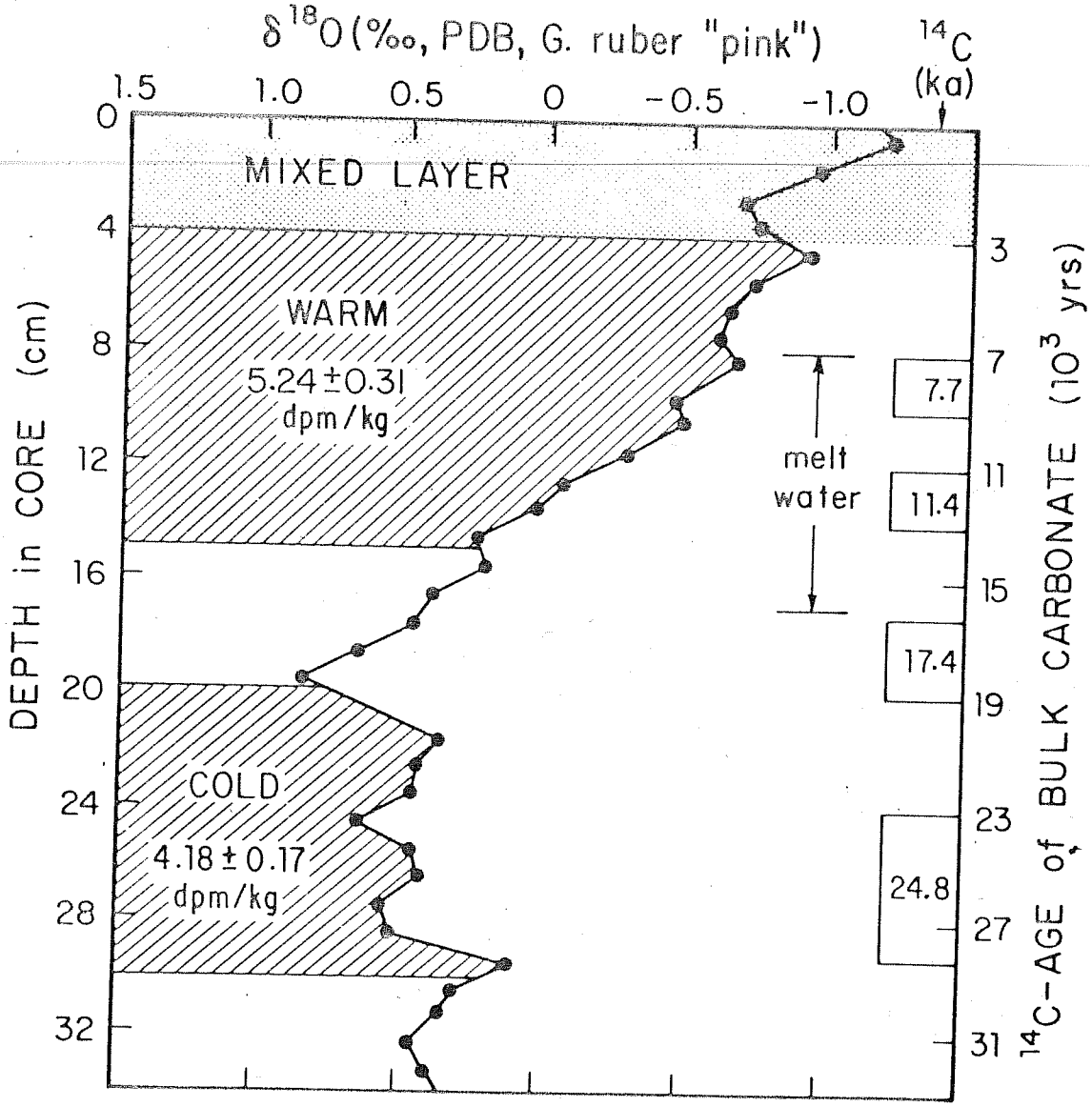
δ18O (‰, PDB, G. ruber "pink")
1.5
1.0
0.5
0
-0.5
-1.0
14C (ka)
MIXED LAYER
WARM
5.24±0.31
dpm/kg
COLD
4.18±0.17
dpm/kg
melt water
7.7
11.4
17.4
24.8
DEPTH in CORE (cm)
0
4
8
12
16
20
24
28
32
14C-AGE of BULK CARBONATE (10³ yrs)
3
7
11
15
19
23
27
31

mixed layer (Nozaki et al., 1977; Peng et al., 1979). But the data on the box core INMD do not show this simple pattern. Although there is a high value of 2 dpm $^{210}Pb_{exc}$/g in the section 0-0.7 cm, the value increases again after going through a minimum of 0.7 dpm/g between 1 and 2 cm and becomes zero after 4 cm. This pattern is similar to that found by Krishnamurthy et al. (1979) in the western equatorial Pacific and by Finkel et al. (1981) in the eastern equatorial Pacific. Finkel et al. (1981) ascribed the increase of ^{210}Pb to scavenging of radioisotopes by manganese whose distribution shows downcore maxima. It is clear from the Table III.5 that the mixed layer thickness is about 4 cm which agrees well with that obtained by U-Th method (described in the next paragraph) and with the ash layer data of Ruddiman and Glover (1972) on a box core north to the INMD core.

The Table III.6 shows $CaCO_3$ and U-Th isotope data. The ^{238}U and ^{232}Th ranges from 2.3 to 1.7 dpm/g and from 21.6 to 15.7 ppm. respectively while $^{230}Th_{exc}$ (dpm/g) and $^{230}Th_{exc}$/ ^{232}Th(A.R.) vary from 11.6 to 6.0 and from 28.2 to 10.0 respectively.

Fig.IV.2 : ^{14}C ages of the sediment core INMD-Box 50 as a function of depth. Number shown by arrow is the accumulation rate (cm/10^3 yrs).

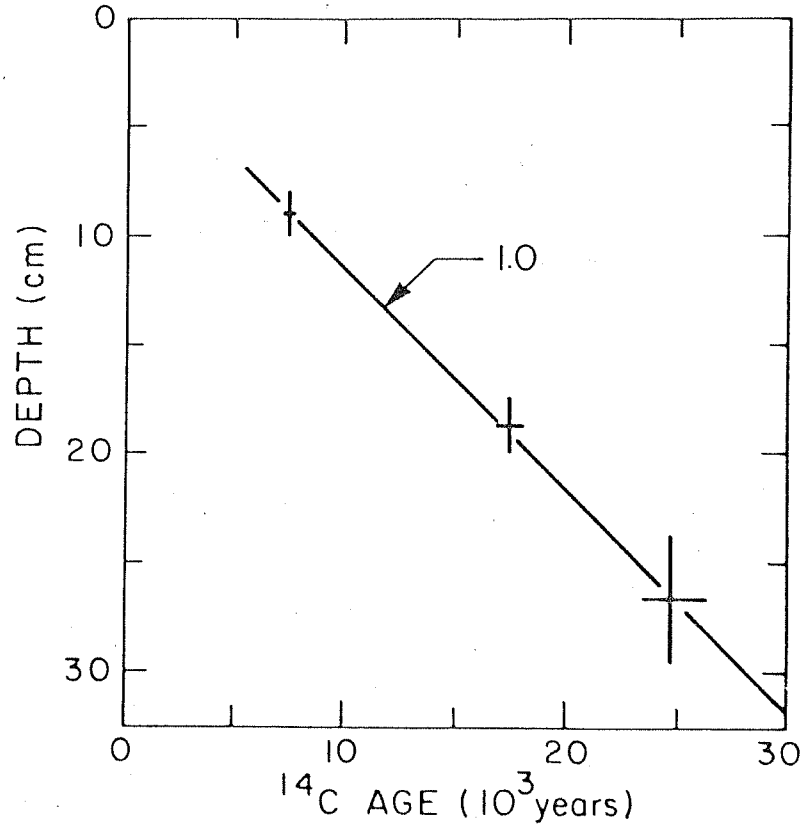
0
10
20
30
DEPTH (cm)
1.0
0
10
20
30
^{14}C AGE (10^3 years)

to reduce contamination with glacial sediments. The Table III.2 lists the ^{10}Be results on a carbonate-free basis. The change from inter glacial sediments (4-15 cm) to glacial sediments (20-30 cm) is from 4.56±0.27 to 4.18±0.17 dpm/kg. The difference of 0.38±0.31 dpm/kg [(0.38/4.18)x100=9%] can be explained as due to the meltwater deposition as discussed below:

The average $\delta^{18}O$ for the 4-15 cm (warm) is calculated to be $-0.46^{o}/_{oo}$ whereas the corresponding average value for the 20-30 cm (cold) period comes out to be $+0.45^{o}/oo$. Using these two values and assuming that molten snow had a $\delta^{18}O$ averaging $-30^{o}/oo$ (Johnsen et al., 1972), it is calculated that 3% of meltwater was introduced into the ocean water during the period of deposition of the 4-15 cm section. The ^{10}Be concentration of Greenland ice sheet was measured by McCorkell et al. (1967) to be $18x10^{-6}$ dpm/l - a value almost identical to that measured in Antarctica by Raisbeck et al. (1978). From the published ^{10}Be data on ocean waters (Raisbeck et al., 1980; Krishnaswami et al., 1982), it is calculated that Greenland ice sheet is about 7 times enriched in ^{10}Be compared to mean oceanwater. Consequently the 3% meltwater input would result in an excess ^{10}Be concentration of 18% which is approximately what has been observed within the uncertainties of the measurements i.e. (9±7)%.

The above calculation is based on the assumption that the difference of ^{10}Be activities during the warmer and cooler periods is due to melt water only. The possible changes in cosmic ray flux should also be taken into consideration. It is known that the intensity of both CR as well as the earth's magnetic field have varied in the past (Kawai et al., 1975; Somayajulu, 1977; Sharma et al., 1982b). The measured ^{10}Be values can be corrected for the production changes due to earth's magnetic field as discussed in the section IV.3. The average intensity variations of the earth's magnetic field during the two periods represented by the samples viz. (4-15) cm and (20-30)cm were obtained from the data of Kawai et al. (1975) and the corresponding changes in ^{10}Be production have been computed. It turns out that the measured ^{10}Be activity of the (4-15) cm section has to be multiplied by a factor of 1.15 (due to 15% decreased in ^{10}Be production as a result of a 31% increased in magnetic field intensity compared to the 20-30 cm sample). This increases the ^{10}Be activity of the (4-15) cm section from 4.56 ± 0.27 to 5.24 ± 0.31 dpm/kg. The difference between this value and that of the (20-30) cm value is 1.06 ± 0.35 dpm/kg. The 18% increase (due to meltwater input) in the ^{10}Be activity compared to the (20-30) cm value is 0.75 dpm/kg. The remaining excess activity of 0.31 dpm/kg which amounts to 7% may be ascribed to the CR intensity variations, other factors being constant.

IV.4(b) CR intensity variations in the past 2 m.y. :

The CR intensity is defined as the intensity of those CR particles which are responsible for ^{10}Be production in the earth's atmosphere. The variations in CR intensity could represent the variations in galactic CR particles impinging on the earth's atmosphere. These variations in CR intensity can be derived from ^{10}Be measurements in deep-sea sediment. The ^{10}Be activity in sediment core is governed by the following equation :

$$C = \frac{P}{S} e^{-\lambda t} \qquad \text{.....(3)}$$

where

P = ^{10}Be production rate (dpm cm^{-2} yr^{-1})

S = Sedimentation rate (g cm^{-2} yr^{-1})

C = Activity of ^{10}Be (dpm g^{-1})

λ = Decay constant of ^{10}Be(yr^{-1})

t = Time of deposition of the sediment(yr)

Equation (3) can be written as

$$Y = \frac{P}{S} \qquad \text{.....(4)}$$

where $Y = Ce^{\lambda t}$ = Decay corrected activity

If P and S are constant than

$$Y = \text{constant} \qquad \text{.....(5)}$$

i.e. if decay corrected activities are plotted against time t, the points should lie on a constant activity line provided P and S remain constant. The various causes which can affect P and S are already discussed. The ^{10}Be activities have been measured in ten sections of NOVA III-16 (Table III.2). These range from 4.90±0.19 to 6.50±0.30 dpm/kg.

The Th isotope data on this core obtained by Amin et al.(1975) reveals that (i) it has a uniform accumulation rate 1.6 mm/10^6 yrs throughout its length (155 cm), which is identical to that obtained using magnetic reversal technique (Amin et al., 1972b) and (ii) the mixed layer thickness would be smaller than about 3 cm. Since the sample thickness 10-21 cm is much larger than the mixed layer thickness, bioturbation effects in this core are not important. The sedimentation rate 1.6 mm/10^3 has been used to convert the 'depth interval' of each section into 'time interval' and the measured ^{10}Be activities have all been decay corrected. These decay corrected activities (A_d) range from 5.79±0.21 to 9.88±0.46 dpm/kg (Table IV.2, Fig.IV.3a).

This core has uniform bulk chemistry, based on major elements compositions. The two major elements which are effective in scavenging elements like Be, Th etc. are Al and Fe, the concentrations of which are 6.5±0.5 and 4.5±0.5% respectively. Hence one does not expect significant differences in the scavenging of Be isotopes from seawater during the period of deposition of NOVA III-16(less than 1 m.y.).

Fig.IV.3 : Plots of parameters (a) A_d (decay corrected ^{10}Be activity), (b) P/P_o and (c) A_{dm} (decay and magnetic field corrected ^{10}Be activity) as a function of time (Before Present) for NOVA III-16.

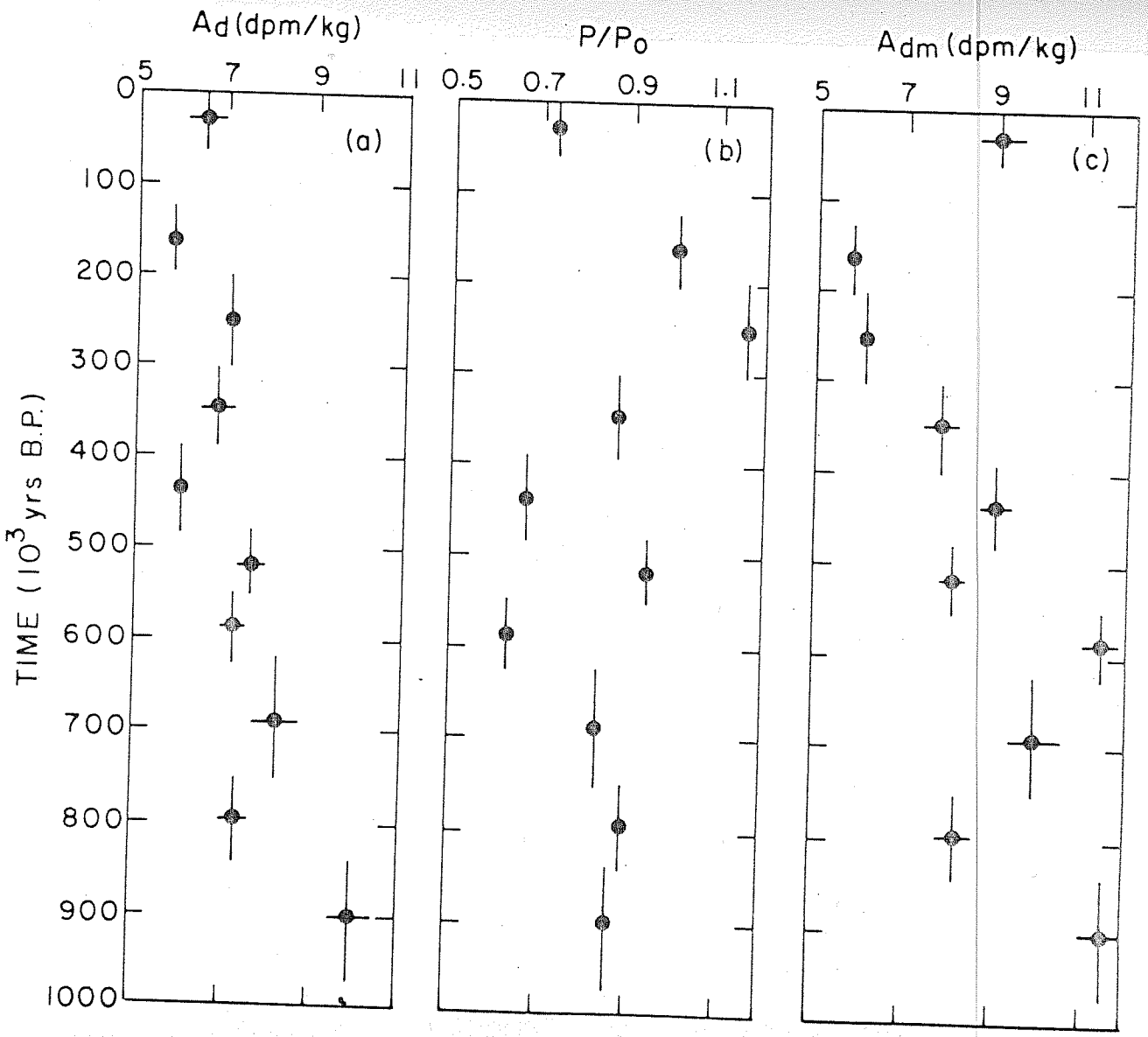
Ad (dpm/kg)
P/Po
Adm (dpm/kg)
5
7
9
11
0.5
0.7
0.9
1.1
(a)
(b)
(c)
0
100
200
300
400
500
600
700
800
900
1000
TIME (10^3 yrs B.P.)

Table IV.2 : ^{10}Be activities of sediment cores corrected for decay and magnetic field variations.

Sediment core	Depth interval (cm)	Time interval (X 10^3 yrs.)	Measured ^{10}Be activity+ (dpm/kg)	P/P_o (ratio)	^{10}Be activity (dpm/kg)	
					Decay corrected A_d	Magnetic field corrected A_{dm}**
1	2	3	4	5	6	7
	0-40	0-191	4.50 ± 0.64	0.82	4.70 ± 0.67	5.7 ± 0.8
	40-80	191-381	3.90 ± 0.51	1.00	4.45 ± 0.58	4.5 ± 0.6
	80-120	381-571	6.30 ± 0.93	0.73	7.85 ± 1.16	10.8 ± 1.6
	120-160	571-762	4.96 ± 0.67	0.78	6.75 ± 0.91	8.7 ± 1.2
	160-190	762-905	4.02 ± 0.63	1.06	5.91 ± 0.93	5.6 ± 0.9
	190-223	905-1062	3.63 ± 0.62	1.11	5.72 ± 1.29	5.2 ± 1.2
KH 70-2-7*	223-236	1062-1124	3.25 ± 0.54	1.07	5.38 ± 0.90	5.0 ± 0.8
	236-265	1124-1262	3.62 ± 0.62	1.05	6.28 ± 1.08	6.0 ± 1.0
	265-295	1262-1405	2.77 ± 0.40	1.09	5.13 ± 0.74	4.7 ± 0.7
	295-330	1405-1571	2.90 ± 0.44	1.01	5.77 ± 0.88	5.7 ± 0.9
	330-365	1571-1738	2.05 ± 0.36	1.12	4.40 ± 0.77	3.9 ± 0.7
	365-387	1738-1843	2.84 ± 0.43	1.22	6.50 ± 0.98	5.3 ± 0.8
	387-420	1843-2000	3.22 ± 0.56	1.16	7.82 ± 1.36	6.7 ± 1.2

1	2	3	4	5	6	7
	0-45	0-225	7.18 ± 0.94	0.83	7.56 ± 0.99	9.1 ± 1.2
	45-95	225-475	5.37 ± 0.80	0.82	6.32 ± 0.94	7.7 ± 1.1
	95-145	475-725	5.25 ± 0.71	0.73	6.92 ± 0.94	9.5 ± 1.2
KH 68-4-15*	145-195	725-925	7.91 ± 1.12	1.04	11.71 ± 1.66	11.3 ± 1.6
	195-245	975-1225	6.88 ± 0.97	1.16	11.43 ± 1.61	9.9 ± 1.4
	245-297	1225-1485	5.38 ± 0.75	1.08	10.06 ± 1.40	9.3 ± 1.3
	297-342	1485-1710	6.67 ± 0.85	1.11	13.95 ± 1.78	12.6 ± 1.6
	342-387	1710-1935	5.23 ± 0.66	1.22	12.14 ± 1.35	10.0 ± 1.3
B-52-39*	7-9	23-30	5.6 ± 0.2	1.01	5.6 ± 0.2	9.3 ± 0.33
	0-35	0-103	7.38 ± 0.96	0.66	7.56 ± 0.98	11.5 ± 1.5
	35-75	103-221	6.54 ± 0.83	1.08	7.05 ± 0.90	6.5 ± 0.8
	75-110	221-324	4.80 ± 0.68	0.98	5.44 ± 0.77	5.6 ± 0.8
	110-155	324-456	5.21 ± 0.63	0.70	6.24 ± 0.75	8.9 ± 1.1
	155-190	456-559	5.00 ± 0.72	1.04	6.32 ± 0.91	6.1 ± 0.9
	190-230	559-677	4.04 ± 0.54	0.67	5.37 ± 0.72	8.0 ± 1.1
	230-265	677-779	5.71 ± 0.83	0.90	7.99 ± 1.16	8.9 ± 1.3

1	2	3	4	5	6	7
	265-300	779-882	4.54 ± 0.63	1.10	6.67 ± 0.93	6.1 ± 0.9
KH 68-4-18*	300-335	882-985	4.57 ± 0.65	0.91	7.04 ± 1.00	7.7 ± 1.1
	335-365	985-1074	5.17 ± 0.87	1.27	8.32 ± 1.40	6.6 ± 1.1
	415-465	1221-1368	2.39 ± 0.35	1.02	4.35 ± 0.64	4.3 ± 0.6
	465-515	1368-1515	5.58 ± 0.75	1.08	10.86 ± 1.46	10.1 ± 1.4
	515-570	1515-1677	4.21 ± 0.54	1.25	8.80 ± 1.13	7.0 ± 0.9
	570-625	1677-1838	4.96 ± 0.70	1.20	11.17 ± 1.58	9.3 ± 1.3
	625-675	1838-1985	3.46 ± 0.46	1.24	8.37 ± 1.11	6.8 ± 0.9
	0-10	0-63	6.44 ± 0.37	0.73	6.54 ± 0.38	9.0 ± 0.5
	20-32	125-200	5.37 ± 0.19	1.00	5.79 ± 0.21	5.8 ± 0.2
	32-48	200-300	6.34 ± 0.22	1.16	7.11 ± 0.25	6.1 ± 0.2
	48-63	300-394	5.77 ± 0.27	0.87	6.77 ± 0.32	7.8 ± 0.4
	63-77	394-481	5.90 ± 0.19	0.67	6.00 ± 0.23	9.0 ± 0.3
NOVA III-16	77-88	481-550	6.01 ± 0.24	0.94	7.63 ± 0.31	8.1 ± 0.3
	88-99	550-619	5.48 ± 0.21	0.63	7.18 ± 0.28	11.4 ± 0.4

1	2	3	4	5	6	7
	99-120	619-750	5.99 ± 0.35	0.83	8.22 ± 0.48	9.9 ± 0.6
	120-135	750-844	5.04 ± 0.22	0.89	7.28 ± 0.32	8.2 ± 0.4
	135-155	844-969	6.50 ± 0.30	0.86	9.88 ± 0.46	11.5 ± 0.5

* Data for the cores KH70-2-7, KH68-4-15, B52-39 and KH68-4-18 have been taken from Inoue and Tanaka (1979), Krishnaswami et al. (1982) and Tanaka and Inoue (1979).

\+ Sedimentation rates of cores KH70-2-7, KH68-4-15 and KH68-4-18 are 2.1, 2.0, 3.0 and 3.4 mm/10^3 yrs (Kobayashi et al., 1971; Amin et al., 1975; Tanaka and Inoue, 1979).

** $A_{dm} = A_d(P/P_o)^{-1}$

According to the present day glacial ice distribution (Flint, 1971) 85% of the total ice resides in the Antarctica and little less than 9% in Greenland. All the rest of the world's glaciers together constitute about 6% (=1.14×10^{18}kg). Assuming that 6% of the ice formed during glacial period on the continents melts totally during interglacial period and the meltwater spreads uniformly over the Pacific, Atlantic and Indian oceans (area = 3.2×10^{18} cm^2, Sverdrup et al., 1942), the increase in the oceanic ^{10}Be inventory will be less than 1% of that present in the water column. In this calculation average values 23×10^{-6} and 2.5×10^{-6} dpm/kg have been used for snow and ocean water respectively(McCorkell et al., 1967; Raisbeck et al., 1978,1979a, 1980; Krishnaswami et al., 1982). Hence the meltwater input at the core location (central equatorial Pacific) is negligible.

Now the only other factor to be considered is the variation of the earth's magnetic field intensity. Using the magnetic field intensity data of Wollin et al.(1978), the factor P/P_o has been calculated for several closely spaced time intervals (about 25×10^3) during the past 2 m.y. The average P/P_o for each analysed section of NOVA III-16 is then calculated. The decay and magnetic field corrected ^{10}Be activity (A_{dm}) is derived from the corresponding decay corrected activity A_d and the P/P_o ratio using the relation

$$A_{dm} = A_d.(P/P_o)^{-1} \qquad \ldots\ldots\ldots\ldots(6)$$

The (P/P_o) and A_{dm} values are given Table IV.2 and plotted in Fig.IV.3(b) and IV.3(c) respectively. The A_{dm} values range from 5.8±0.2 to 11.5±0.5 dpm/kg. This range must be a measure of the CR intensity variations. From Fig.IV.3(c) it is seen that these variations are as much as ±33% over the mean during the past about 1 m.y. These variations are statistically significant as some of the points lie well outside the 1 sigma (standard deviation) over the mean and the errors of the individual measurements. The CR intensity appears to be low at about 200 kyr and high at about 600 and 900 kyr. Since the variations do not show any systematic linear trends, Power Spectrum Analysis of the data was done by Maximum Entropy Method (MEM) for lag 9 (Burg 1967, 1978; Murty, 1981). This method requires the data points to be at equal intervals. A total of 13 points were read off at 75 kyr intervals from the curve obtained by joining the mid points of the data. The analysis yielded periodicities of 1250, 500, 300 and 197 kyr (Fig.IV.4a) of which the last three are prominent ones as NOVA III-16 data is only for the past less than 1000 kyr.

Though less precise compared to NOVA III-16 measurements, a lot of data on ^{10}Be in ocean cores are available due to the pioneering efforts of Tanaka's group

Fig.IV.4 : Power spectrum for (a) NOVA III-16 data and (b) combined data. Numbers indicated near the peaks are the periodicities (k.y).

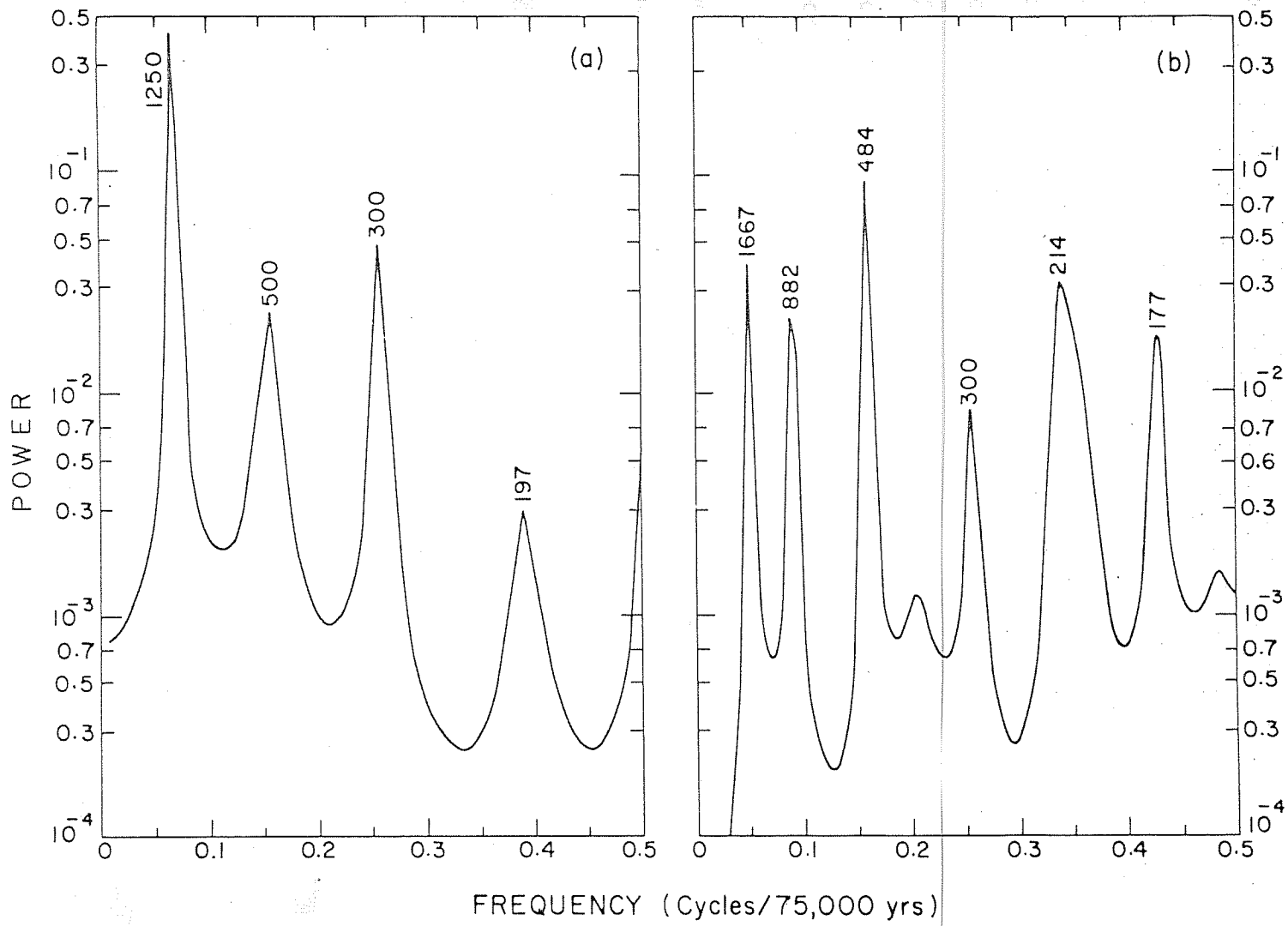
(a)
(b)
POWER
FREQUENCY (Cycles/75,000 yrs)
1250
500
300
197
1667
882
484
300
214
177
0.5
0.3
10^{-1}
0.7
0.5
0.3
10^{-2}
0.7
0.5
0.3
10^{-3}
0.7
0.5
0.3
10^{-4}
0.6
0
0.1
0.2
0.3
0.4
0.5

(Inoue and Tanaka, 1976, 1979; Tanaka et al., 1977; Tanaka and Inoue, 1979) and most of their cores were independently dated by the magnetic reversal technique (Kobayashi et al., 1971). I have selected only those cores which had constant deposition rates, which are free from volcanic effects and which are from a closeby location to NOVA III-16 (Table IV.2). Though this data extends upto 3 m.y., it could be used upto 2 m.y. since the magnetic field intensity variations beyond 2 m.y. are not known. The combined data on A_{dm} are plotted as a function of time (Fig.IV.5). It should be noted that the P/P_o correction factor for all the samples amounts to less than $\pm 30\%$.

Though there is large scatter in the data (Fig. IV.5), an attempt was made to fit a least square line (to find out if any gradual increase or decrease of CR existed) through the data; it yielded a poor correlation coefficient of - 0.11 for 26 data points. The χ^2 - test for 'goodness of fit' was also applied and the value of χ^2 is 617 (Bevington, 1969). This high value of χ^2 implies that a straight line fitting through the data points is poor and the ^{10}Be data has no systematic linear relationship with time.

The combined data shows variations as much as $\pm 50\%$ over the mean. It is clear from the Fig.IV.5 that CR intensity was low at about 200,1300 and 1700 kyr and

Fig.IV.5 : Plot of decay and magnetic field corrected ^{10}Be activities (A_{dm}) as a function of time (B.P.) for the composite data (ours plus the ones selected from the measurements of Tanaka's group). The solid curve is drawn by joining the weighted-mean of data points in each 75 k.y. interval. Where there is no point in a given interval the preceding and succeeding ones are interpolated. This curve should represent the CR intensity variations.

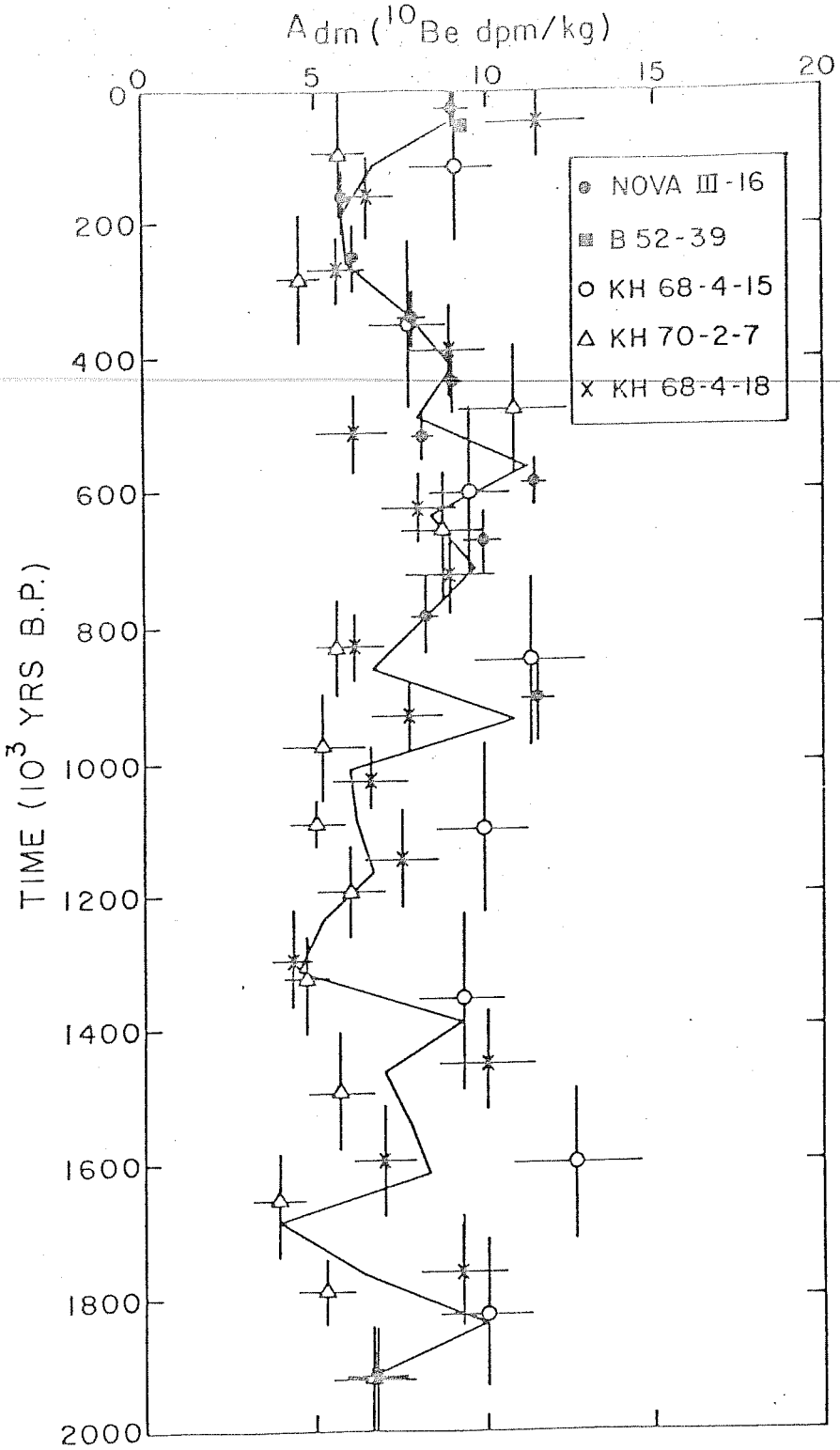
Adm (^{10}Be dpm/kg)
0
5
10
15
20
TIME (10^3 YRS B.P.)
0
200
400
600
800
1000
1200
1400
1600
1800
2000
NOVA III-16
B 52-39
KH 68-4-15
KH 70-2-7
KH 68-4-18

it was high at about 550, 950 and 1800 kyr. The MEM power spectrum method is again used for the combined data. Twenty six points were obtained by taking the weighted average of the points in each 75 kyr interval. In two cases since there is no data point in the interval, interpolations were made between the weighted-average values of the points before and after the interval. The power spectrum analysis for lag 18 has yielded periodicities 1667, 882, 484, 300, 214 and 177 kyr (Fig.IV.4b). The common periodicities to both the NOVA III-16 and combined data sets are 500, 300 and about 200 k.y. and represent CR intensity variations which had been as much as ±50% based on the combined data during the past 2 m.y. During the past 1 m.y. the variations based on our more precise data on NOVA III-16 had been upto ±33%. The possible causes for these long term CR intensity variations have been discussed by Forman and Schaeffer (1979). These are :

i) Variations in the distant sources.

ii) Time variations in the propagation conditions in the galaxy.

iii) Variations in the position of the solar system with respect to stationary spatial distribution of CR in the galaxy.

iv) Local events e.g. supernova explosions (Higdon and Lingenfelter, 1973; Lingenfelter, 1979).

The observed periodicities 500, 300 and 200 kyr are much smaller than the only expected periodic increase in the CR flux of the 10^8 yr time scale, which is supposed to be caused by the passage of our solar system through the spiral arm of our galaxy. The observed periodicities and variations obtained in the present investigation should be useful in understanding the origin of CR and its propagation conditions.

IV.4 Ferromanganese nodules' studies :

The results of the studies of the growth rates, composition and mineralogy of the manganese nodules from the Pacific, Atlantic and Indian oceans are discussed separately. Besides, the implications of these results towards understanding the depositional history of the authigenic elements are also indicated.

IV.4(a) Growth rates :

The distribution of a radionuclide in the nodule is governed by the following equation

$$C = C_o \exp(- \lambda \frac{Z}{S}) \qquad \text{.....} \quad (7)$$

where

C = Activity (dpm/g) of radionuclide at depth Z.

C_o = Initial activity (dpm/g) of radionuclide at Z=0

λ = Decay constant of the radionuclide ($m.y.^{-1}$)

Z = Depth (cm), origin fixed at the nodule surface, positive axis into the nodule.

S = Average growth rate of the nodule (cm/m.y.)

Logarithm of equation (9) yields,

$$\ln C = \ln C_o - \frac{\lambda}{S} Z \qquad \text{.....(8)}$$

or

$$\frac{d\ln C}{dZ} = - \frac{\lambda}{S} \qquad \text{.....(9)}$$

So the slope of activity versus depth plot gives a measure of the nodule growth rate. The assumptions made in calculating the growth rates are :

(1) The radionuclide is incorporated into the nodule matrix at a constant rate over the dating interval (constant flux assumption).

(2) The radionuclide is immobile in the nodule material over the dating interval (closed system assumption).

IV.4(a)(i) <u>^{10}Be and $^{10}Be/^{9}Be$ methods</u> :

The ^{10}Be activity and $^{10}Be/^{9}Be$ specific activity data are given in Tables III.3, III.4 and IV.1 and have been shown in Figs. IV.6, IV.7, IV.8 and IV.9. The average growth rates of the thirteen nodules analysed range from 1-8 mm/10^6 yrs over the past 5-10 m.y. These are in good agreement with the previously reported measurements using ^{10}Be on different nodules (Somayajulu, 1967; Bhat et al., 1970; Krishnaswami et al., 1972 , 1979; Guichard

Fig.IV.6 : Variations of ^{10}Be activity (dpm/kg) and $^{10}Be/^{9}Be$ specific activity (dpm/mg) as a function of depth for eight large nodules (obtained by decay counting method). Computer-based-best-fit-lines are drawn through the data points to obtain the growth rates (mm/10^6 yrs) which are also indicated.

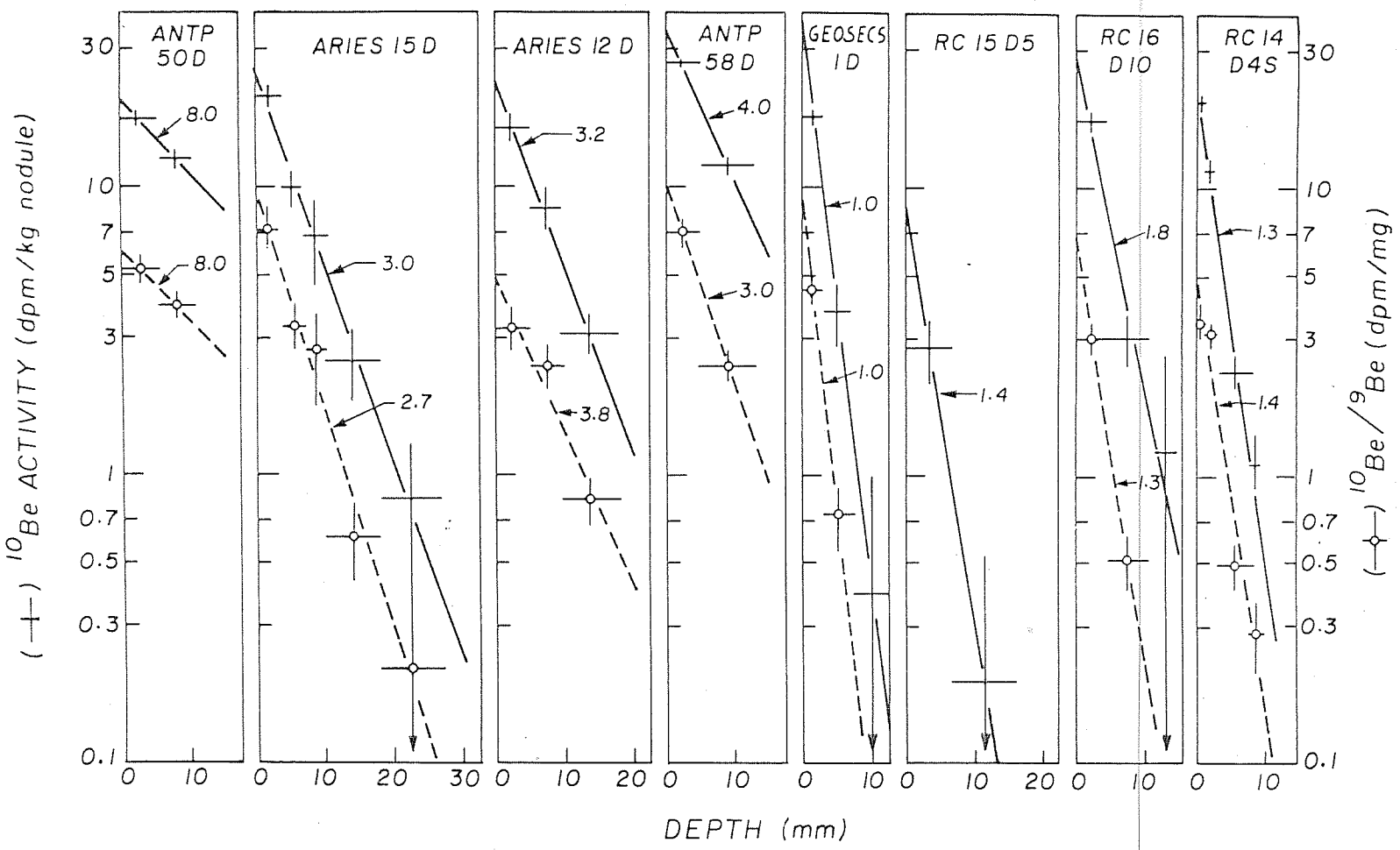
ANTP 50D
ARIES 15 D
ARIES 12 D
ANTP 58 D
GEOSECS 1D
RC 15 D5
RC 16 D10
RC 14 D4S
8.0
8.0
3.0
2.7
3.2
3.8
4.0
3.0
1.0
1.0
1.4
1.8
1.3
1.3
1.4
(—+—) 10Be ACTIVITY (dpm/kg nodule)
(—◇—) 10Be/9Be (dpm/mg)
DEPTH (mm)

Fig.IV.7 : Variations of ^{10}Be activity (dpm/kg) and $^{10}Be/^{9}Be$ specific activity (dpm/mg) as a function of depth for the RC 14 D4F nodule (using decay counting method). The possible explanations for the observed 'V' patterns are discussed in the section IV.4(a).(i).

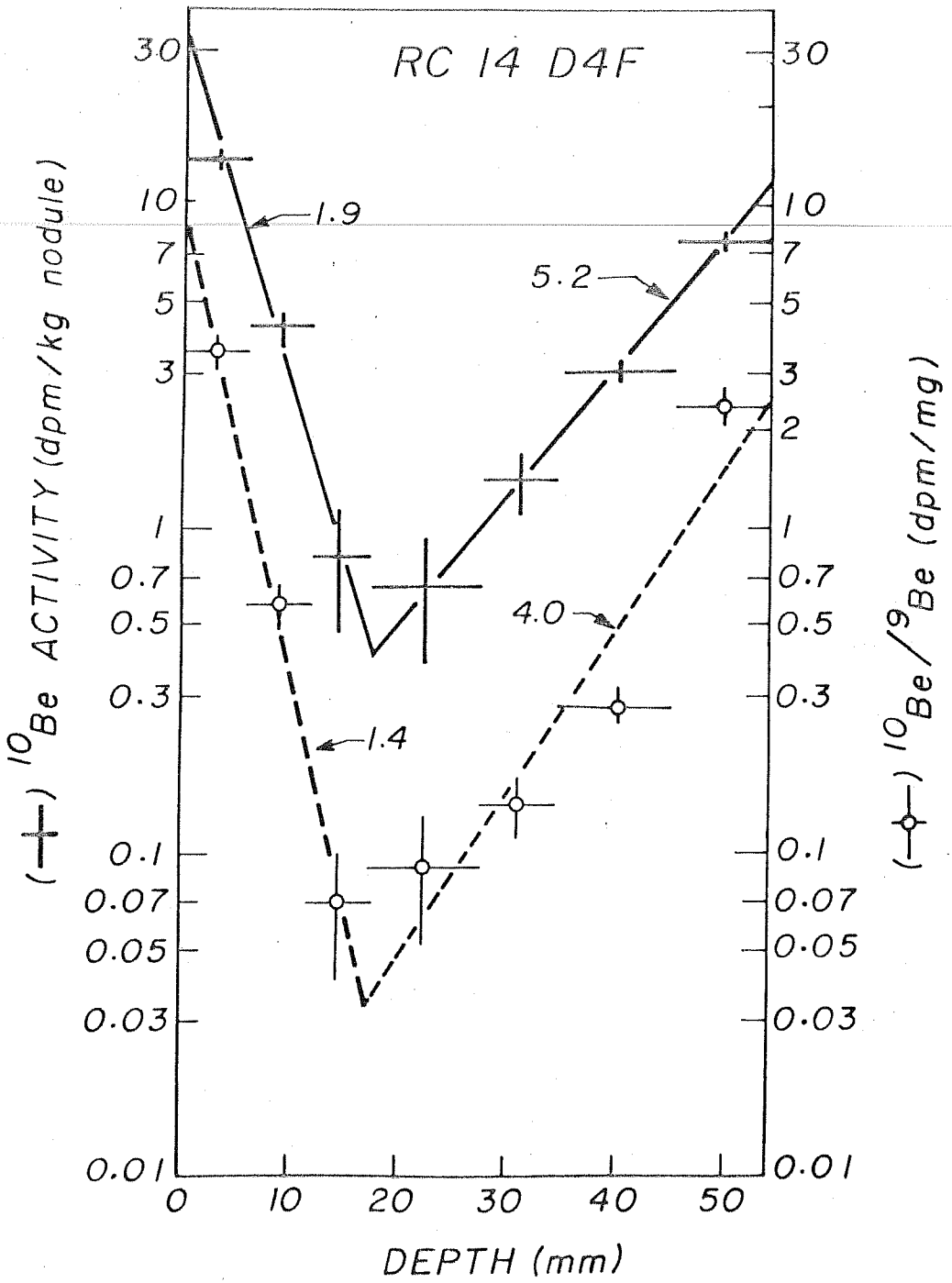
RC 14 D4F
30
10
7
5
3
1
0.7
0.5
0.3
0.1
0.07
0.05
0.03
0.01
1.9
5.2
4.0
1.4
2
0
10
20
30
40
50
DEPTH (mm)
(—+—) 10Be ACTIVITY (dpm/kg nodule)
(—○—) 10Be/9Be (dpm/mg)

Fig.IV.8 : Variations of ^{10}Be activity (atoms/g) and $^{10}Be/^{9}Be$ specific activity (atoms/μg) as a function of depth in three small nodules (using atom counting method). Numbers indicated are the growth rates (mm/10^6 yrs) obtained by drawing least square lines through the data points.

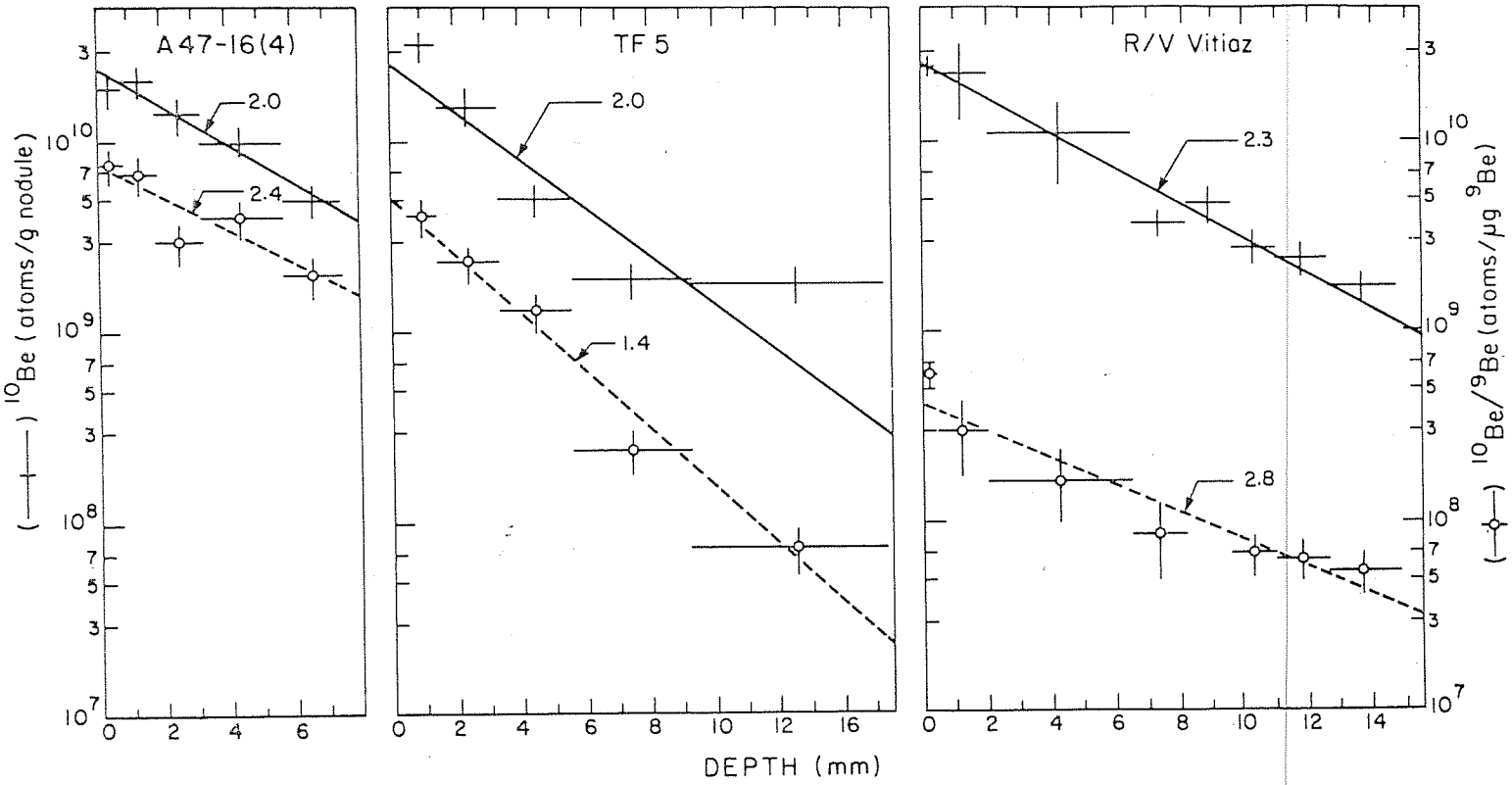
A47-16(4)
TF 5
R/V Vitiaz
2.0
2.4
2.0
1.4
2.3
2.8
(—+—) ^{10}Be (atoms/g nodule)
(—○—) ^{10}Be/^{9}Be (atoms/μg ^{9}Be)
DEPTH (mm)

Fig.IV.9 : Intercomparison of ^{10}Be growth rates ($mm/10^6$ yrs) for nodule ANTP 58D determined by decay counting and atom counting techniques.

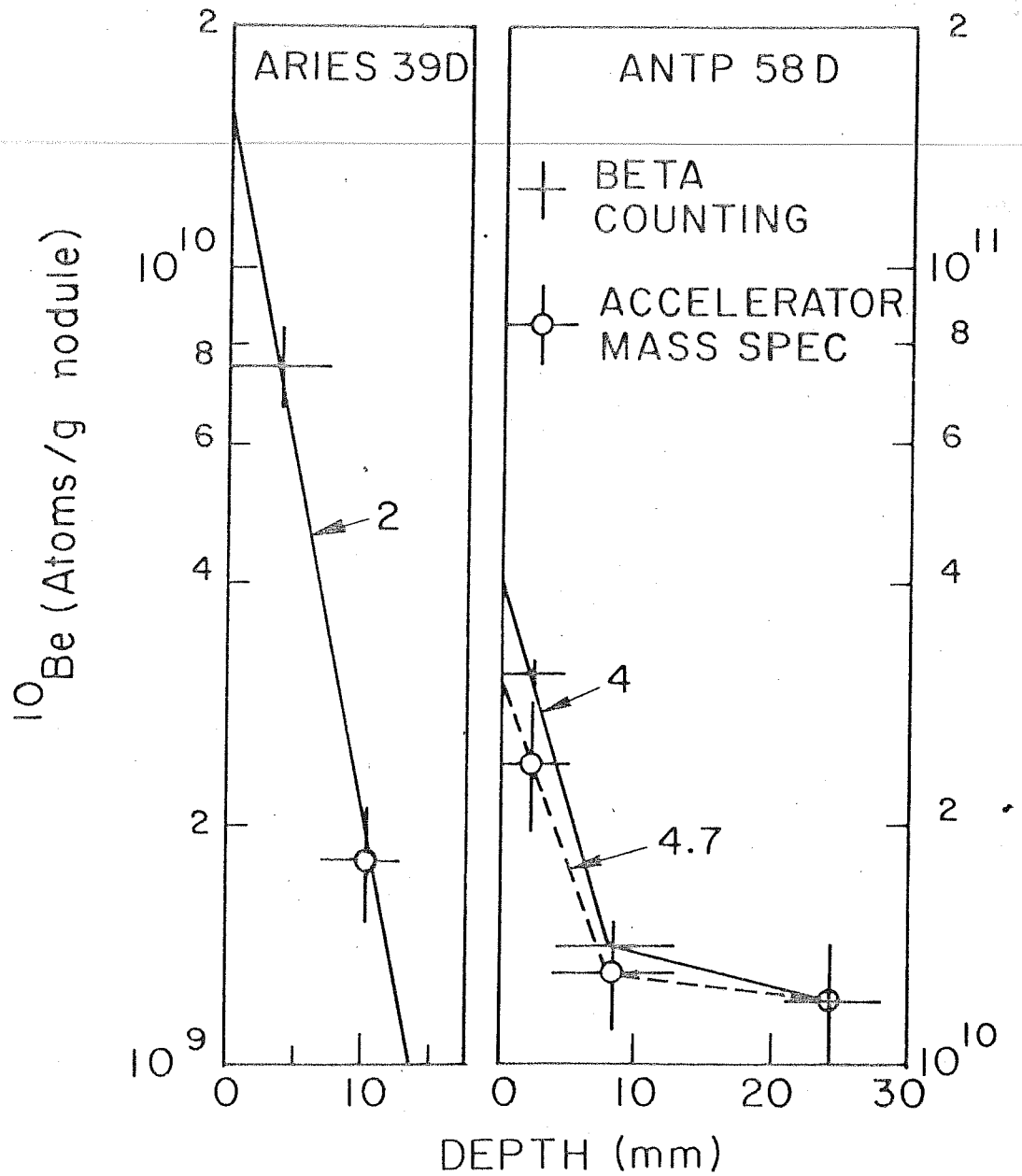
ARIES 39D
ANTP 58 D
BETA COUNTING
ACCELERATOR MASS SPEC
^{10}Be (Atoms/g nodule)
10^{10}
10^{9}
10^{11}
10^{10}
2
4
4.7
DEPTH (mm)
0
10
20
30

et al., 1978; Ku et al., 1979, 1981; Reyss, 1979; Turekian et al., 1979; Nelson et al., 1980). The growth rates calculated by ^{10}Be and $^{10}Be/^{9}Be$ methods are in good agreement (within ±35%). It shows that although ^{10}Be and ^{9}Be have different source functions, the parameter $^{10}Be/^{9}Be$ can be used as a good index of growth rate since it avoids possible uncertainties arising from temporal variations in the uptake of ^{10}Be by nodules.

It should be noted here that, todate including the present work, thirty nodules have so far been dated by the ^{10}Be method and all the growth rates fall in the range 1-8 mm/10^6 yrs (Fig.IV.10a, Table IV.3). Fig.IV.10(a) is the histogram of ^{10}Be growth rates of the nodules. It is clear that most of the nodules have growth rates 1-4 mm/10^6 yrs, a range similar to that obtained on different nodules using U-Th by Ku and Broecker (1969) viz. 2-4 mm/10^6 yrs.

In the case of ANTP 58D the ^{10}Be activity flattens off after 12.8 mm (Table IV.1. Fig.IV.9). The growth rates calculated for this nodule in the interval (0-12.8) mm by decay counting (4 mm/10^6 yrs) and atom counting (4.7 mm/10^6 yrs) are in excellent agreement (within ±15%).

Fig.IV.10 (a) Histogram of the growth rates of the nodules. In addition to the data obtained in this work all the data that are existing as of 1982 are compiled. (Bhat et al., 1970; Krishnaswami et al., 1972 , 1979; Guichard et al., 1978; Ku et al., 1979; Reyss et al., 1979; Turekian et al., 1979; Nelson et al., 1980).

(b) Histogram of ^{10}Be inventory in nodules. Here also all the data are compiled from references given in Fig.10(a).

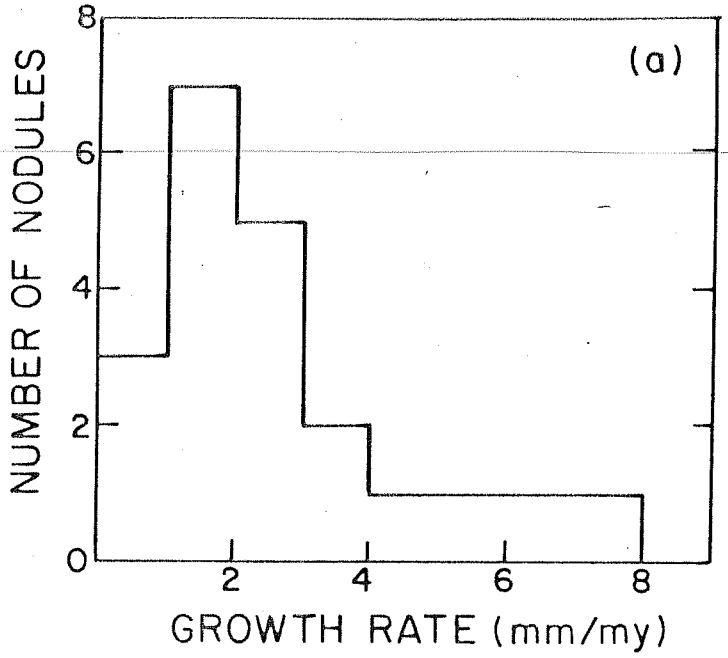
(a)
NUMBER OF NODULES
0
2
4
6
8
2
4
6
8
GROWTH RATE (mm/my)

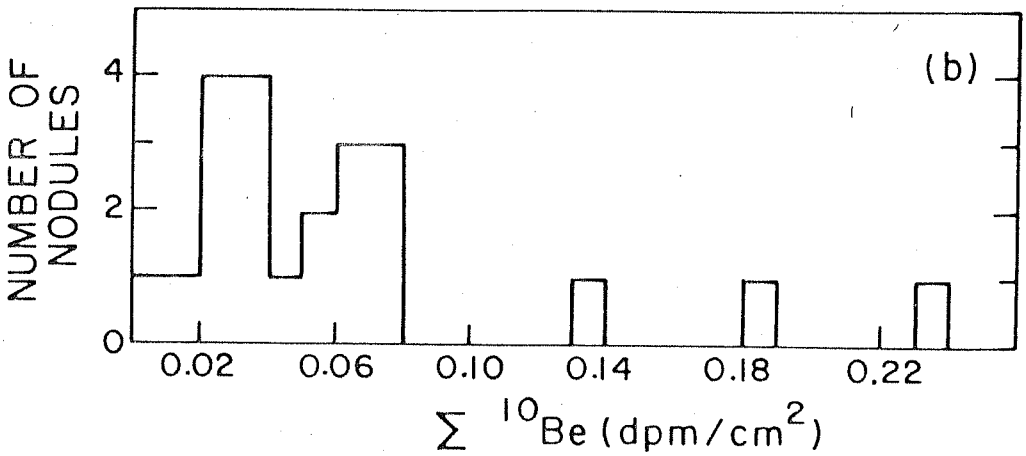
(b)
NUMBER OF NODULES
0
2
4
0.02
0.06
0.10
0.14
0.18
0.22
Σ 10Be (dpm/cm2)

Table IV.3 : Average growth rates, extrapolated-to-surface activities and $\Sigma^{10}Be$ of nodules*

Nodule	Growth rate (mm/10^6 yrs)					Extrapolated-to-surface activity ^{10}Be (dpm/kg)	$\Sigma^{10}Be$ (dpm/cm^2)	Reference
	^{10}Be	$^{10}Be/^{9}Be$	$^{230}Th_{exc}$	$^{230}Th_{exc}/^{232}Th$ (A.R.)	$^{231}Pa_{exc}$			
1	2	3	4	5	6	7	8	9
Zetes 3D	1.3	1.3	2.3	1.4	-	130.0	0.183	Krishnaswami et al.(1972)
ARIES 39D	2.0	-	-	-	-	14.0	o.012	Sharma et al. (1982a)
ANTP 50D	8.0	8.0	-	-	-	20.0	0.139	This work
ARIES 15D	3.0	2.7	-	-	-	24.5	0.032	This work
ARIES 12D	3.2	3.8	-	-	-	23.3	0.032	This work
ARIES 13D	2.4	-	-	-	-	68.0	0.071	Ku et al.(1979)
Tripod 2D	6.3	-	4.0	4.0	-	35.0	0.239	Bhat et al.(1970)
Mn 139	1.3	-	4.1	-	5.5	120.0	0.068	Ku et al.(1979)
DoDO 15-1	3.0	-	-	-	-	20.0	0.065	Bhat et al.(1970)
ANTP 58D	4.0	3.0	-	-	-	33.5	0.058	This work
C57-58-2	∿2	-	-	-	-	-	0.027	Krishnaswami et al.(1979)

1	2	3	4	5	6	7	8	9
A47-16(3)	~2	-	-	-	-	-	0.040	Krishnaswami et al.(1979)
A-47-16(4)	2.0	2.4	5.1	5.0	7.2	19.4	0.074	Krishnaswami et al.(1982)
TECHNO-1	2.8	-	2.3	-	-	27.0	0.033	Guichard et al.(1980)
TF 5	2.0	1.4	1.1	1.1	2.2	37.0	0.064	Krishnaswami et al.(1982)
GEOSECS 1D	1.0	1.0	1.7	1.6	-	38.5	0.017	This work
K-9-21	1.5	-	-	3.5	-	-	-	Nelson et al.(1980)
RC 15 D5	1.4	-	1.2	1.4	-	7.8	0.005	This work
RC 16 D10	4.4	-	-	-	-	28.2	0.055	Turekian et al. (1979)
RC16 D10**	1.8	1.3	3.4	3.5	-	27.0	0.021	This work
MD 13	1.2	-	-	-	-	12.1	-	Reyss (1979)
	(1.6)	-	-	-	-	(11.8)	-	
RC14 D4F+	1.9	1.4	1.3	1.5	-	29.7	0.024	This work
	(5.2)	(4.0)	-	-	-	(11.0)	(0.025)	
RC14 D4	1.3	1.4	3.1	3.3	-	21.6	0.049	This work
R/V VITIAZ	2.3	2.8	1.1	1.0	1.0	26.4	0.073	Krishnaswami et al.(1982)

A.R. = Activity Ratio

* ^{10}Be growth rates for two manganese crusts and four manganese nodules ranging from 1-5 mm/10^6 yrs (Ku et al., 1981) are not included in the table as details are not available.

** The average growth rates using $^{230}Th_{exc}$ and $^{230}Th_{exc}/^{232}Th$ methods are given for the top 1 mm section. The data indicates changes in growth rates which can be seen from Fig.IV.11.

\+ Numbers in parentheses represent measurements made on the other side of the nodule.

The sample ARIES 39D (6.9 - 12.3) mm did not show any measurable ^{10}Be activity by decay counting technique (Fig.IV.9), however it could be measured by accelerator mass spectrometry in the laboratory of Prof.Wolfli at Zurich. The growth rate based on two points (one by decay counting and the other by atom counting) is 2 mm/10^6 yrs.

Nodule RC14 D4F

This flat nodule from the south Indian ocean, (Table VI.3) showed measurable activity of ^{10}Be on both sides which decrease towards the centre. Both the ^{10}Be and $^{10}Be/^{9}Be$ ratio show an identical distribution pattern (Fig.IV.7) and increase from the centre towards the sides. The deduced growth rates on the two sides differ by a factor of 2-3 from each other (1.9 and 1.4 on one side and 5.2 and 4.0 mm/10^6 yrs on the other side by ^{10}Be and $^{10}Be/^{9}Be$ methods respectively. - Fig.IV.7 and Table IV.3). The corresponding ^{10}Be activities extrapolated to the surface are 29.7 and 11.0 dpm/kg whereas the $^{10}Be/^{9}Be$ ratios are 9.4 and 2.5 dpm/mg. respectively. U and Th isotopes have been measured only on one side, i.e. the side that has the slower growth rate by ^{10}Be method, and it is found that $^{230}Th_{exc}$ - based rates are in excellent agreement with the ^{10}Be based ones (Figs.IV.7, IV.10 and Table IV.3).

It is interesting to note that Reyss (1979) reported ^{10}Be and nuclear track data on a nodule which showed the same behaviour as RC14 D4F and which also comes from a nearby location. In his case the extrapolated-to-surface values for both sides are about the same showing thereby that it has been growing simultaneously from both sides.

This is the second observation of its kind which has no unique and satisfactory explanation. However two possible scenarios can be considered :

i. The nodule was growing on both sides simultaneously at rates differing by a factor of about 3. It is not known how this nodule was lying on the ocean floor and how it had different growth rates. Based on trace metal analysis, it is seen that the side with a faster growth rate has higher Mn (22.2%) and Ni (0.91%) compared to the other side which has 14.4% Mn, and 0.39% Ni. Fe showed the opposite trend (Appendix).

ii. The nodule was growing at a faster rater (4.0-5.2) mm/10^6 yrs and it flipped at about 3 m.y. B.P. and started growing slowly (1.4-1.9 mm/10^6 yrs). This is a case similar to that proposed by Krishnaswami and Cochran (1978) based on Th isotope studies on smaller and somewhat spherical nodules. Being flat, RC14 D4F is not expected to flip frequently. However, if the

nodule flipped about 3 m.y B.P. and started growing at a slower rate, one should not see any gradient beyond 6 mm. (Fig.IV.7). Unfortunately, Th isotope measurements were not made on both the sides and so the ''flipping'' age by ^{230}Th method cannot be calculated.

Moore et al. (1981) based on U-Th decay series nuclides and nuclear track measurements on the two sides of another nodule considered both the scenarios discussed above and found the first one is more appropriate i.e. the nodule was simultaneously growing from both the sides.

IV.4(a).(ii) $^{230}Th_{exc}$ and $^{230}Th_{exc}/^{232}Th$ methods :

In Fig.IV.11 and IV.12 the depth variations of $^{230}Th_{exc}$ and $^{230}Th_{exc}/^{232}Th$ activity ratios in the eight nodules are presented. Based on least square lines drawn through the data, the average growth rates upto 1 m.y. are calculated (Table IV.3). Both the methods yield rates that are in good agreement (within $\pm 15\%$) and fall in the range of 1-5 mm/10^6 yrs, similar to that obtained (1-6 mm/10^6 yrs) by earlier workers (Ku and Broecker, 1969; Krishnaswami and Cochran, 1978; Krishnaswami et al., 1979).

Fig.IV.11 : $^{230}Th_{exc}$(dpm/g) and $^{230}Th_{exc}/^{232}Th$ (A.R.) variations with depth in five large nodules. Computer-based-best-fit-lines are drawn to get the growth rates (mm/10^6 yrs). In the case of RC 16 D10 the best fit lines drawn through all the points yield growth rates 3.4 and 3.5 mm/10^6 yrs by $^{230}Th_{exc}$ and $^{230}Th_{exc}/^{232}Th$ methods. These rates are used for comparison with ^{10}Be rates (Table IV.3).

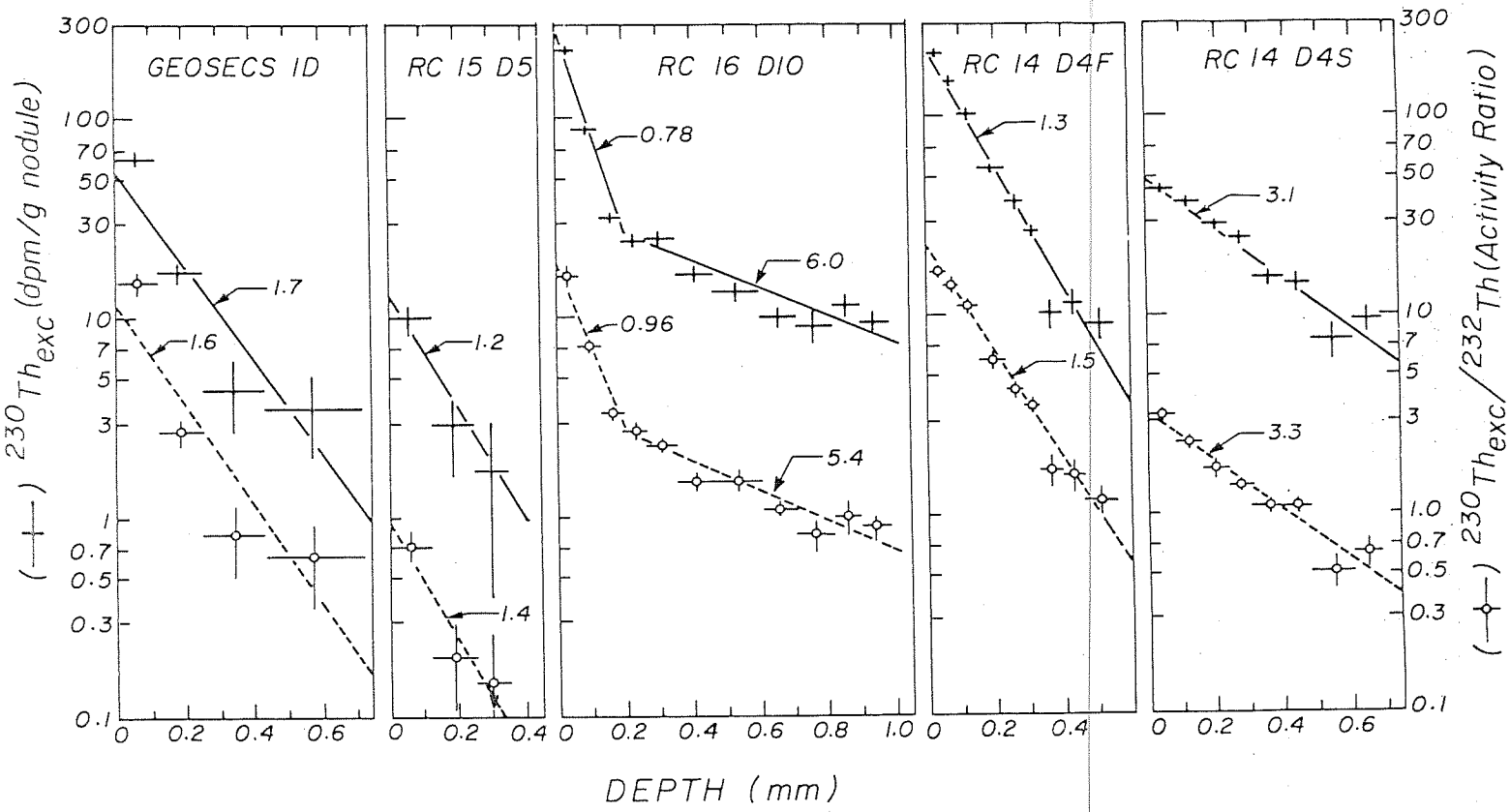
GEOSECS 1D
RC 15 D5
RC 16 D10
RC 14 D4F
RC 14 D4S
1.7
1.6
1.2
1.4
0.78
6.0
0.96
5.4
1.3
1.5
3.1
3.3
(—+—) 230Th exc (dpm/g nodule)
(—+—) 230Th exc/232Th (Activity Ratio)
DEPTH (mm)

Fig.IV.12 : Depth variations of $^{230}Th_{exc}$(dpm/g) and $^{230}Th_{exc}/^{232}Th$ (A.R.) in three small nodules. Growth rates (mm/10^6 yrs) are obtained by drawing least square lines through the data points.

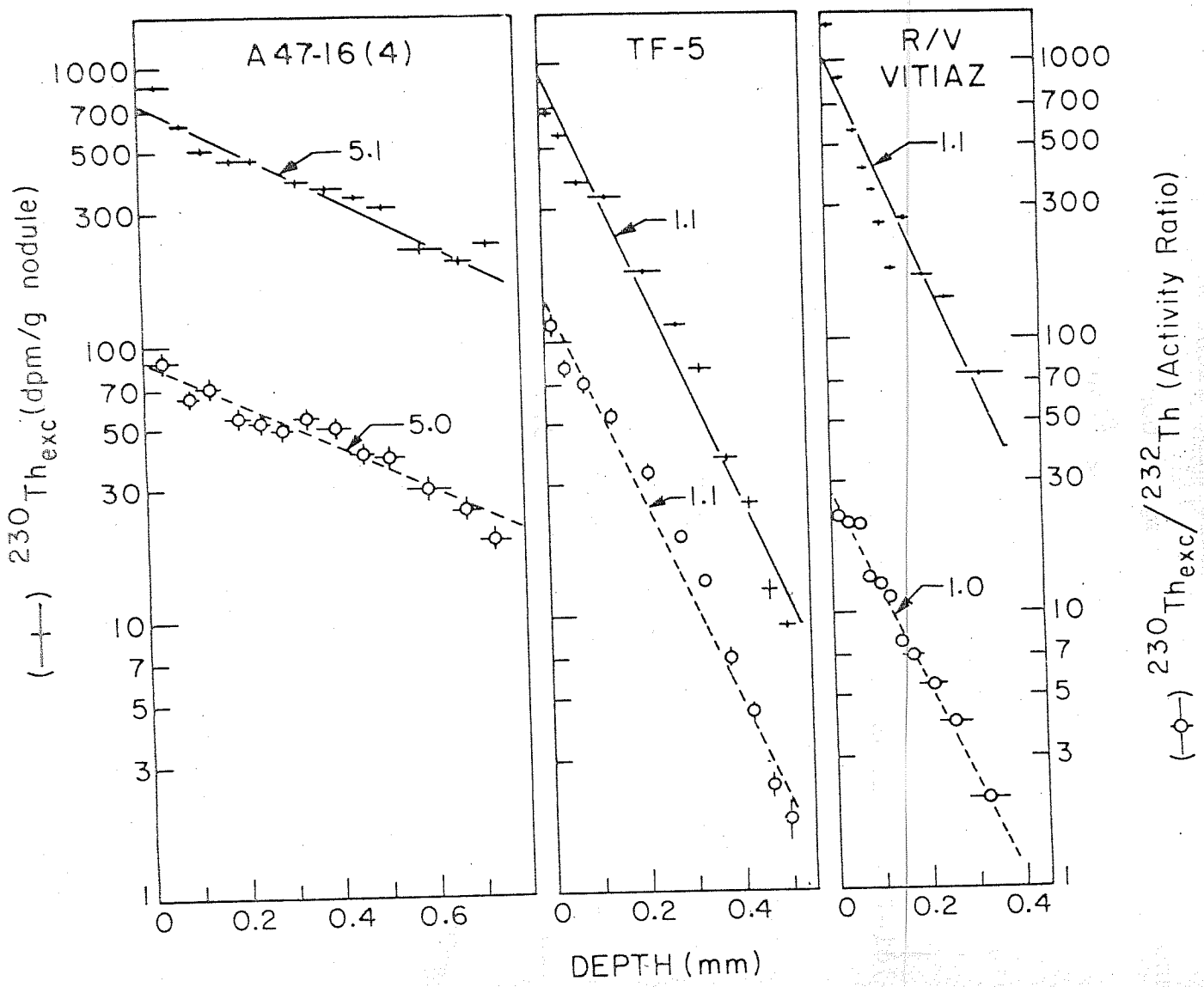
A47-16(4)
TF-5
R/V VITIAZ
5.1
5.0
1.1
1.1
1.1
1.0
1000
700
500
300
100
70
50
30
10
7
5
3
1
0
0.2
0.4
0.6
DEPTH (mm)
(—+—) 230Thexc (dpm/g nodule)
(—o—) 230Thexc/232Th (Activity Ratio)

There may be short term variations (of the order of 10^4-10^5 yrs) in the nodule growth rates. Such variations cannot be seen by the ^{10}Be decay technique used here because of large sampling intervals. However it is possible to study these variations by analysing closely spaced thin sections (1-2)mm using the accelerator mass spectrometry method. In the four nodules, A47-16(4), TF-5, RC 16 D10 and R/V VITIAZ, the depth profiles of Th isotopes have shown discontinuities. The detailed fine structure study can be used to infer the growth histories on the assumption that there has been no sampling artifacts. The growth rates have been found to vary from 0.8 to 7.3 mm/10^6 yrs (Krishnaswami et al., 1982; Sharma and Somayajulu, 1982).

IV.4(a).(iii) $^{231}Pa_{exc}$ method :

The data given in Table III.8 has been plotted in Fig.IV.13 and the average growth rates are calculated (Table IV.3). These growth rates range 1-7.2 mm/10^6 yrs which are in good agreement with the growth rates obtained by the same method on different nodules by other workers (Ku and Broecker, 1969; Krishnaswami and Cochran, 1978).

Fig.IV.13 : $^{231}Pa_{exc}$ activity (dpm/g) variations with depth in three small nodules. Growth rates (mm/10^6 yrs) are obtained by drawing best-fit-lines through the data sets.

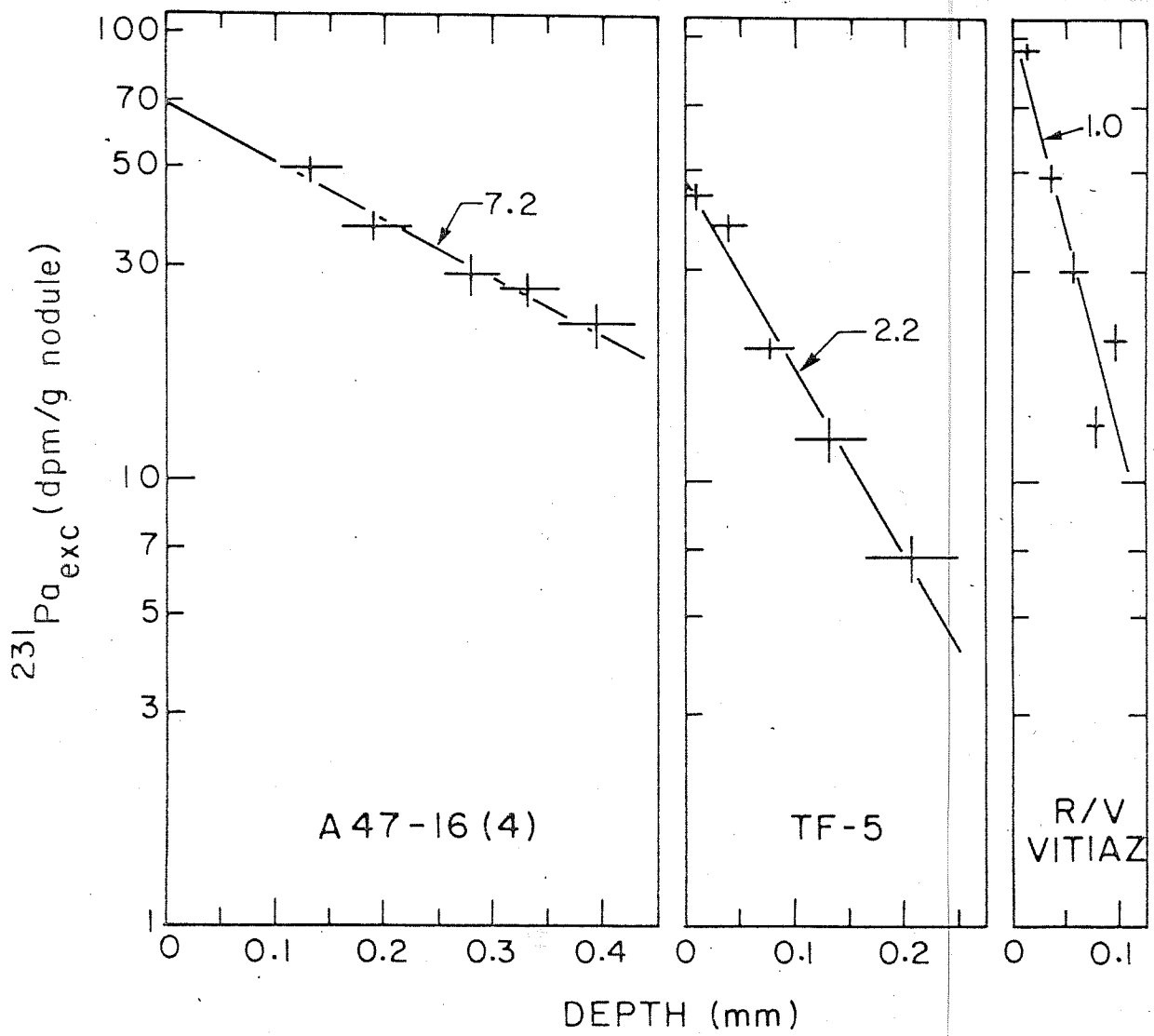
100
70
50
30
10
7
5
3
1
$^{231}Pa_{exc}$ (dpm/g nodule)
7.2
2.2
1.0
A47-16(4)
TF-5
R/V
VITIAZ
0
0.1
0.2
0.3
0.4
0
0.1
0.2
0
0.1
DEPTH (mm)

IV.4(a).(iv) Intercomparison of growth rates by different methods and growth models :

The average growth rates of the thirteen nodules obtained by different methods are given in Table IV.3 along with other published data. In most of the cases the agreement of the growth rates determined by ^{10}Be and ^{230}Th methods on the same nodule is very good. (Fig.IV.14). However in few cases there is discordancy as discussed below.

The depth distribution of the chronometric tracers (^{10}Be, $^{230}Th_{exc}$ and $^{231}Pa_{exc}$) within the nodules can be modelled to yield growth rates if the tracer nuclide is immobile in the nodule after its incorporation in the matrix. Most of the controversy in establishing nodule growth rates from the distribution of radionuclides centres around the validity of this condition.

The distribution of any radionuclide within a nodule can be described in terms of one of the three possible models : (1) The growth model-in which the radionuclide depth profiles in the nodules can be described in terms of its incorporation through nodule growth and removal

Fig.IV.14 : Comparison of growth rates by ^{10}Be and $^{230}Th_{exc}$ methods. If growth rates by both the methods are identical, points will fall on the dotted line.

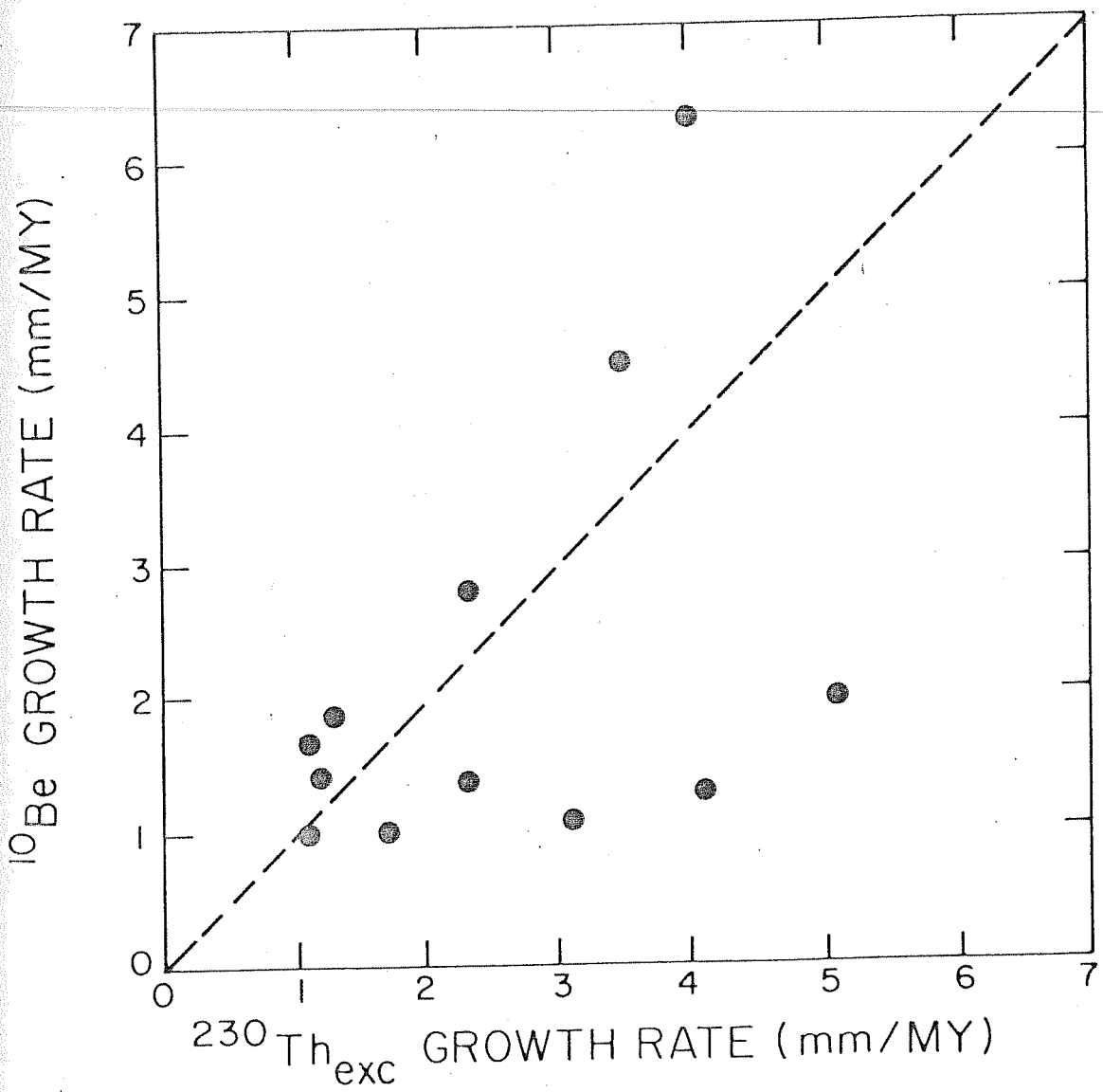
^{10}Be GROWTH RATE (mm/MY)
^{230}Th$_{exc}$ GROWTH RATE (mm/MY)
0
1
2
3
4
5
6
7

through radioactive decay. This model predicts an exponential decrease in the concentration of the radionuclide with depth, if the growth rate of the nodule has remained constant over the dating interval. Within the resolution of the data most of the radionuclide profiles reported in the literature do in fact show an exponentially decreasing trend with depth (2) The diffusion model-in which the depth distribution of the radionuclide is assumed to be controlled by its diffusion inward from the nodule surface accompanied by its radioactive decay. This model assumes a continuous supply of the radionuclide to the surface (e.g. by adsorption of nuclides on pre-existing nodules). It is implicit in this model that the nodule has been in existence on the ocean floor in its present size for an indeterminate period of time (3) The diffusion - growth model-which combines features of the above two models and includes terms for nodule growth, redistribution of radionuclides through diffusion/mixing and radioactive decay. This also predicts an exponentially decreasing concentration - depth profile for the radionuclides analogous to the growth model. The concepts and mathematical formulation of this model are identical to the commonly used bioturbation/mixing models for lake and marine sediments (Goldberg and Koide, 1962; Guinasso and Schink, 1975; Nozaki et al., 1977).

Mathematically the above three models can be summarized as follows :

(1) Growth model

$$S \frac{dC}{dZ} - \lambda C = 0 \qquad \text{.....(10)}$$

$$\text{Solution } C = C_o \exp\left[-\left(\frac{\lambda}{S}\right) Z\right]$$

(2) Diffusion model

$$K \frac{d^2C}{dZ^2} - \lambda C = 0 \qquad \text{.....(11)}$$

$$\text{Solution } C = C_o \exp\left[-\left(\frac{\lambda}{K}\right)^{1/2} Z\right]$$

(3) Diffusion growth model

$$K \frac{d^2C}{dZ^2} - S \frac{dC}{dZ} - \lambda C = 0 \qquad \text{.....(12)}$$

$$\text{Solution } C = C_o \exp\left[\frac{S-(S^2+4K\lambda)^{1/2}}{2K} Z\right]$$

Where

S = Growth rate, C = Concentration of radionuclide

λ = Decay constant, Z = Depth, K = Diffusion coefficient

Recently Ku et al. (1979) developed a mathematical model to describe radionuclide profiles in nodules - resulting from ''diffusion'' and ''diffusion-Growth''

concepts. They showed that for the diffusion model (termed as ''exposure - diffusion'' model in their paper), the logarithm of the concentration of the nuclide would have complex dependence with depth Z (ln C would vary approximately as Z^2) rather than the simple exponential decrease commonly observed. Ku et al. (1979) observed a pattern in the growth rates : $^{10}Be < ^{230}Th < ^{231}Pa$, for their nodule Mn-139. They have argued that any homogenization processes such as diffusion and mixing (largely due to sampling on crenulated growth surfaces) would tend to reduce the concentration gradients of shorter-lived radioisotopes more than those of longer lived ones. Thus they attributed the higher growth rates derived from $^{230}Th_{exc}$ and $^{231}Pa_{exc}$ data relative to that estimated from ^{10}Be profiles to diffusion/mixing of $^{230}Th_{exc}$ and $^{231}Pa_{exc}$. Although their hypothesis could explain the observed pattern of growth in Mn-139, the major problem associated with such a model is the assumption of constant growth rate for the nodule in the past several million years, an assumption very difficult either to substantiate or deny independent of radiometric data. Available data on the growth rates of nodules based on ^{10}Be and $^{230}Th/^{232}Th$ indicate that the pattern observed for A47-16(4) and Mn-139 (i.e. the ^{10}Be rate less than ^{230}Th rate) is not

unique and that for nodules TRIPOD 2D and R/V VITIAZ, the ^{10}Be rate faster than the ^{230}Th rate has also been observed (Table IV.3, Fig.IV.15). This observation i.e. the ^{10}Be rate $>^{230}Th_{exc}$ rate, would not be expected to result from mixing processes, since mixing would decrease the gradients in the concentration-depth profile of $^{230}Th_{exc}$ more than that of ^{10}Be, thereby the growth rates estimated from $^{230}Th_{exc}$ data are relatively higher.

This allows one to conclude that discordant growth rates deduced from ^{10}Be and $^{230}Th_{exc}$ most likely document changes in nodule growth rates with time, rather than homogenization of nuclide profiles by mixing processes. Therefore the observed radionuclide profiles in the nodules are interpreted as a reflection of their growth rates.

IV.4(b) <u>Fractional inventories and surface-extrapolated activities of radioisotopes</u> :

In Figs.IV.10(b) and IV.15 are shown the growth rates, extrapolated - to - surface activities and the inventories of ^{10}Be of nodules so far analysed from the world oceans. There is no clear-cut variation of these parameters either as a function of latitude in a given ocean or from ocean to ocean. It is also seen that Σ ^{10}Be (dpm/cm^2) of the nodules is 0.4-22% of what is present in the overhead

Fig.IV.15 : Growth rates (mm/10^6 yrs) of nodules from the world oceans obtained by the ^{10}Be method. Numbers in parentheses are the extrapolated-to-surface activities (dpm/kg nodule). 'X' indicate locations from where two nodules are analysed.

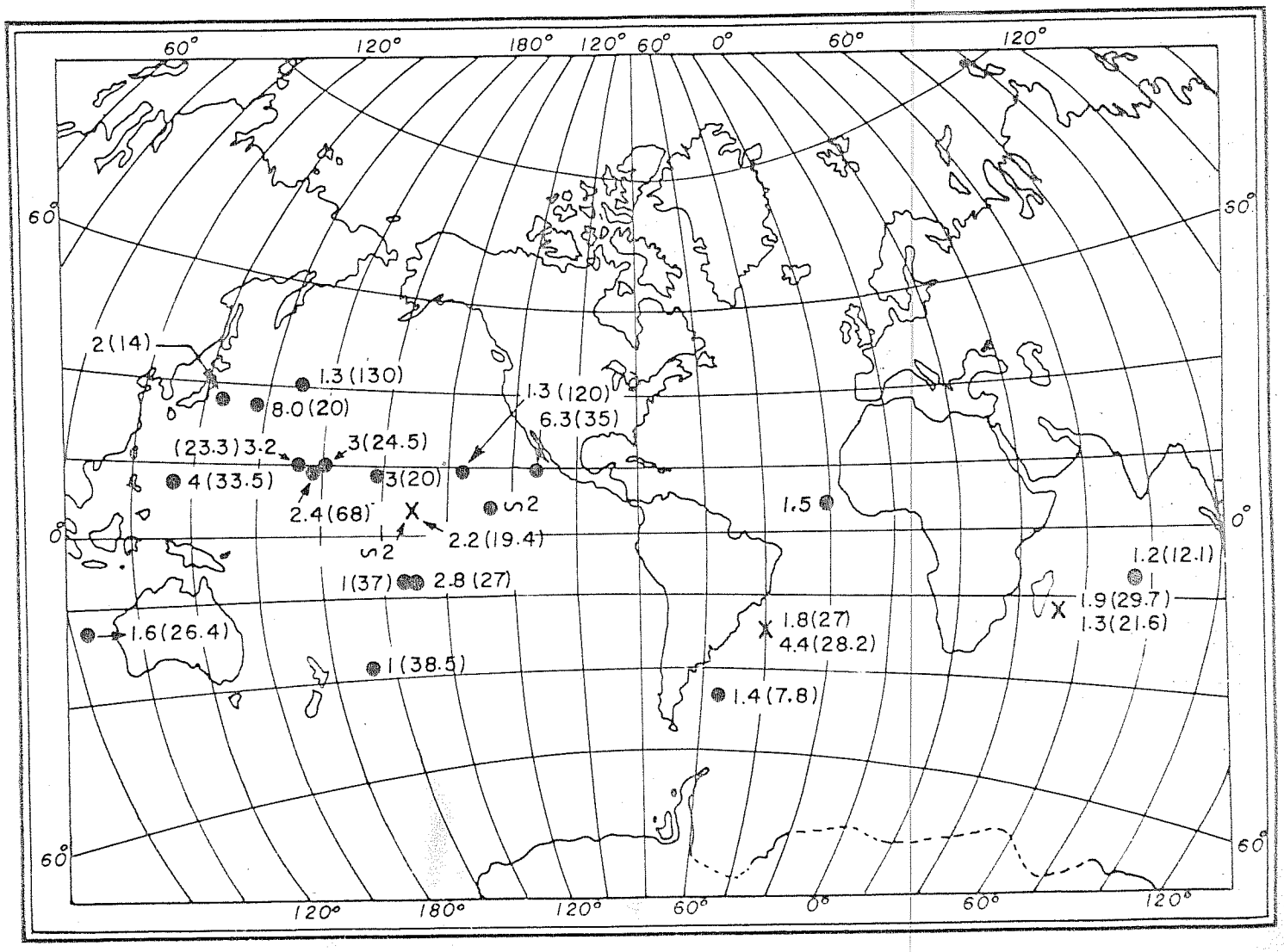
60°
120°
180°
120°
60°
0°
60°
120°
60°
60°
0°
0°
60°
60°
120°
180°
120°
60°
0°
60°
120°
2(14)
1.3(130)
8.0(20)
1.3(120)
6.3(35)
(23.3)3.2
3(24.5)
4(33.5)
3(20)
2.4(68)
2
2.2(19.4)
2
1.5
1.2(12.1)
1(37)
2.8(27)
1.9(29.7)
1.3(21.6)
1.6(26.4)
1.8(27)
4.4(28.2)
1(38.5)
1.4(7.8)

water column viz. 1.08 dpm/cm^2 (a case similar to that for ^{230}Th). Three possible explanations have already been put forward by Bhat et al. (1970); Sharma and Somayajulu (1979) viz. (1) Sporadic growth of nodules, (2) growth and erosion such that the net growth is <20% and (3) that the growing nodule on the ocean floor is effectively scavenging elements from a few hundred meters of the water column above its position.

I have also looked at the variation of all the three ^{10}Be parameters as a function of water depth at the nodule stations. No correlation could be seen which means that the nodule growth as determined by radiometric methods is indpendent of water depth. In such a case the third explanation appears important if one assumes that nodule growth had been continuous, one can calculate the effective thickness of the water column on the assumption that the ^{10}Be standing crop over the nodule is 1.08 dpm/cm^2 that the average oceanic depth of 4000 m and taking into account the ^{10}Be inventory of the nodule. The water column thickness for various nodules so far studied comes out to be 20-900 m for ^{10}Be and 2-800 m for ^{230}Th (Figs. IV.16a and b). In the above calculations it is assumed that the nodules grow continuously. In the case of sporadic growth it would be more, but may never be equal to the entire water column over the nodule.

Fig.IV.16 : Histograms showing the effective thicknesses (in meters) of water column from which nodules scavenge (a) $^{230}Th_{exc}$ and (b) ^{10}Be.

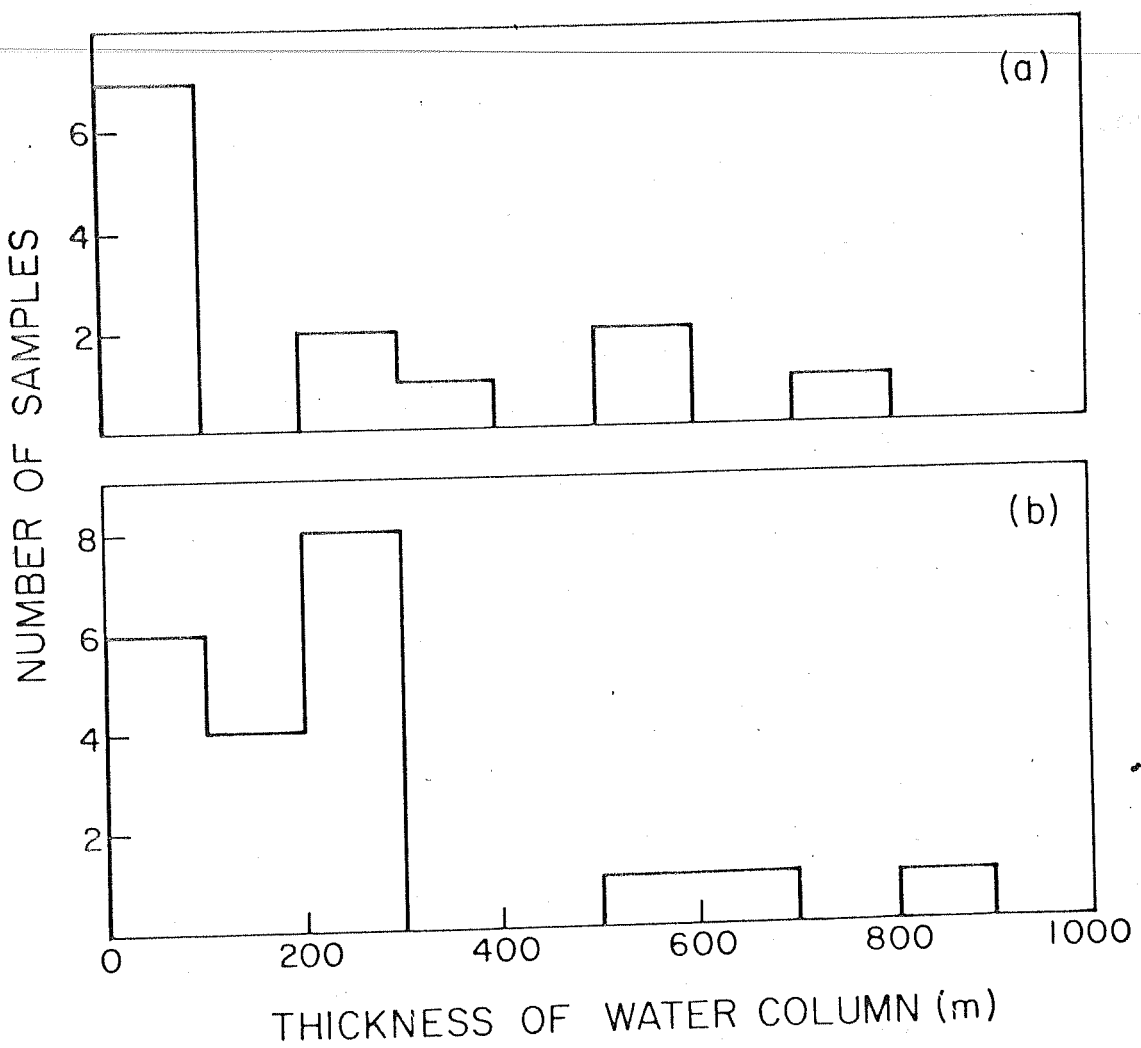
(a)
(b)
NUMBER OF SAMPLES
2
4
6
8
0
200
400
600
800
1000
THICKNESS OF WATER COLUMN (m)

IV.4(c) ^{9}Be in ocean water :

Since the direct ^{10}Be measurements on seawater have now been made (Raisbeck et al., 1979a, 1980; Krishnaswami et al., 1982) one can calculate the oceanic concentrations of ^{9}Be by using the ^{10}Be data and the $^{10}Be/^{9}Be$ ratios of the nodules (extrapolated-to-surface value). Taking $^{10}Be/^{9}Be$ range as (2.5-15) dpm/mg and a mean ^{10}Be concentration of $2x10^{-6}$ dpm/kg seawater (Table I.1), it is estimated that ^{9}Be in seawater is in the range of $(2-8)x10^{-10}$ g/kg - which is in good agreement with the range of ^{9}Be measurements so far made in seawater (Merrill et al., 1960; Measures and Edmond,1981). This means that most of the ^{9}Be in the nodules is authigenic. The assumption made in above calculation is that nodule matrix scavenges ^{10}Be and ^{9}Be in the same ratio as present in the ocean water and hence the above calculated value for ^{9}Be will correspond to the present day ^{9}Be concentration at the nodule location. It has been shown that like Be, Th in the nodules is also authigenic (Krishnaswami and Cochran, 1978; Moore, 1981).

IV.4(d) Mineralogy:

The various manganese mineral phases identified in the bulk samples from different depths of the nodules are given in Table III.9. All the nodules

contain δ-MnO_2 while some of them contain δ-MnO_2 and todorokite (10Å manganite) and some others have δ-MnO_2, birnessite (7Å manganite) and todorokite (10Å manganite). Thus nodules can be classified into three groups on the basis of these three phases as revealed in the X-ray diffractograms (Barnes, 1967). The group labeled δ-MnO_2 contains only δ-MnO_2. The group labeled 10Å manganite contains both 10Å manganite and δ-MnO_2. The group labeled 7Å manganite contains all the three mineral phases.

Out of a total thirteen nodules, ten nodules (ANTP 50D, ARIES 15D, ARIES 12D, ANTP 58D, TF 5, GEOSECS 1D, RC 16 D10, RC 15 D5, RC 14 D4S and R/V VITIAZ) belong to the δ-MnO_2 group while A47-16(4) belongs to 7Å manganite group. The X-ray diffraction patterns of different depth sections in these nodules do not show any significant change in their mineralogy. In the case of the other two nodules ARIES 39D and RC 14 D4F, mineralogy of different depth sections is not the same. The section 0-6.9 cm of ARIES 39D has todorokite, birnessite and δ-MnO_2 while section 12.3-15.9 cm has only δ-MnO_2 as the principal manganese phase. Similarly all the sections from 0 to 45.9 mm of RC 14 D4F have δ-MnO_2 except the section 45.9-54.1 cm which has todorokite, birnessite and δ-MnO_2. The depth variation in mineralogy has been reported by Piper and Williamson (1981) on a 3 cm radius

noddule by X-ray method. Their study showed that birnessite was present in the outer layers and todorokite in the inner layers.

IV.4(e) Chemical Composition :

The measurements of fourteen elements (Mn, Fe, Co, Ni, Cu, Zn, Cr, Pb, Be, Mg, Ca, Sr, Ba and Al) in different sections of the nodules are given in Appendix. These measurements are mainly carried out either in the 10% $NH_2OH.HCl$ or 6M HCl leaches and in a few cases in the residues left after leaching. In those cases where the residues have not been analysed the weight percentage of the elements have been calculated based on the leach data only.

In Fig.IV.17, a number of histograms of percentage of elements in 10% $NH_2OH.HCl$ or 6M HCl leach are given from which the following inferences can be made :

(1) $NH_2OH.HCl$ and 6M HCl are good leachants for most of the elements. The elements Mn, Fe, Co, Ni, Cu, Zn, Pb, Be, Mg, Ca and Sr can be leached more than 90% with these reagents. Hereafter these elements are termed as 'Authigenic elements' in the discussions that follows.

(2) Al and Cr are leached less efficiently with $NH_2OH.HCl$ compared to HCl. Their leaching efficiencies vary from 20 to 100% and from 10 to

Fig.IV.17 : Histograms showing the percentages of elements leached by 10% $NH_2OH.HCl$ and 6M HCl.

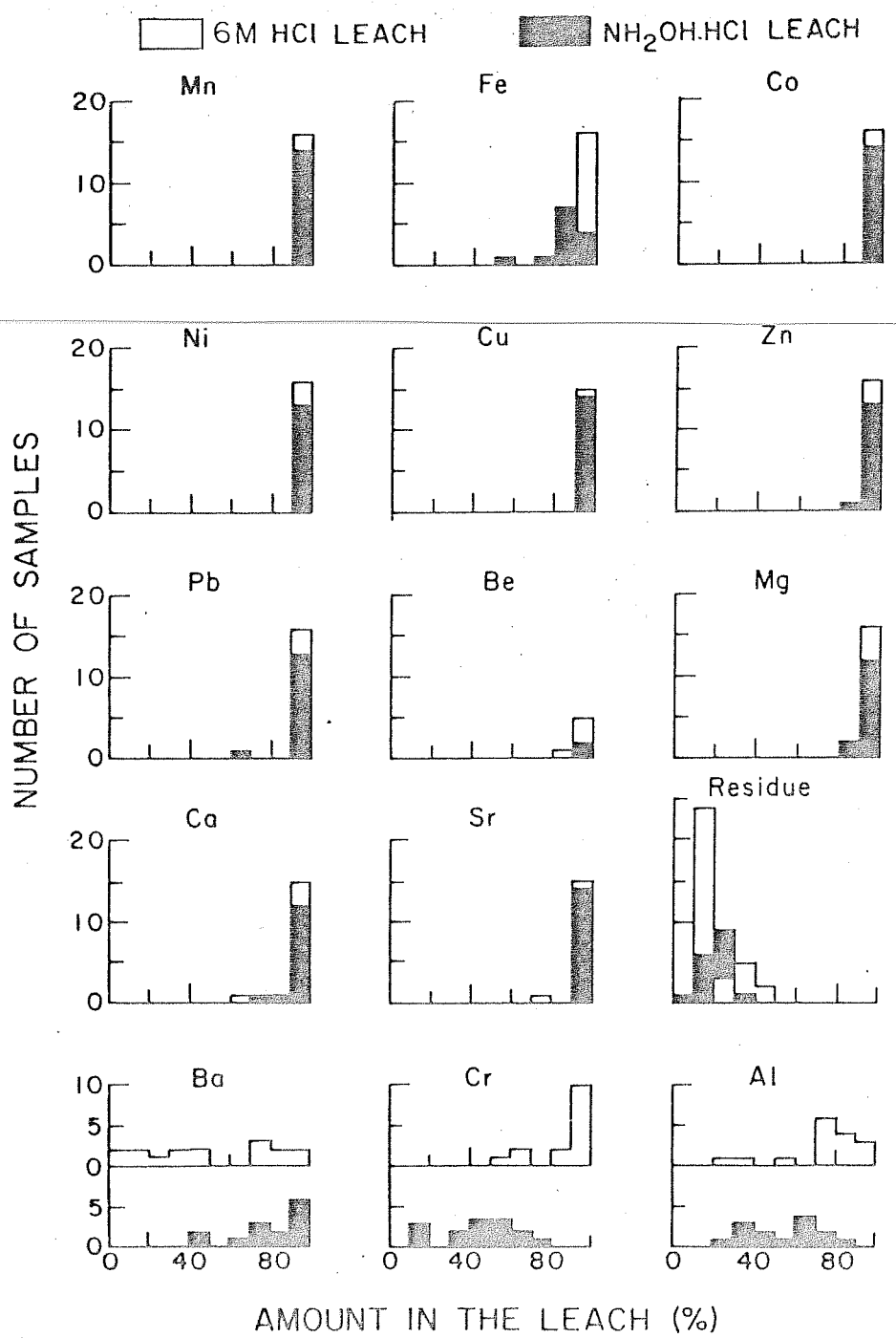
6M HCl LEACH
NH2OH.HCl LEACH
Mn
Fe
Co
Ni
Cu
Zn
Pb
Be
Mg
Ca
Sr
Residue
Ba
Cr
Al
NUMBER OF SAMPLES
AMOUNT IN THE LEACH (%)
0
10
20
5
40
80

100% respectively. This may be because that part of these elements reside in the anthigenic phases and the rest in the deterital phases.

(3) Ba shows a complex behaviour. The $NH_2OH.HCl$ leaching efficiency varied from 40 to 100% while for 6M HCl from 10 to 100%. In manganese nodules some of the Ba is known to be in the form of barite (Church, 1979) which can explain the poor leaching efficiency of the reagents for this element.

(4) The percentage of residues left after leaching with $NH_2OH.HCl$ or 6M HCl vary from negligible to 50%. On the average, $NH_2OH.HCl$ leach yields more residue compared to 6M HCl leach. It is because of the fact that $NH_2OH.HCl$ is a milder leachant of the two.

The above results are in good agreement with the measurements reported earlier (Arrhenius, 1963; Moore et al., 1981).

The range, mean and ratio of maximum to minimum concentrations of the various elements in the analysed nodules are given in Table IV.4. The measured mean concentrations are in good agreement with the average values reported for the world oceans (Cronan, 1976).

Table IV.4 : Concentration ranges and means for the analysed elements in nodules

Element wt(%)	Percentage of element Minimum	Maximum	Geometric mean*	Ratio = $\frac{\text{Maximum}}{\text{Minimum}}$
Mn	10.2	36.2	22.2(16.2)	3.6
Fe	5.0	29.1	16.2(15.6)	5.8
Co	0.14	1.2	0.49(0.30)	8.6
Ni	0.14	1.7	0.40(0.49)	12.1
Cu	0.030	1.6	0.12(0.26)	53.3
Zn	0.040	0.17	0.067(0.071)	4.3
Pb	0.035	0.38	0.13(0.087)	10.9
Be^{+}	2.2	12.1	4.8 (-)	5.5
Mg	0.85	2.55	1.2(3.1)	3.0
Ca	1.1	5.5	2.3(2.5)	5.0
Sr	0.035	0.27	0.13(0.083)	7.7
Residue	~ 0	47.1	-	-
Mn/Fe	0.63	6.7	1.3	10.6

* Numbers in parentheses are the values quoted from Cronan (1976).

\+ Concentration of Be is in ppm

The most striking feature of manganese nodules is perhaps their compositional heterogeneity. All the measured elements show large variations. The maximum to minimum ratios of the various elements vary even upto a factor of 50 (Table IV.4). The variations in nodule compositions have been attributed to the following causes (Cronan and Tooms, 1969; Cronan, 1975; Heath, 1980).

(1) Variations in the sources and rate of supply of the elements in the ocean,

(2) Local variations in the hydrothermal input due to submarine volcanic activity,

(3) Variations in the activity of bacteria capable of fixing manganese (and other metals).

(4) Variations in the mineralogy of manganese and iron oxyhydroxides and their capacity to accommodate other trace metals,

(5) Variations in the interstitial pore water composition,

(6) Variations in the chemistry of seawater.

The interelement - correlation matrix for the nodules is given in Table IV.5. Mn is well correlated with Ni, Cu and Mg while Fe does not show correlation with any of the elements except with Sr for which

Table IV.5 : Inter-element-correlation matrix in the nodules

	Mn	Fe	Co	Ni	Cu	Zn	Pb	Be	Mg	Ca	Sr	Residue	Mn/Fe
Mn	1.0	-0.29	0.21	0.80	0.70	0.38	0.04	0.16	0.84	0.28	0.01	-0.47	0.75
Fe		1.0	0.16	-0.65	-0.58	-0.12	0.08	0.31	-0.43	-0.10	0.47	-0.21	-0.72
Co			1.0	-0.28	-0.43	-0.24	0.70	0.03	-0.19	-0.24	0.44	-0.34	-0.07
Ni				1.0	0.94	0.63	-0.39	-0.34	-0.92	0.09	-0.38	-0.14	0.91
Cu					1.0	0.63	-0.51	-0.23	0.85	0	-0.47	0	0.94
Zn						1.0	-0.28	-0.12	0.69	0.14	0	-0.27	0.16
Pb							1.0	0.08	-0.19	0.27	0.76	-0.55	-0.24
Be								1.0	0.39	0.39	0.38	-0.14	-0.22
Mg									1.0	0.13	-0.22	-0.27	0.88
Ca										1.0	0.40	-0.1	0.06
Sr											1.0	-0.49	-0.51
Residue												1.0	-0.09
Mn/Fe													1.0

For 64 observations

correlation coefficient(r) is 0.47, Ni-Cu, Zn-Ni, Zn-Cu, Mg-Cu, Ni-Mg, Mg-Zn, Sr-Pb and Co-Pb are internally well correlated (r>0.6). Similar correlations have also been found by earlier workers (Mero, 1960; Willis and Ahrens, 1962; Cronan and Tooms, 1967; Cronan, 1969, 1970, 1975). Be does not show any correlation with any of the elements.

The nodule A47-16(4) is from a mining rich area, the 'Clarion Clipperton fracture zone' (Halbach, 1980). It has 1.7% Ni and 1.6% Cu and contains todorokite, birnessite and δ-MnO_2 as the main Mn phases (Appendix, Table III.9). This result is in good agreement with the earlier observations (Chave and Mackenzie, 1961; Barnes, 1967; Cronan and Tooms, 1969; Cronan, 1975; Piper et al., 1979) that the nodules rich in Ni and Cu have todorokite and δ-MnO_2 as the principal manganese phases. This probably results from the ability of Ni^{2+} and Cu^{2+} ions to replace the divalent manganese in todorokite structure $(Ca, Na, Mg, Mn^{+2})2\ Mn_5{}^{+4}\ O_{12}.3H_2O$ as suggested by Burns and Burns (1978).

The elemental abundances and flux contrasts of various elements in the nodule RC 14 D4F is given in Table IV.6. The two sides of this nodule significantly differ in their chemical compositions and have shown

Table IV.6 : Elemental abundance and flux contrasts in RC 14 D4F nodule.

Element	Elemental abundance contrast, top/bottom	Flux contrast*, top/bottom
Mn	0.65	0.24
Fe	1.23	0.45
Co	1.9	0.33
Ni	0.39	0.16
Cu	1.9	0.15
Zn	0.78	0.67
Pb	3.2	1.1
Be	1.1	0.46
Mg	0.75	0.27
Ca	1.7	0.63
Sr	2.1	0.80
Residue	0.47	-
Mn/Fe	0.53	-

* Growth rates used are 1.9 and 5.2 mm/10^6 yrs for the top and bottom respectively.

different surface-extropolated ^{10}Be activities (Section IV.4(a).(i). The side which has shown relatively higher surface-extrapolated value is named as 'top' compared to the other side as 'bottom'. The bottom layer (45.9 - 54.1 mm) is enriched in Mn, Ni, Zn, Mg and depleted in Fe, Co, Cu, Pb, Ca and Sr compared to the top layer (0-5.8 mm). The bottom has 50% more residue compared to the top (Fig.IV.18). The elements Mn, Co, Ni, Cu and Mg were depositing four times faster in the bottom layer compared to the top layer while the fluxes of Fe, Zn, Pb, Be, Ca and Sr are same in both these layers within a factor of two. Moore et al. (1981) have also found a similar behaviour of the elements in the oriented 'Apple' nodule. If it is assumed that the bottom layer was in contact with the sediments, in which case the high abundance of Mn, Ni and Zn in this may be explained as due to their delivery from pore waters present in the underlying sediments (Manheim, 1976).

IV.4(f) <u>Deposition of authigenic elements in the past 10 m.y.</u> :

Once the time scale is well established for each nodule, the element abundance data can be used to unravel the oceanic history of authigenic elements Mn, Fe, Co, Ni, Cu, Zn, Pb, Be, Mg, Ca and Sr on the assumption that these elements are authigenically precipitating from seawater. In order to convert depth interval into time

Fig.IV.18 : Elemental abundance contrasts in the nodule RC 14 D4F on the two sides. Elements falling below the horizontal line show enrichment in the bottom (45.9-54.1 mm) compared to the top (0-5.8 mm).

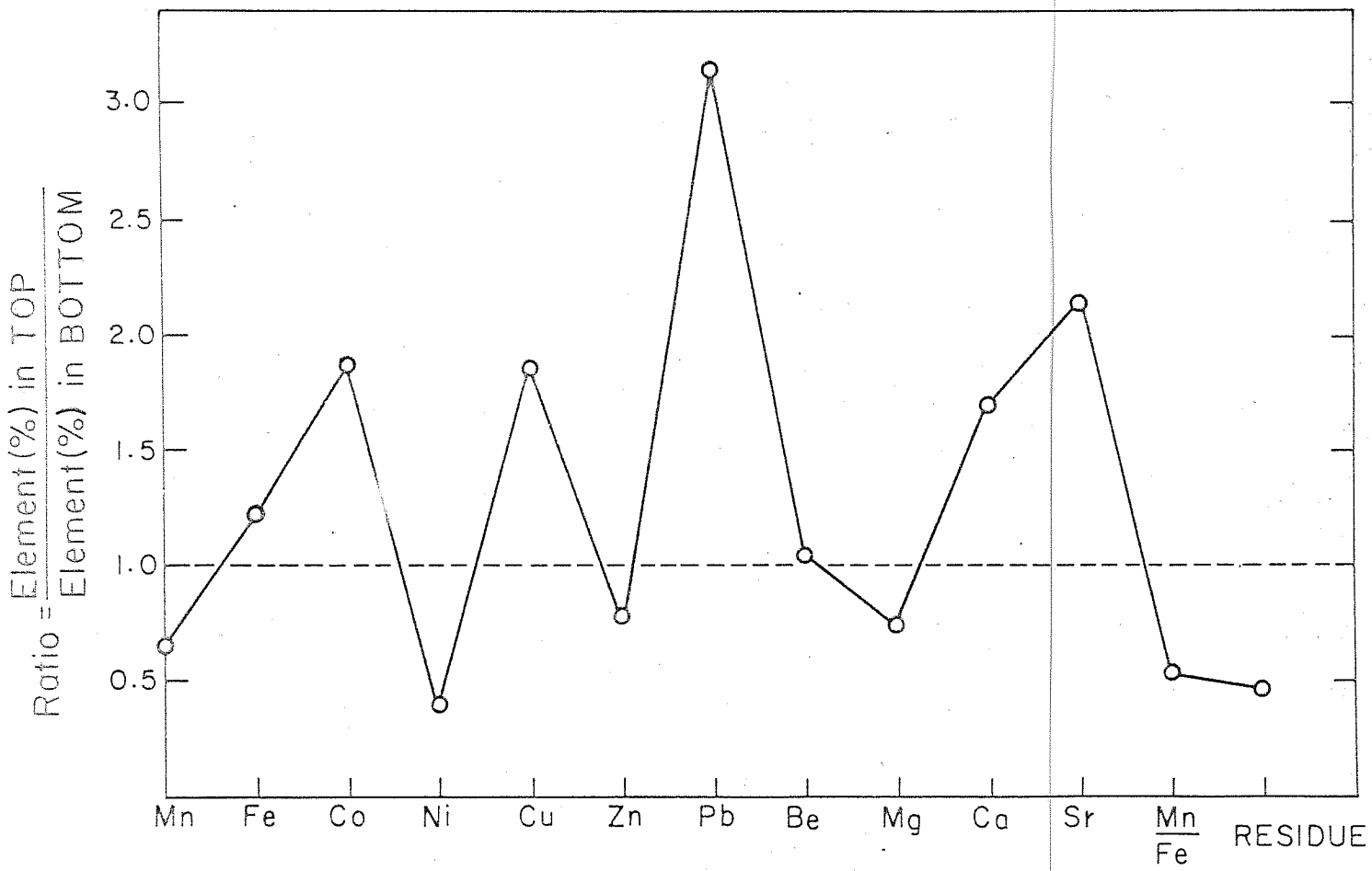
Ratio = Element (%) in TOP / Element (%) in BOTTOM
3.0
2.5
2.0
1.5
1.0
0.5
Mn
Fe
Co
Ni
Cu
Zn
Pb
Be
Mg
Ca
Sr
Mn/Fe
RESIDUE

interval in each nodule I have used 'average' growth rates as obtained by ^{10}Be method (Table IV.3) except for TF 5 for which $^{10}Be/^{9}Be$ growth rate has been used. Only those nodules which do not show any variation in the mineralogy with depth have been used for interpretation.

Based on Mn, Fe, (Co+Ni+Cu)x10 concentrations, trilinear plots for three different time spans viz. present, 4 m.y. B.P. and 8 m.y. B.P. have been made. In all cases the points cluster in the centre of the triangles (Fig.IV.19). According to Bonatti et al. (1972) this central field, is for hydrogenous deposits formed by slow precipitation of the elements from seawater under oxidising environments. Such hydrogenous ferromanganese deposits are also characterised by a Mn/Fe ratio between 0.5 to 5 and relatively higher concentration of trace metals. In the present investigation the Mn/Fe ratio varies between 0.6 to 6.7 with a mean value of 1.3 (Table IV.4). Thus all the analysed nodules appear to have a hydrogenous origin. Since the points in Fig.IV.10 do not shift with time from the central field and mineralogy do not change with depth, it implies that mechanisms/conditions in which these nodules had grown from seawater remained about the same during the entire growth period of the nodules.

Although nodules show a large variation in their chemical composition, an attempt has been made to delineate

Fig.IV.19 : Trilinear plots of the nodules at three different times during their growth period. All nodules during the three periods fall in the central field of hydrogeneous deposits (Bonatti et al., 1972). The areas near the left and right corners have been assigned for hydrothermal and diagenetic deposits respectively.

Present

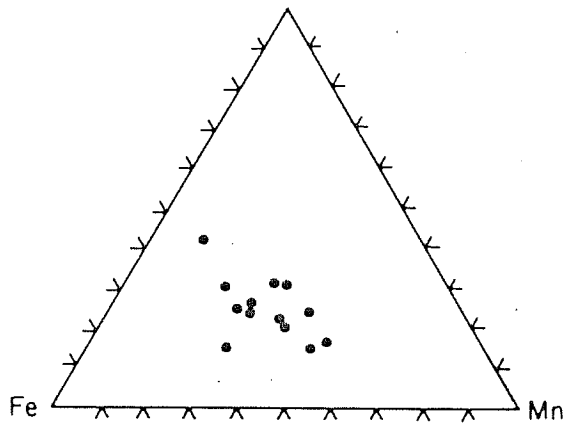

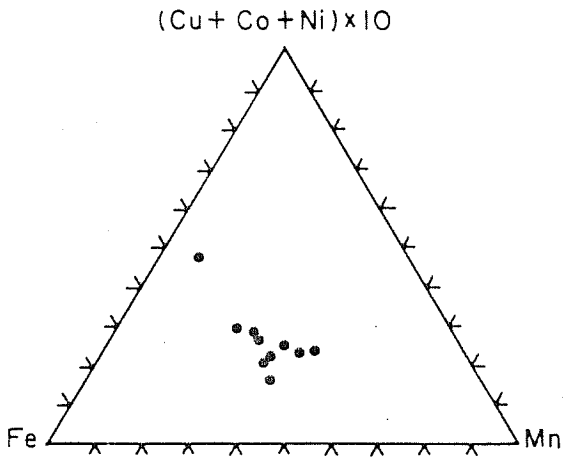

4 m.y. B.P.

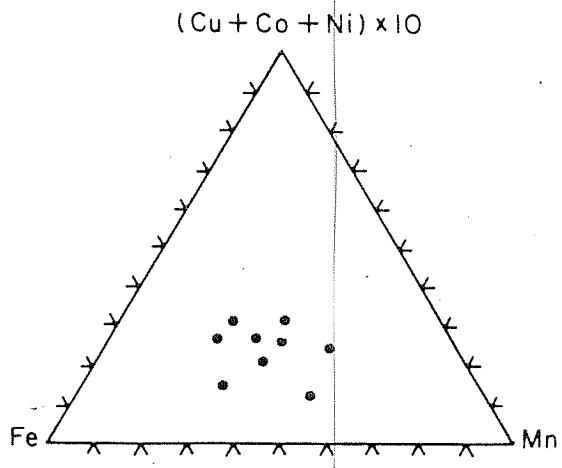

8 m.y. B.P.

the depositional history of authigenic elements Mn, Fe, Co, Ni, Cu, Zn, Pb, Be, Mg, Ca and Sr during the past about 10 m.y. The concentrations of the elements in the deeper sections have been normalized to those of the surface sections (recent deposition) and these ratios have been plotted separately for Pacific ocean and for Atlantic plus Indian oceans (Figs.IV.20 and IV.21). The data on Pacific ocean show a much larger scatter compared to those from Atlantic and Indian oceans.

In the Pacific ocean, during the past 10 m.y. the deposition rate of Mn, Fe, Co, Ni, Zn, Pb, Be, Mg, Ca and Sr has varied upto ± 50%, whereas Cu shows higher depositional rate by as much a factor of 4 compared to the present deposition rate.

During the same period, in the Atlantic and Indian oceans the deposition rate of Mn, Fe, Co, Ni, Pb, Mg, Ca and Sr were low by 20-60% whereas Cu shows a 20% higher deposition rate compared to the present day value. Zn and Be show variations by as much as ±80%.

Ni and Cu deposition rates

In the case of these two elements a more critical evaluation was made. Both Ni and Cu show high correlation (0.8 and 0.7 respectively - Table IV.5) with Mn which is

Fig.IV.20 : Ratio C_t/C_o (elemental concentration C_t of the element in the past normalised with respect to the concentration C_o in top most layer of nodule) as a function of time for Pacific ocean nodules.

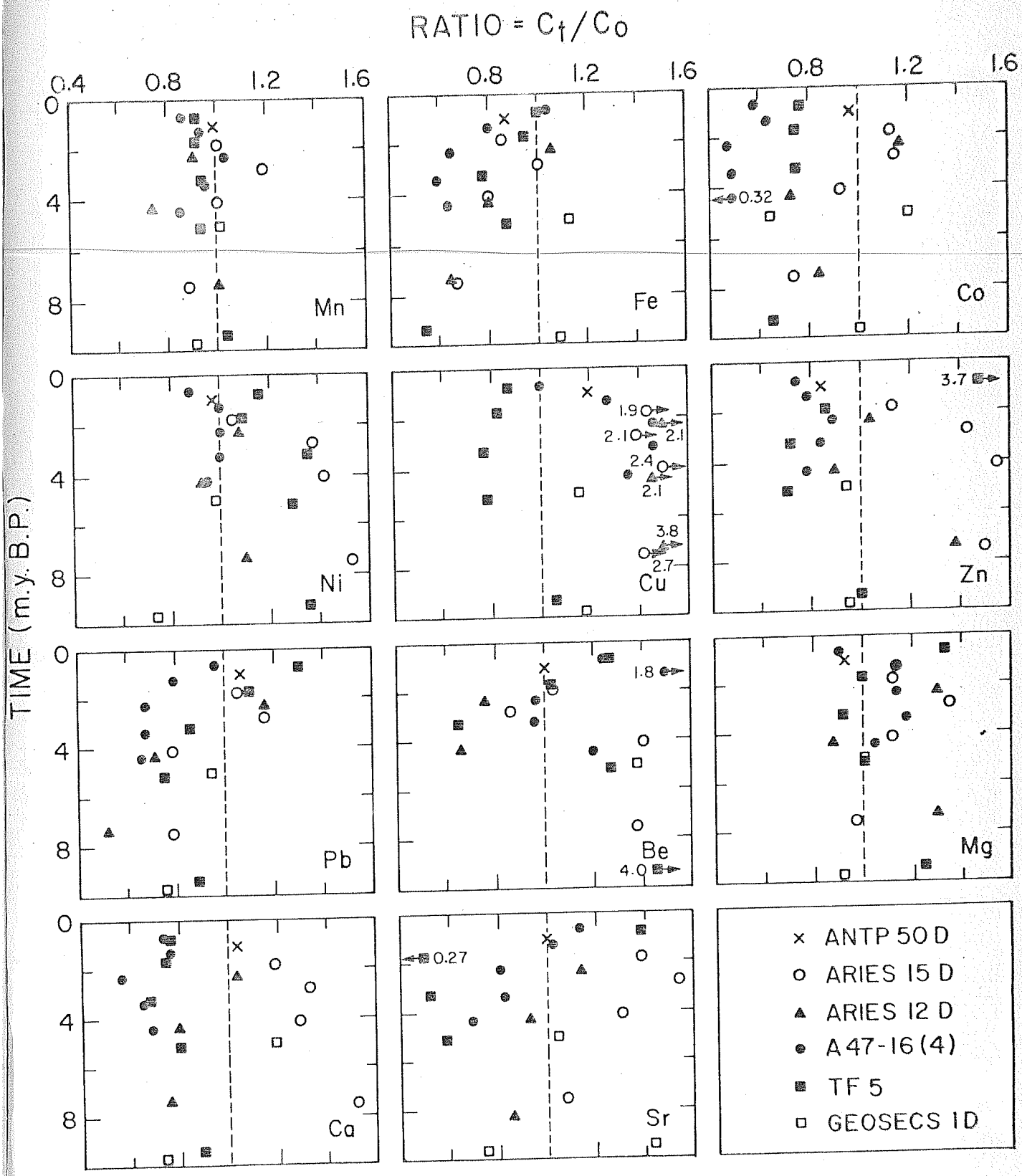
RATIO = Ct/Co
TIME (m.y. B.P.)
0.4
0.8
1.2
1.6
0
4
8
Mn
Fe
Co
Ni
Cu
Zn
Pb
Be
Mg
Ca
Sr
0.32
1.9
2.10
2.1
2.4
2.1
3.8
2.7
3.7
1.8
4.0
0.27
× ANTP 50 D
○ ARIES 15 D
▲ ARIES 12 D
● A47-16(4)
■ TF 5
□ GEOSECS 1D

Fig.IV.21 : Ratio C_t/C_o (elemental concentration C_t of the element in the older section normalised to that of the top most layer C_o of the nodule) as a function of time for Atlantic and Indian ocean nodules.

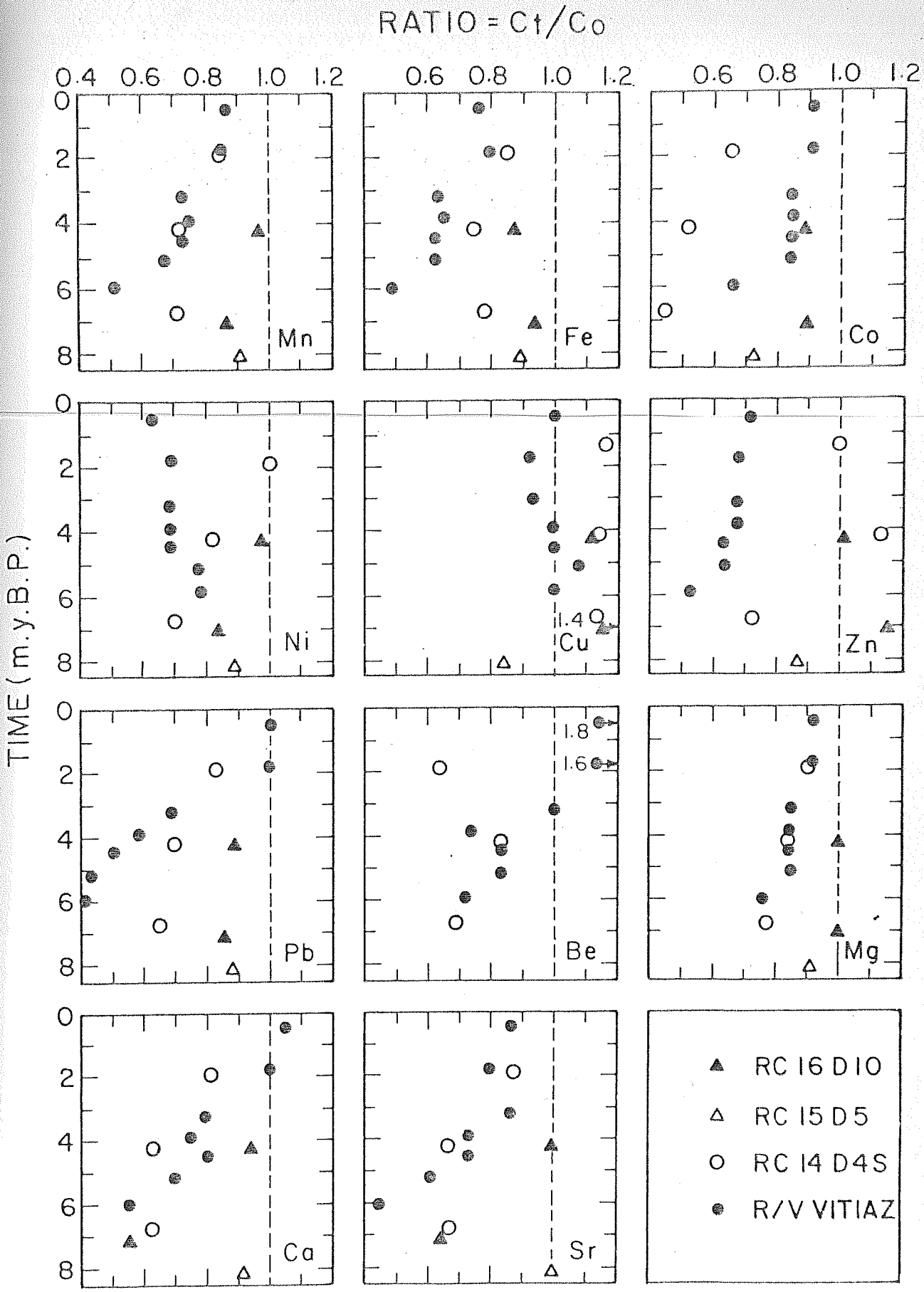
RATIO = Ct/Co
TIME (m.y.B.P.)
0.4 0.6 0.8 1.0 1.2
0.6 0.8 1.0 1.2
0.6 0.8 1.0 1.2
0 2 4 6 8
Mn
Fe
Co
Ni
Cu
1.4
Zn
Pb
1.8
1.6
Be
Mg
Ca
Sr
RC 16 D10
RC 15 D5
RC 14 D4S
R/V VITIAZ

further improved if I take Mn/Fe instead of Mn. The corresponding correlation coefficients for Ni-Mn/Fe and Cu-Mn/Fe are 0.91 and 0.94 respectively. If one plots Ni/(Mn/Fe) and Cu/(Mn/Fe) normalized to the corresponding surface values as a function of time (Figs.22a and b). One can expect a better trend as the Mn and Fe scavenging effects have also been considered. Here again there is large scatter($\pm$150% for all the oceans). The scatter probably reflects the chemical reactivities of the elements. Mn, Fe, Co, Ni, Cu, Zn, Pb and Be have residence times about 10^2-10^4 years (Brewer, 1975) which are either less or comparable to the oceanic mixing times (about 10^4 yrs). Hence these elements do not get homogenized in seawater with respect to any small perturbation in their supply. On the other hand the residence times of Mg, Sr and Ca (about 10^6 - 10^7 yrs) is more than oceanic mixing time. Even these elements show a scatter which is probably due to their involvement in biocycles.

If one accepts the theory that nodules scavenge their authigenic material from <1000 m of their overhead water column (as in the case of ^{10}Be and ^{230}Th) the observed variations in the C_t/C_o and R_t/R_o rates can be attributed to the bottom waters. It is likely that there

Fig.IV.22 : Ratio R_t/R_o as a function of time (a) for Ni and (b) for Cu for all the analysed nodules. R_t and R_o are the concentrations of Ni and Cu corrected with Mn/Fe ratio at times t and o .

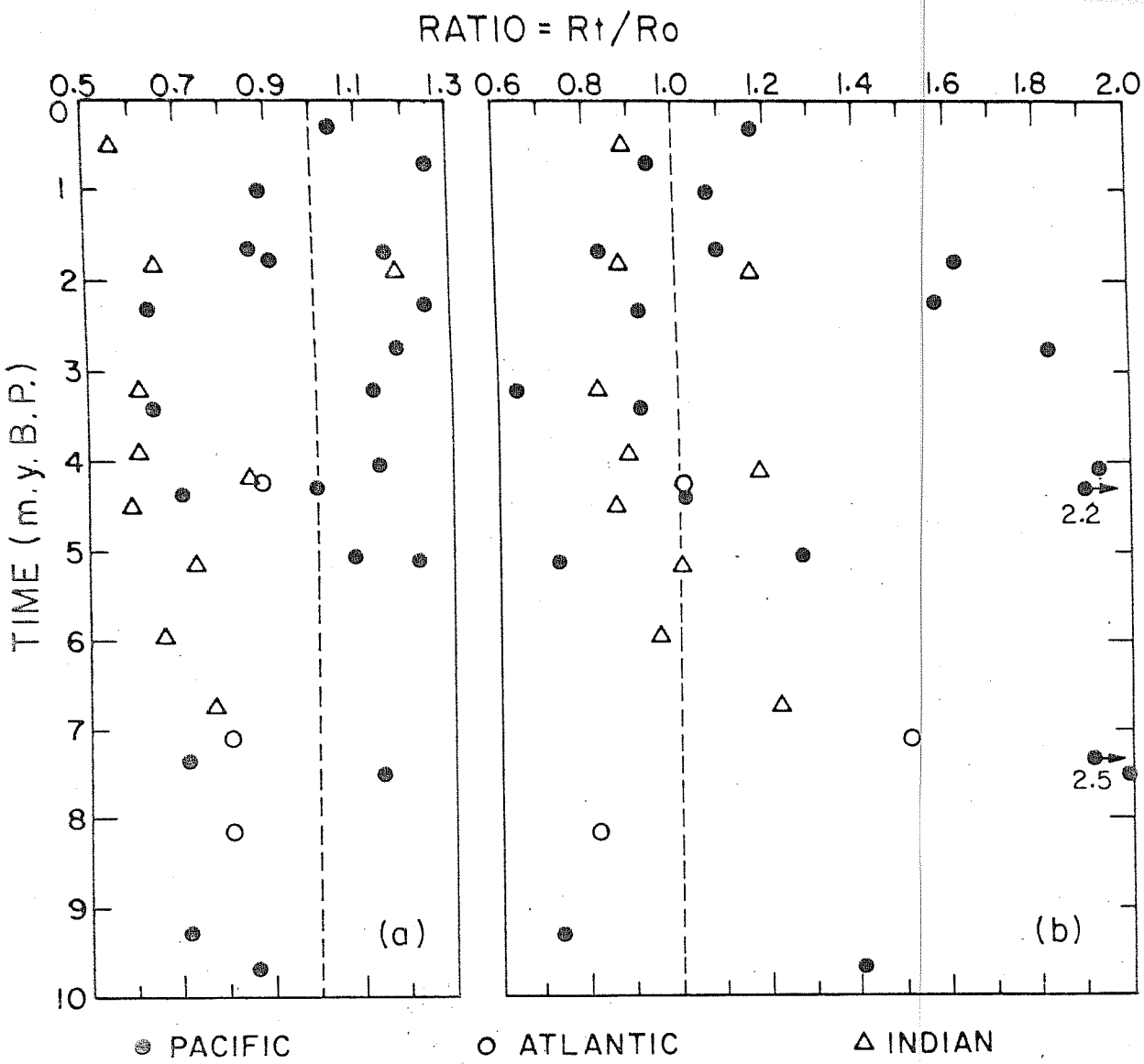
RATIO = Rt/Ro
0.5
0.7
0.9
1.1
1.3
0.6
0.8
1.0
1.2
1.4
1.6
1.8
2.0
TIME (m.y.B.P.)
0
1
2
3
4
5
6
7
8
9
10
2.2
2.5
(a)
(b)
PACIFIC
ATLANTIC
INDIAN

is a substantial change with time in the concentration of the analysed elements in the bottom waters. It thus appears that regional and local factors are much more important in controlling the chemical composition of the nodules.

CHAPTER - V

CONCLUSIONS

The primary aim of this thesis has been to obtain information on meltwater input, CR intensity variations, growth rates of oceanic ferromanganese nodules using cosmogenic ^{10}Be and on the paleochemistry of ocean water using ^{10}Be and measurements of major and trace elements in the nodules. The following are the important conclusions drawn in this regard:

1. In properly chosen sediments the ^{10}Be excess due to meltwater input during interglacials is measurable as evidenced by the study on INMD Box core.

2. CR intensity variations have occurred during the past 2 m.y. These have been upto $\pm 30\%$ in the past 1 m.y. based on precise ^{10}Be measurements reported here. Based on the combined data of mine and that of Tanaka's group the variations had been as much as $\pm 50\%$ over the mean during the past 2 m.y. The important periodicities of these variations are deduced to be 500, 300 and 200 k.y.

3. The most suitable radionuclide for dating small as well as large nodules from the world oceans is ^{10}Be. These nodules have growth rates of 1-4 mm/10^6 yrs. The comparison of the long term (millions of

years) average growth rates based on Be isotope data with the recent (<400,000 yrs) rates deduced from U-Th series nuclides show that these rates are concordant in most cases.

4. There appears to be no global trends in the depositional pattern of elements in manganese nodules. Whereas the Pacific ocean nodules show a large compositional diversity with time, those from Atlantic and Indian oceans, though limited in number, indicate that on the average the deposition of most of the elements have been less in the past about 10 m.y. compared to the present day deposition.

REFERENCES

Agrawal, D.P., Kusumgar, S. and Lal, D., 1965. The measurement of radiocarbon activity and some determination of ages of archaeological samples. Curr. Sci., 34, 394-397.

Amin, B.S., 1970. Dating of ocean sediments by radioactive methods. M.Sc. Thesis, Bombay University, Bombay, pp 100.

_____, Kharkar, D.P. and Lal, D., 1966. Cosmogenic ^{10}Be and ^{26}Al in marine sediments. Deep Sea Res., 13, 805-824.

_____, Biswas, S., Lal, D. and Somayajulu, B.L.K., 1972a. Radiochemical measurements of ^{10}Be and ^{7}Be formation cross sections in oxygen by 135 and 550 MeV protons. Nuclear Phy., A195, 311-320.

_____, Likhite, S.D., Radhakrishnamurty, C. and Somayajulu, B.L.K., 1972b. Susceptibility stratigraphy and paleomagnetism of some deep Pacific cores. Deep Sea Res., 19, 249-252.

_____, Lal, D. and Somayajulu, B.L.K., 1975. Chronology of marine sediments using ^{10}Be method: Intercomparison with other methods. Geochim.Cosmochim. Acta, 39, 1187-1192.

Anderson, M.E. and McDougall, J.D., 1977. Accumulation rates of manganese nodules and sediments : An alpha track method. Geophys. Res. Lett., 4, 351-353.

Arnold, J.R., 1956. Beryllium-10 produced by cosmic rays. Science, 124, 584.

_____, Honda, M., and Lal, D., 1961. Record of cosmic ray intensity in meteorites. J. Geophys. Res., 66, 3519-3531.

Arrhenius, G., 1963. Pelagic sediments. In The Sea (Editor M.N. Hill) Wiley Interscience Publishers, New York, 3, 658-627.

_____, 1967. Deep sea sedimentation : A critical review of U.S. work. Trans. Am. Geophys. Union, 48, 604-631.

_____, Kjellburg, G. and Libby, W.F., 1951. Age determination of Pacific Chalk Ooze by radiocarbon and titanium content. Tellus, 31, 222.

Aumento, F., 1969. The Mid-Atlantic ridge near 45°N; Fission-Track and ferromanganese chronology. Can. J. Earth Sci. , 6, 1431-1440.

Bada, J.L., 1972. The dating of fossil bones using recemization of isoleucine. Earth Planet. Sci. Lett., 15, 223-231.

_____, Luyendyk, B.P. and Maynard, J.B., 1970. Marine sediments : Dating by the recemization of amino-acids. Science, 170, 730.

Barnes, S.S., 1967. The formation of oceanic manganese nodules. Ph.D. Thesis, University of California, San Diego.

_____, and Dymond, J.R., 1967. Rates of accumulation of ferromanganese nodules. Nature, 213, 1218-1219.

Berger, W.H. and Heath, G.R., 1968. Vertical mixing in pelagic sediments. J. Mar. Res., 26, 134-143.

_____, and Gardner, J.V., 1975. On the determination of Pleistocene temperature from planktonic foraminifera J. Foram. Res., 5, 102-113.

_____, Johnson, R.F. and Killingley, J.S., 1977. Unmixing of the deep-sea record and the glacial meltwater spike. Nature, 269, 661-663.

Bevington,P.R., 1969. (Editor) Data reduction and error analysis for the physical sciences. McGraw-Hill Book Company, New York, pp.187.

Bhandari, N., 1969. A selective and versatile low-level β, X and γ ray detector assembly, Nucl. Instrum. Methods, 67, 251-256.

Bhat, S.G., Krishnaswami, S., Lal, D., Rama and Moore, W.S., 1969. $^{234}Th/^{238}U$ ratios in the ocean. Earth Planet. Sci. Lett., 5, 483-491.

_____, Krishnaswami, S., Lal, D., Rama and Somayajulu, B.L.K., 1970. Radiometric and trace elemental studies of ferromanganese nodules. In Proc. Symp. Hydrogeochem. Biogeochem. Tokyo. The Clarke & Co., Washington,D.C., 1, 443-462, 1973.

_____, Krishnaswami, S. and Rama, 1974. Radon concentration of air over the eastern Arabian sea. Proc. Ind. Acad. Sci., 80, 109-116.

Black, D.I., 1967. Cosmic ray effects and faunal extinctions at geomagnetic field reversals. Earth Planet. Sci. Lett., 3, 225-236.

Bonatti, E., and Nayudu, Y.R., 1965. Origin of manganese nodules on the ocean floor. Am. Jour. Sci., 263, 17-39.

Bonatti, E., Kraemer, T. and Rydell, H., 1972. Classification and genesis of submarine iron manganese deposits. In Ferromanganese deposits on the ocean floor. (Editor D.R.Horn) N.S.F. Washington D.C., 149-166.

Brewer, P.G., 1975. Minor elements in seawater, In Chemical Oceanography (Eds.J.P.Riley and G.Skirrow). Academic Press, London, 1, 415-496.

Broecker, W.S., 1965. An application of natural radon problems in ocean circulation. In Proc. Symposium on diffusion in oceans and fresh waters (Editor T.Ichiye) Lamont Doherty Geological Observatory, Palisades, New York, 116-145.

Brown, L., Sacks., I.S., Tera, F., Klein,J. and Middleton, R., 1981. Beryllium-10 in continental sediments. Earth Planet. Sci. Lett., 55, 370-376.

Burg, J.P., 1967. Maximum entropy spectral analysis. Paper presented at 37th Meeting, Soc. of Explor, Geophys., Oklahoma, City Okla.

_____, 1968. A new analysis technique for time series data. Paper presented at the advanced study institute on signal processing with emphasis on underwater Acoustics, NATO, Enschede, Netherlands.

Burns, V.M., and Burns, R.G., 1978. Post-depositional metal enrichment processes inside manganese nodules from the north equatorial Pacific. Earth Planet. Sci. Lett., 39,341-348.

Burns, R.G. and Burns, V.M., 1977. Mineralogy. In Marine manganese deposits (Editor G.P. Glasby) Elsevier Scientific Publishing Company, Amsterdam, 185-248.

Burton, J.D., 1975. Radioactive nuclides in the marine environment. In Chemical Oceanography (Editors J.P. Riley and G.Skirrow) Academic Press, London and New York, 3, pp.92-191.

Chave, K.E., and Mackenzie F.T., 1961. A statistical technique applied to the geochemistry of pelagic muds. J. Geol., 69, 572-582.

Church, T.M., 1979. Marine barite. In Marine minerals (Editors R.G.Burns) Short Course Notes, Mineralogical Society of America, Washington D.C., 6, 175-207.

Cochran, J.K., 1979. The geochemistry of ^{226}Ra and ^{228}Ra in marine deposits Ph.D. Thesis, Yale University, Connecticut, pp.260.

Crecelius, E.A., Carpenter, R. and Merrill, R.T., 1971. Magnetism and Magnetic reversals in ferromanganese nodules. Earth Planet. Sci. Lett., 17, 391-396.

Cronan, D.S., 1969/1970. Interelement association in some pelagic deposits. Chem. Geol., 5, 99-106.

_____, 1975. Manganese nodules and other ferromanganese oxide deposits from the Atlantic Ocean. J. Geophy. Res., 80, 3831-3837.

_____, 1976. Manganese nodules and ferromanganese oxide deposits. In Chemical Oceanography (Editors J.P.Riley and Chester, R.) Academic Press, London, 5, 217-263.

_____, and Tooms, J.S., 1969. The geochemistry of manganese nodules and associated pelagic deposits from the Pacific and Indian oceans. Deep Sea Res., 16, 335-359.

Dymond, J.R., 1966. Potassium argon geochronology of deep-sea sediments. Science, 152, 1239.

Ehrlich, H.L., 1972. The role of microbes in manganese nodule genesis and degradation. In Ferromanganese deposits on the ocean floor (Editor D.R. Horn) National Science Foundation, Washington,D.C., 63-69.

Fairhall, A.W., 1960. The radiochemistry of beryllium. National Academy of Sciences, National Research Council, NAS-NS 3013, Washington D.C., pp.58.

Finkel, R., Krishnaswami, S. and Clark, D.L., 1977. ^{10}Be in Arctic Ocean sediments. Earth Planet. Sci. Lett., 35, 199-204.

_____, Berger, W.H. and Chung, Y.C., 1981. Manganese distributions in eastern equatorial Pacific sediments - evidence for an historical effect. AGU Abstract, EOS, 62, #45, 899.

Flanagan, F.G., 1973. 1972 values for international geochemical reference samples. Geochim. Cosmochim. Acta., 37, 1189-1200.

Flint, R.F., 1971. Glacial and Quaternary Geology, John Wiley and Sons, New York, pp.81-84.

Forman, M.A., and Schaeffer, O.A., 1979. Cosmic ray intensity over long time scales, Preprint, Max Plank Institut fur Kernphysik, Heidelberg, MPIH-1979-V20.

Glasby, G.P., 1977. (Editor) Marine manganese deposits. Elsevier Publishing Co., New York.

Goel, P.S., Kharkar, D.P., Lal, D., Narasappaya, N., Peters, B. and Yatirajam, V., 1957. Beryllium-10 concentration in deep-sea sediments. Deep Sea Res., 4, 202-210.

Goldberg, E.D., and Arrhenius, G.O.S., 1958. Chemistry of Pacific pelagic sediments. Geochim. Cosmochim. Acta., 13, 153-212.

_____, and Koide, M., 1962. Geochronological studies of deep sea sediments by the ionium/thorium method. Geochim. Cosmochim. Acta, 26, 417-450.

_____, and Bruland, K., 1974. Radioactive Geochronologies. In The Sea (Editor E.D.Goldberg) Wiley Interscience, New York, 5, 451-489.

Gooch, F.A. and Havens, F.S., 1896. A method of separation of aluminium and iron. Am. J. Sci. 4, 416.

Gove, H.E., 1978. (Editor) Proceedings of the first conference on radiocarbon dating with accelerators. University of Rochester, Rochestor.

Graham, J.W., 1959. Metabolically induced precipitation of trace elements from seawater. Science, 129, 1428-1429.

Graham, J.W., and Cooper, S.C., 1959. Biological origin of manganese-rich deposits on the sea floor. Nature, 183, 1050-1051.

Greenslate, J., 1974. Microorganisms participate in the construction of manganese nodules. Nature, 249, 181-183.

Guichard, F., 1980. De l' utilisation du ^{10}Be a des fins de datation dans des materiaux marins. Ph.D.Thesis. University of Paris, pp.246.

_____, Reyss, J.L. and Yokoyama, Y., 1978. Growth rates of manganese nodules measured with ^{10}Be and ^{26}Al. Nature 272, 155-156

Guinasso, N.L., and Schink, D.R., 1975. Quantitative estimates of biological mixing rates in abyssal sediments, 80, 3032-3043.

Halbach, P., 1980. The metallic minerals of the Pacific sea floor. Geojournal, 45, 407-422.

Harrison, C.G.A., and Funnell, B.M., 1964. Relationship of paleomagnetic reversals and micropaleontology in two late caenozoic cores from the Pacific Ocean, Nature, 204, 566.

Heath, G.R., 1980. Manganese nodules and mineral deposits. In Marine Sciences and Ocean Policy Symposium (Editor D.S.Simonett) University of California, Santa Barbara, 129-142.

Higdon, J.C., and Lingenfelter, R.E., 1973. Sea sediments, cosmic rays, and pulsars. Nature, 246, 403-405.

Hillas, A.M., 1975. Some recent developments in cosmic rays. Phy. Lett., 20, 59-136.

Inoue, T., and Tanaka, S., 1976. ^{10}Be in marine sediments. Earth Planet. Sci. Lett., 29, 155-160.

_____, and Tanaka, S., 1979. Beryllium-10 in marine sediments, Earth's environment, and cosmic rays. Nature, 277, 209-210.

Johnsen, S.J., Dansgaard, W., Clausen, H.B. and Langway, C.C., 1972. Oxygen isotope profiles through the Antarctic and Greenland ice sheets. Nature, 235, 429-434.

Kawai, N., Yaskawa, K., Nakajima, T., Torii, M. and Natsuhara, N., 1975. Voice of geomagnetism from lake Biwa. In Paleolimnology and the Japanese Pleistocene (Editor S.Horie), 3, 143-158.

Kharkar, D.P., Lal, D. and Somayajulu, B.L.K., 1963. Investigations in marine environments using radio-isotopes produced by cosmic rays. Proc. IAEA Symp. on Radioactive Dating, Vienna, 175-187.

_____, Turekian, K.K. and Scott, M.R., 1969. Comparison of sedimentation rates by ^{32}Si and uranium decay series determinations in some silicous Antarctic cores. Earth Planet. Sci. Lett., 6, 61-68.

Krishnamurthy, R.V., Lal, D., Somayajulu, B.L.K. and Berger, W.H., 1979. Radiometric studies of box cores from Ontong-Java Plateau. Proc. Indian Acad. Sci., 88A, 273-283.

Krishnaswami, S., Lal, D., Martin, J.M. and Meybeck, M., 1971. Geochronology of lake sediments. Earth Planet. Sci. Lett., 11. 407-414.

_____, and Lal, D., 1972a. Manganese nodules and budget of trace solubles in the ocean. In Proc. The changing chemistry of oceans, Noble Symp. 20 (Eds. D. Dyrssen and D.Jagner), Almqvist and Wiksell, Stockholm, 307-320.

_____, Somayajulu, B.L.K. and Moore, W.S., 1972b. Dating of manganese nodules using beryllium-10 In Ferromanganese deposits on the ocean floor (Ed.D.R. Horn) National Science Foundation, Washington,D.C.,117-122.

Krishnaswami, S., and Sarin, M.M., 1976. Procedure for the simultaneous determination of Th, Pu, Ra isotopes, ^{210}Pb, ^{55}Fe, ^{32}Si and ^{14}C in marine suspended phases. Anal. Chim. Acta., 83, 143-156.

_____, and Cochran, J.K., 1978. Uranium and Thorium series nuclides in oriented ferromanganese nodules : growth rates, turnover times and nuclide behaviour. Earth Planet. Lett., 40, 45-62.

_____, Cochran, J.K., Turekian, K.K. and Sarin, M.M., 1969. Time scales of deep-sea ferromanganese nodule growth based on ^{10}Be and alpha track distributions and their relation to uranium decay series measurements. In La genese des nodules manganese (Editor C. Lalou) Colloq. Int. C.N.R.S., 289, pp.251-260.

_____, and Lal, D., 1980. Deep sea sedimentation: Processes and chronology. In ACS Symposium on Nuclear and Chemical Dating Techniques. (in press).

_____, Mangini, A., Thomas, J.H., Sharma, P., Cochran, J.K., Turekian, K.K. and Parker, P.D., 1982. ^{10}Be and Th isotopes in manganese nodules and adjacent sediments : nodule growth histories and nuclide behaviour. Earth Planet. Sci. Lett., (in press).

Kobayashi, K., Kitazawa, K., Kanaya, T. and Sakai, T., 1971. Magnetic and micropaleontological study of deep-sea sediments from the west-central equatorial Pacific. Deep Sea Res., 18, 1045-1062.

Koide, M., Soutar, A. and Goldberg, E.D., 1972. Marine geochronology with ^{210}Pb. Earth Planet. Sci. Lett., 14, 442-446.

_____, Bruland, K.W. and Goldberg, E.D., 1973. Th-228/Th-232 and Pb-210 geochronologies in marine and lake sediments. Geochim. Cosmochim.Acta.,34, 3-24.

_____, Bruland, K. and Goldberg, E.D., 1976. Ra-226 chronology of a coastal marine sediment. Earth Planet. Sci. Lett., 31, 31-36.

Ku, T.L., 1976. The uranium-series methods of age determination. Ann. Rev. Earth. Planet. Sci., 4, 347-379.

_____, 1977. Rates of accretion, In Marine manganese deposits (Ed. Glasby, G.P.) Elsevier Publishing Co., N.Y., 249-267.

_____, and Broecker, W.S., 1967. Uranium, thorium and protactinium in a manganese nodule. Earth Planet. Sci. Lett., 2, 317-320.

Ku, T.L., and Broecker, W.S., 1969. Radiochemical studies of manganese nodules of deep sea origin. Deep Sea Res., 16, 625-637.

_____, Omura, A. and Chen, P.S., 1979. ^{10}Be and uranium series isotopes in manganese nodules from the central north Pacific. In Marine Geology and Oceanography of the Pacific manganese nodule province (Editors Bischoff, J.L. and Piper, D.Z.) Plenum Press., N.Y., pp.791-814.

_____, Kusakabe, M., Huh, C.A., Nelson, D.E., Southon, J., Novikov, I. and Vogel, J., 1981. Has the ^{10}Be flux changed? EOS, 62, O2-2-A-12 (Abstract)

Lal, D., 1963. On the investigations of geophysical processes using cosmic ray produced radioactivity. In Earth Science and Meteoritics (Editors J.Geiss and E.D. Goldberg). North Holland Publ. Co., Amsterdam, 115-142.

_____, and Schink, D.R., 1960. Low background thin wall flow counters for measuring beta activities of solids. Rev. Sci. Instrum., 31, 305-308.

Lal, D., and Peters, B., 1967. Cosmic ray produced radioactivity on the earth. Handbuch der Physik (Ed. by S. Flugge), Springer-Verlag, Berlin, 46, 551-612.

Lalou, C., and Brichet, E., 1972. Signification des measures radiochimiques dane l' evaluation de la vitesse de croissance des nodules de manganese. C. R. Acad. Sci. Paris, 275D, 815-818.

_____, Brichet, E. and Ranque, M.D., 1973. Certains nodules de manganese trouves en surface des sediments sontils des formation contemporaries de la sedimentation? C. R. Acad. Sci. Paris, 276D, 1661-1664.

_____, Brichet, E. and Bonte, P., 1976. Some new data on the genesis of manganese nodules. In Geology and Geochemistry of Manganese, Publishing House of the Hungarian Academy of Sciences, Budapest, 3, 31-90.

Lanford, W.A., Parker, P.D., Bauer, K., Turekian K.K., Cochran, J.K. and Krishnaswami, S., 1980. Measurement of ^{10}Be distributions using a Tandem Van De Graaff Accelerator. Nucl. Inst. Methods, 168, 505-510.

Lederer, C.M., Hollander, J.M. and Perlman, I., 1967. Table of Isotopes. John Wiley and Sons, Inc., New York, pp594.

Lingenfelter, R.E., 1979. Cosmic ray propagation. 16th Int. Cosmic Ray Conf., Kyoto, Japan, 14, 135-145.

Lynn, D.C., and Bonatti, E., 1965. Mobility of manganese in diagenesis of deep sea sediments. Mar. Geol., 3, 457-474.

Manheim, F.T., 1976. Interstitial waters of marine sediments. In Chemical Oceanography (Eds. J.P. Riley and R.Chester), 6, 115-186.

Martin, J.M., and Meybeck, M., 1979. Elemental mass-balance of material carried by world rivers. Mar. Chem., 7, 173-206.

Mast, T.S., and Mullar, R.A., 1979. Radioisotope detection and dating with accelerators. LBL-10072, (Preprint).

McCorkell, R.H., Fireman, E.L. and Langway, C.C. Jr., 1967. Aluminium-26 and Beryllium-10 in Greenland Ice. Science, 158, 1690.

Measures, C.I., and Edmond, J.M., 1981. Beryllium in the water column of the central north Pacific at MANOP site R. (Preprint).

Mero, J.L., 1960. Mineral resources on the ocean floor. Mining Congr., 46, 48-53.

_____, 1965. The mineral resources of the sea. Elsevier, Amsterdam, pp.312.

Merrill, J.R., Lyden, E.F.X., Honda, M. and Arnold, J.R., 1960. The sedimentary geochemistry of beryllium isotopes. Geochim. Cosmochim. Acta., 18, 108-129.

Moore, W.S., 1981. The thorium isotope content of ocean water. Earth Planet. Sci. Lett., 53, 419-426.

_____, and Somayajulu, B.L.K., 1974. Age determination of fossil corals using $^{230}Th/^{234}Th$ and $^{230}Th/^{227}Th$. J. Geophys. Res., 79, 5065-5068.

_____, Ku, T.L., Macdougall, J.D., Burns, V.M., Burns, R., Dymond, J., Lyle, M.W. and Piper, D.Z., 1981. Fluxes of metals to a nodule : radiochemical, chemical, structural and mineralogical studies. Earth Planet. Sci. Lett., 52, 151-171.

Mullar, R.A., 1977. Radioactive dating with a cyclotron. Science, 196, 489-494.

Murray, J., and Renard, A.F., 1891. Deep sea deposits, Rep. Sci. Results Explor. Voyage Challenger, pp.525.

Murty, C.S.R., 1981. A programming system on maximum entropy spectral analysis. PRL Technical Note TN-81-01.

Nozaki, Y., Cochran, J.K. and Turekian, K.K., 1977. Radiocarbon and ^{210}Pb distribution in submersible-taken deep-sea cores from project famous. Earth Planet. Sci. Lett., 34, 167-173.

Nelson, D.E., Suthon, J., Novikov, I., Korteling, R., Kusobe, M. and Ku, T.L., 1980. ^{10}Be measurements on a manganese crust. AGU Fall Meeting 46, Abstract 0203.

Opdyke, N.D., 1972. Paleomagnetism of deep-sea cores. Rev. Geophys. Space Phy., 10, 213-249.

Peng, T.H., Broecker, W.S., Kipphut, G., and Shackleton, N., 1977. Benthic mixing in deep sea cores as determined by ^{14}C dating and its implications regarding climate stratigraphy and the fate of fossil fuel Co_2. In Fate of fossil fuel CO_2 in the Oceans (Editors N.R.Anderson and A.Malahoff). Mar. Sci. Ser.6, Plenum Press, New York, 355-373.

Peng, T.H., Broecker, W.S. and Berger, W.H., 1979. Rates of benthic mixing in deep-sea sediment as determined by radioactive tracers, Quat. Res., 11, 141-149.

Peters, B., 1955. Radioactive beryllium in the atmosphere and on the earth. Proc. Ind. Acad. Sci., 41, 67.

Picciotto, E., and Wilgain, S., 1954. Thorium determination in deep-sea sediments. Nature, 173, 632-633.

Piper, D.Z., Leong, K. and Cannon, W.F., 1979. Manganese nodules and surface sediment compositions : DOMES Sites A, B, and C. In Marine Geology and Oceanography of the Pacific Manganese Nodule Province (Eds.J.L. Bischoff and D.Z. Piper). Plenum Press, New York, 437-474.

_____, and Williamson, M.E., 1981. Mineralogy and composition of concentric layers within a manganese nodule from the north Pacific ocean. Mar. Geol.,40, 255-268.

Pomerantz, M.A., 1971. Cosmic-rays. Van Nostrand Reinhold Co., New York.

Raisbeck, G.M., Yiou, F., Fruneau, M., Lieuvin, M. and Loiseaux, J.M., 1978. Measurement of ^{10}Be in 1000 and 5000 year old Antartic Ice. Nature 275, 731-733.

_____, Yiou, F., Fruneau, M., Loiseaux, J.M. and Lieuvin, M., 1979a. ^{10}Be concentration and residence time in the ocean surface layer. Earth Planet. Sci. Lett., 43, 237-240.

_____, Yiou, F., Fruneau, M., Loiseaux, J.M., Lieuvin, M. and Raval J.C., 1979b. Deposition rate and seasonal variations in precipitation of cosmogenic ^{10}Be. Nature, 282, 279-280.

_____, Yiou, F., Fruneau, M., Loiseaux, J.M., Ravel, J.C. and Hays, J.D., 1979c. A search in a marine sediment core for ^{10}Be concentration variation during a geomagnetic field reversal. Geophy. Res. Lett., 6, 717-719.

_____, Yiou, F., Fruneau, M., Loiseaux, J.M., Lieuvin, M., Ravel, J.C., Reyss, J.L. and Guichard, F., 1980. ^{10}Be concentration and residence time in the deep ocean. Earth Planet. Sci. Lett., 51, 275-278.

Raisbeck, G.M., Yiou, F., Fruneau, M., Loiseaux, J.M., Lieuvin, M., Ravel, J.C. and Lorius, C., 1981. Cosmogenic ^{10}Be concentrations in Antarctic ice during the past 30,000 years. Nature, 292, 825-826.

Ramaty, R., 1965. The influence of geomagnetic shielding on ^{14}C production and content. In Magnetism and the Cosmos, NATO Advanced Study Institute on Planetary and Stellar Magnetism, The School of Physics, the University, New castle-upon-Tyne, (Oliver and Boyd. Ltd., Edinburgh), p.66-78.

Reyss, J.L., 1979. Repartition de deux radioisotopes des periodes differentes, ^{230}Th et ^{10}Be, sur les faces opposes d'un nodule de manganese oriente. C. R. Acad. Sc. Paris, t.289 Serie. D-233.

_____, Yokoyama, Y. and Guichard, F., 1981. Production cross section of ^{26}Al, ^{7}Be from nitrogen : Implications for production rates of ^{26}Al and ^{10}Be in the atmosphere. Earth Planet. Sci. Lett., 53, 203-210.

Rosholt, J.N., Emiliani, C., Geiss J., Koczy, F.F. and Wangersky, P.J., 1961. Absolute dating of deep-sea cores by $^{231}Pa/^{230}Th$ method. J. Geol., 69, 162-185.

Ruddiman, W.F., and Glover, L.K., 1972. Vertical mixing of ice-rafted volcanic ash in North Atlantic sediments. Geol. Soc. Am. Bull., 83, 2817-2836.

Sarin, M.M., Borole, D.V. and Krishnaswami, S., 1979. Geochemistry and geochronology of sediments from the Bay of Bengal and equatorial Indian ocean, Proc. Ind. Acad. Sci., 88A, Part II, 2, 131-134.

Sackett, W.M., 1965. Deposition rates by the proto-actinium method. In symposium on marine chemistry (Editors D.R. Schink and J.T.Corless) Univ. Rhode Island, Rhode Island, 29-40.

Sarma, T.P., 1964. Dating of marine sediments by Ionium and Protoactinium methods. Ph.D. Theis, Carneigie Institute of Technology, Pittsburgh, U.S.A.

Schaeffer, O.A., 1975. Constancy of galactic cosmic rays in time and space. Proc. 14th Int. Cosmic Ray Conf., 11, 3508-3520.

Sharma, P., and Somayajulu, B.L.K., 1979. Growth rates and composition of two ferromanganese nodules from the central North Pacific. In La Genese des Nodules de Manganese (Editor C.Lalou) Colloq. Int. C.N.R.S., No.289, 281-288.

_____, Somayajulu, B.L.K., Lal, D., Wolfli, W., Bonani, G., Beer, J., Stoller, Ch. and Suter, M., 1982a. Particle accelerator measurements of ^{10}Be in marine accumulations : Intercomparison with beta counting method (in preparation).

Sharma, P.. Bhattacharya, S.K. and Somayajulu, B.L.K., 1982b. ^{10}Be in deep-sea sediments and Cosmic-Ray intensity variations (submitted to Science).

_____, and Somayajulu, B.L.K., 1982c. ^{10}Be dating of large manganese nodules from the world oceans. Earth Planet. Sci. Lett. (in press).

Somayajulu, B.L.K., 1967. ^{10}Be in a manganese nodule. Science, 156, 1219-1220.

_____, 1977. Analysis of causes for the beryllium-10 variations in deep-sea sediments. Geochim. Cosmochim. Acta, 41, 909-193.

_____, Heath, G.R., Moore, T.C., Jr. and Cronan, D.S., 1971. Rates of accumulation of manganese nodules and associated sediment from the equatorial Pacific. Geochim. Cosmochim. Acta, 35, 621-624.

_____, Sharma, P. and Berger, W.H., 1982. ^{10}Be and U-Th decay series nuclides in a box core from the central North Atlantic (Submitted to Nature).

Sorem, R.K., 1973. Manganese nodules as indicators of long-term variations in sea floor environment. In Papers on the origin and distribution of manganese nodules in the Pacific and prospects for exploration, Hawaii Inst. of Geophy., Honolulu, 151-164.

Suter, M., Balazer, R., Bonani, G., Stoller, Ch., Wolfli, W., Beer, J., Oeschger, H. and Stauffer, B, 1981. Paper presented at symposium on Accelerator Mass Spectrometry, Argonne National Laboratory, Illinois.

Sverdrup, M.U., Johnson, M.W. and Fleming, R.H., 1942. The Oceans, Their physics, chemistry and general biology. Prentice Hall, Inc., N.Y., pp.15.

Tanaka, S., Inoue, T. and Imamura, M. 1977. The ^{10}Be method of dating marine sediments - comparison with the paleomagnetic method. Earth. Planet. Sci. Lett., 37, 55-60.

_____, and Inoue, T., 1979. Beryllium-10 dating : Beryllium-10 concentration and beryllium-10/beryllium-9 ratios in North Pacific sediment cores upto 2.5 million years B.P. Earth. Planet. Sci. Lett., 45, 181-187.

Thomas, J., Parker, P., Mangini, A., Cochran, J.K., Turekian, K.K., Krishnaswami, S. and Sharma, P. ^{10}Be in manganese nodules. (to appear in Proc. Symp. on Accelerator Mass Spectrometry held at Argonne National Laboratory, Illinois).

Thurber, D.L., 1963. Anamalous $^{234}U/^{238}U$ and an investigation of the potential of ^{234}U for Pleistocene chronology, Ph.D. thesis, Columbia University, New York.

Turekian, K.K., and Cochran, J.K., 1978. Determination of marine chronologies using natural radionuclides. In Chemical Oceanography (Editors J.P.Riley and R. Chester) Academic Press, London, 7, 313-360.

_____, Cochran, J.K., Krishnaswami, S., Lanford, W.A., Parker, P.D. and Bauer, K., 1979. The measurement of ^{10}Be in manganese nodules using a Tandem Vande Graff accelerator. Geophys. Res. Lett., 6, 417-420.

Volchok, M.L., and Kulp, J.L., 1952. Age determination of deep-sea sediments. Nature, 173, 632.

Willis, J.P., and Ahrens, L.H., 1962. Some investigations on the composition of manganese nodules, with particular reference to certain trace elements. Geochim. Cosmochim. Acta, 26, 751-764.

Wollin, G., Ryan, B.F.W. and Ericson, D.B., 1978. Climatic changes, magnetic intensity variations and fluctuations of the eccentricity of the earth's orbit during the past 2000,000 years and a mechanism which may be responsible for the relatitionship. Earth Planet. Sci. Lett., 41, 395-397.

Yiou, F. and Raisbeck, G.M., 1972. Half life of ^{10}Be. Phys. Rev. Lett., 29, 372-375.

Yokoyama, Y., Guichard, F., Reyss, J.L. and Yan, N.M., 1978. Oceanic residence times of dissolved beryllium and aluminium deduced from cosmogenic traces ^{10}Be and ^{26}Al. Science, 201, 1016-1017.

APPENDIX

Concentration of elements in manganese nodules

ARIES 39D

Element	Total Wt(%)	0-6.9 mm Fractional (%) 1	2	3	6.9 - 12.3 mm Wt(%) 1	12.3 - 15.9 mm Wt(%) 1
Mn	20.7	99.9	0.1	0	24.9	19.2
Fe	12.5	80.7	18.7	0.6	10.9	9.7
Co	0.23	99.9	0.1	0	0.46	0.34
Ni	0.7	99.5	0.5	0	0.46	0.31
Cu	0.15	98.1	1.8	0.1	0.14	0.11
Zn	0.079	97.5	2.1	0.4	0.073	0.055
Cr*	20.0	58.3	31.5	10.2	5.3	4.0
Pb	0.11	99.8	0.2	0	0.19	0.16
Be*	2.2	91.4	6.1	2.5	NM	NM
Mg	1.3	90.5	7.7	1.8	1.1	0.97
Ca	2.0	88.4	7.4	4.2	1.7	3.5
Sr	0.12	97.9	1.3	0.8	0.13	0.13
Ba	0.11	65.8	32.6	1.6	0.040	0.055
Al	1.8	32.5	48.7	18.8	0.54	0.41
Residue	24.9	37.8	60.6	1.6	14.0	14.0

ANTP 5OD

Element	0 - 5.5 mm Total Wt(%)	Fractional (%) 1	2	3	5.5 - 10.6 mm Total Wt(%)	Fractional (%) 1	3
Mn	18.4	99.9	0.1	0	18.0	99.9	0.1
Fe	19.7	86.2	13.5	0.3	17.4	87.1	12.9
Co	0.38	99.9	0.1	0	0.37	99.8	0.2
Ni	0.33	98.9	1.1	0	0.32	99.8	0.2
Cu	0.048	96.6	2.6	0.8	0.057	96.3	3.7
Zn	0.054	93.5	5.7	0.8	0.060	94.5	5.5
Cr*	51.0	14.5	80.6	4.9	23.0	32.0	68.0
Pb	0.17	97.7	1.9	0.4	0.18	98.3	1.7
Be*	3.3	85.9	11.8	2.3	3.3	NM	NM
Mg	1.2	82.3	16.7	1.0	1.1	98.0	2.0
Ca	2.6	96.2	1.7	2.1	2.7	98.8	1.2
Sr	0.16	98.8	0.6	0.6	0.16	99.7	0.3
Ba	0.022	79.4	12.5	8.1	0.031	87.6	12.4
Al	1.4	27.9	43.5	28.6	0.61	55.2	44.8
Residue	25.5	17.0	73.2	9.8	20.7	93.7	6.3

ARIES 15D

Element	Total Wt(%)	0 - 3.8 mm Fractional (%) 1	2	3	Total Wt(%)	3.8 - 6.8 mm Fractional (%) 1	3
Mn	20.8	99.9	0.1	0	21.0	99.9	0.1
Fe	14.8	81.1	18.8	0.1	12.7	90.7	9.3
Co	0.86	99.9	0.1	0	0.97	100.0	0
Ni	0.38	99.3	0.7	0	0.40	NM	MM
Cu	0.030	97.0	2.8	0.2	0.057	90.0	10.0
Zn	0.040	92.6	7.2	0.2	0.045	97.1	2.9
Cr*	20.0	11.0	81.7	7.3	22.0	48.9	51.1
Pb	0.19	96.8	3.2	NM	0.20	99.0	1.0
Be*	2.9	NM	NM	NM	3.0	NM	NM
Mg	0.89	94.1	4.5	1.4	1.0	99.0	1.0
Ca	2.1	98.6	0.6	0.8	2.5	99.6	0.4
Sr	0.13	99.4	0.1	0.5	0.18	99.7	0.3
Ba	0.11	94.6	3.2	2.2	0.14	89.4	10.6
Al	0.72	35.4	25.4	39.2	0.54	63.3	36.7
Residue	13.5	46.6	47.4	8.0	10.6	87.1	12.9

ARIES 15D

Element	6.8 - 9.7 mm Total Wt(%)	Fractional (%) 1	Fractional (%) 3	9.7 - 17.9 mm Total Wt(%)	Fractional (%) 1	Fractional (%) 3	17.9 - 27.0 mm Total Wt(%)	Fractional (%) 1	Fractional (%) 3
Mn	24.7	99.5	0.5	21.1	99.8	0.2	18.6	99.9	0.1
Fe	15.0	54.7	45.3	11.9	86.7	13.3	9.9	91.8	8.2
Co	0.99	99.8	0.2	0.80	99.3	0.6	0.64	99.9	0.1
Ni	0.52	99.2	0.8	0.54	99.4	0.6	0.58	99.8	0.2
Cu	0.064	95.4	4.6	0.073	97.5	2.5	0.082	98.6	1.4
Zn	0.057	91.0	9.0	0.062	96.5	3.5	0.060	98.4	1.6
Cr*	24.0	34.3	65.7	17.0	53.5	46.5	12.0	61.2	38.8
Pb	0.19	69.8	30.2	0.15	97.7	2.3	0.15	97.7	2.3
Be*	2.5	NM	NM	4.1	97.3	2.7	4.0	NM	NM
Mg	1.2	99.3	0.7	1.0	99.4	0.6	0.86	99.7	0.3
Ca	2.8	99.1	0.9	2.7	99.5	0.5	3.2	99.9	0.1
Sr	0.20	98.9	1.1	0.17	96.1	3.9	0.14	99.8	0.2
Ba	0.028	76.5	23.5	0.047	46.8	53.2	0.021	72.8	27.2
Al	0.53	31.1	68.9	0.35	68.0	32.0	0.35	77.8	22.2
Residue	24.4	94.9	5.1	11.6	78.8	21.2	8.4	54.1	45.9

Element	0-4.7 mm Total Wt(%)	0-4.7 mm Fractional(%) 1	0-4.7 mm Fractional(%) 3	4.7 - 9.5 mm Total Wt(%)	4.7 - 9.5 mm Fractional(%) 1	4.7 - 9.5 mm Fractional(%) 3	9.5 - 17.9 mm Total Wt(%)	9.5 - 17.9 mm Fractional(%) 1	9.5 - 17.9 mm Fractional(%) 3	17.9 - 29.1 mm Wt(%) 1
Mn	21.8	99.9	0.1	19.9	100.0	0	16.1	100.0	0	21.9
Fe	15.2	95.7	4.3	16.1	99.3	1.7	12.2	84.8	15.2	9.9
Co	0.69	100.0	0	0.81	100.0	0	0.50	99.8	0.2	0.62
Ni	0.39	99.5	0.1	0.42	100.0	0	0.36	99.9	0.1	0.38
Cu	0.042	99.3	0.8	0.057	99.2	0.8	0.087	98.7	1.3	0.16
Zn	0.050	98.5	1.5	0.052	99.6	0.4	0.045	97.5	2.5	0.063
Cr*	20.0	45.7	54.3	34.0	76.8	23.2	21.0	54.5	45.5	4.0
Pb	0.25	98.3	1.7	0.29	99.1	0.9	0.18	99.3	0.7	0.13
Be*	5.0	NM	NM	3.8	NM	NM	3.3	NM	NM	NM
Mg	1.0	98.4	1.6	1.3	87.0	13.0	0.88	99.7	0.3	1.3
Ca	2.5	99.0	1.0	2.6	98.9	1.1	2.0	98.9	1.1	1.9
Sr	0.14	99.7	0.3	0.16	99.7	0.3	0.13	96.4	3.6	0.12
Ba	0.14	98.3	1.7	0.053	98.5	1.5	0.018	44.7	55.3	0.008
Al	0.78	47.6	52.4	0.70	64.5	35.5	0.54	49.1	50.9	0.29
Residue	22.5	84.3	15.7	19.1	81.5	18.5	19.0	83.2	16.8	20.7

Element	0-0.8 mm Wt(%) 2	0.8-1.8 mm Wt(%) 2	1.8-3.2 mm Wt(%) 2	3.2-5.7 mm Wt(%) 2	5.7-7.5 mm Wt(%) 2	7.5-9.9 mm Wt(%) 2
Mn	34.9	30.5	32.8	36.2	33.5	30.0
Fe	8.3	8.6	6.7	5.4	5.0	5.3
Co	0.44	0.26	0.28	0.21	0.22	0.14
Ni	1.7	1.5	1.7	1.7	1.7	1.6
Cu	1.1	1.1	1.4	1.6	1.6	1.5
Zn	0.19	0.14	0.15	0.17	0.16	0.15
Cr*	0.003	19.0	16.0	14.0	16.0	19.0
Pb	0.053	0.051	0.042	0.036	0.036	0.035
Be*	2.5	3.1	4.6	2.4	2.4	3.0
Mg	2.2	2.0	2.5	2.5	2.6	2.3
Ca	3.5	2.6	2.7	2.0	2.3	2.4
Sr	0.087	0.098	0.090	0.070	0.072	0.061
Ba	0.37	0.18	0.16	0.19	0.19	0.17
Al	1.7	1.7	1.9	2.0	2.1	2.2
Residue	17.6	18.3	16.0	14.5	15.2	17.4

TF 5

Element	0-0.5 mm Wt(%) 2	0.5-1.4 mm Wt(%) 2	1.4-3.3 mm Wt(%) 2	3.3-5.5 mm Wt(%) 2	5.5-8.7 mm Wt(%) 2	8.7-17.3 mm Wt(%) 2
Mn	23.8	21.9	21.8	22.4	22.2	24.6
Fe	24.9	24.9	23.3	19.3	21.7	13.5
Co	0.79	0.64	0.60	0.60	0.51	0.52
Ni	0.34	0.39	0.37	0.46	0.44	0.46
Cu	0.22	0.19	0.18	0.17	0.17	0.23
Zn	0.083	0.304	0.069	0.059	0.058	0.083
Cr*	18.0	22.0	19.0	17.0	23.0	38.0
Pb	0.10	0.13	0.11	0.087	0.076	0.089
Be*	6.2	7.8	6.4	4.0	7.9	24.5
Mg	1.2	1.6	1.2	1.1	1.2	1.5
Ca	3.6	2.8	2.7	2.5	2.9	3.2
Sr	0.21	0.20	0.18	0.16	0.17	0.19
Ba	0.13	0.18	0.035	0.068	0.076	0.19
Al	1.4	1.8	1.6	1.3	2.1	3.3
Residue	6.6	8.3	9.6	7.6	12.8	18.2

Element	o - 4.8 mm Total Wt(%)	Fractional (%) 1	2	3	4.8 - 12.8 mm Total Wt(%)	Fractional (%) 1	3
Mn	12.7	99.4	0.1	0.5	12.2	99.9	0.1
Fe	19.7	75.4	23.0	1.4	19.1	76.9	23.1
Co	0.32	99.5	0.2	0.3	0.28	99.9	0.1
Ni	0.18	98.7	1.1	0.2	0.17	99.8	0.2
Cu	0.094	90.4	6.2	3.4	0.090	94.6	5.4
Zn	0.050	86.2	9.0	4.8	0.047	93.6	6.4
Cr*	100.0	11.5	74.6	13.9	20.0	43.4	56.6
Pb	0.13	98.2	NM	1.8	0.13	98.9	1.1
Be*	3.3	NM	NM	NM	4.9	NM	NM
Mg	1.1	77.7	16.8	5.5	0.79	99.2	0.8
Ca	2.3	79.3	8.7	12.0	1.7	97.8	2.2
Sr	0.14	93.3	1.5	5.2	0.13	99.7	0.3
Ba	0.071	89.8	5.1	5.1	0.017	94.0	0.6
Al	2.0	37.2	55.2	7.6	0.86	60.9	29.1
Residue	33.9	26.5	63.1	10.4	26.8	82.4	17.6

Element	12.8 - 21.0 mm Wt (%)	21.0 - 27.8 mm Total Wt(%)	Fractional (%)	
	1		1	3
Mn	14.9	16.7	99.9	0.1
Fe	16.4	18.1	82.0	18.0
Co	0.32	0.42	99.9	0.1
Ni	0.21	0.34	99.9	0.1
Cu	0.078	0.12	96.5	3.5
Zn	0.051	0.059	94.1	5.9
Cr*	4.0	15.0	64.0	36.0
Pb	0.13	0.13	98.5	1.5
Be*	NM	4.9	NM	NM
Mg	0.89	1.0	99.7	0.3
Ca	1.3	2.1	99.5	0.5
Sr	0.12	0.14	99.7	0.3
Ba	0.012	0.024	97.9	2.1
Al	0.59	1.0	86.9	13.1
Residue	25.1	26.0	81.2	18.8

GEOSECS ID

Element	0 - 3.2 mm Wt(%) 2	3.2 - 6.9 mm Wt(%) 2	6.9 - 12.5 mm Wt(%) 2	12.5 - 16.4 mm Wt(%) 2
Mn	24.4	25.0	22.5	17.8
Fe	15.9	18.0	17.4	13.8
Co	1.0	1.2	1.1	0.81
Ni	0.48	0.47	0.30	0.29
Cu	0.034	0.039	0.040	0.038
Zn	0.065	0.061	0.062	0.061
Cr*	16.0	20.0	22.0	26.0
Pb	0.38	0.36	0.30	0.22
Be*	4.0	5.1	NM	NM
Mg	1.3	1.3	1.2	1.1
Ca	3.1	3.7	2.3	5.6
Sr	0.23	0.24	0.17	0.14
Ba	0.0080	0.0080	0.012	0.007
Al	0.34	0.40	0.46	0.52
Residue	~ 0	~ 0	0.6	6.9

RC 15 D5

Element	0-6.6 mm Wt(%) 2	6.6-16.2 mm Wt(%) 2	16.2-22.6 mm Wt(%) 2	22.6-28.6 mm Wt(%) 2	28.6-36.9 mm Wt(%) 2	36.9-40.9 mm Wt(%) 2
Mn	20.3	18.5	19.7	18.5	17.6	17.7
Fe	27.7	24.6	29.1	25.4	23.5	21.7
Co	0.37	0.27	0.30	0.31	0.39	0.39
Ni	0.26	0.21	0.23	0.24	0.20	0.25
Cu	0.11	0.092	0.092	0.038	0.078	0.066
Zn	0.084	0.073	0.075	0.074	0.063	0.062
Cr*	27.0	31.0	24.0	24.0	15.0	12.0
Pb	0.16	0.14	0.16	0.15	0.18	0.20
Be*	9.3	NM	NM	NM	NM	NM
Mg	1.1	1.0	1.1	1.1	1.0	1.1
Ca	2.5	2.3	2.1	2.3	1.6	1.8
Sr	0.18	0.18	0.19	0.16	0.15	0.16
Ba	0.17	0.063	0.039	0.096	0.034	0.055
Al	0.78	0.72	0.82	0.86	0.70	0.57
Residue	10.4	9.9	9.8	13.6	2.7	9.2

RC 16 D10

Element	0 - 4.6 mm Total Wt(%)	Fractional (%) 2	Fractional (%) 3	4.6 - 10.6 mm Total Wt(%)	Fractional (%) 2	Fractional (%) 3	10.6 - 15.0 mm Wt(%) 2
Mn	25.7	99.9	0.1	24.8	99.7	0.3	22.3
Fe	24.3	99.0	1.0	21.1	99.8	0.2	22.7
Co	1.0	99.9	0.1	0.89	99.8	0.2	0.96
Ni	0.38	100.0	0	0.37	100.0	0.3	0.28
Cu	0.033	99.5	0.5	0.037	99.4	0.6	0.046
Zn	0.054	99.8	0.2	0.055	99.8	0.2	0.062
Cr*	37.0	99.3	0.7	11.0	95.2	4.8	17.0
Pb	0.35	99.9	0.1	0.31	99.7	0.3	0.35
Be*	5.7	NM	NM	5.9	NM	NM	NM
Mg	1.3	99.6	0.4	1.3	99.1	0.9	1.3
Ca	3.2	99.8	0.2	3.0	99.6	0.4	1.6
Sr	0.23	99.9	0.1	0.23	99.6	0.4	0.15
Be	0.010	91.9	8.1	0.030	17.0	83.0	0.014
Al	0.59	91.9	8.1	0.68	84.2	15.8	0.73
Residue	1.3	90.5	9.5	3.3	71.3	28.7	3.3

RC 14 D4F

Element	0 - 5.8 mm Total Wt(%)	Fractional (%) 2	Fractional (%) 3	5.8 - 12.0 mm Total Wt(%)	Fractional (%) 2	Fractional (%) 3
Mn	14.4	99.8	0.2	21.6	99.7	0.3
Fe	13.2	99.6	0.4	19.0	99.5	0.5
Co	0.73	99.9	0.1	0.53	99.7	0.3
Ni	0.39	100.0	0	0.44	99.7	0.3
Cu	0.067	99.9	0.3	0.12	99.7	0.3
Zn	0.064	99.8	0.2	0.074	99.7	0.3
Cr*	18.0	95.0	5.0	22.0	91.9	8.1
Pb	0.28	99.9	0.1	0.22	99.7	0.3
Be*	4.0	98.9	1.1	7.3	98.6	1.4
Mg	1.2	99.8	0.2	1.2	99.5	0.5
Ca	2.7	99.6	0.4	2.2	98.9	1.1
Sr	0.21	99.8	0.2	0.19	99.1	0.9
Ba	0.096	77.4	22.6	0.011	42.0	58.0
Al	0.56	75.4	24.6	0.95	13.4	26.6
Residue	4.7	77.5	22.5	12.1	55.8	44.2

RC 14 D4F

Element	12.0 - 17.4 mm Total Wt(%)	Fractional (%) 2	Fractional (%) 3	17.4 - 27.4 mm Total Wt(%)	Fractional (%) 2	Fractional (%) 3
Mn	32.5	99.4	0.6	21.0	NM	NM
Fe	27.3	99.4	0.6	28.3	99.4	0.6
Co	0.83	99.4	0.6	0.58	99.1	0.8
Ni	0.60	99.3	0.7	0.28	99.2	0.8
Cu	0.18	99.3	0.7	0.094	99.9	0.8
Zn	0.12	99.4	0.6	0.10	99.3	0.7
Cr*	42.0	97.1	2.9	22.0	94.8	5.2
Pb	0.29	99.5	0.5	0.17	99.4	0.6
Be*	12.1	NM	NM	7.2	NM	NM
Mg	1.8	99.5	0.5	0.99	98.4	0.6
Ca	3.0	99.1	0.9	3.2	98.6	1.4
Sr	0.27	98.9	1.1	0.21	98.2	1.8
Ba	0.019	70.5	29.5	0.022	12.1	87.9
Al	1.6	79.9	20.1	0.92	75.6	24.4
Residue	15.0	69.8	30.2	13.3	74.7	25.3

RC 14 D4F

Element	27.4 - 34.5 mm Total Wt(%)	Fractional(%) 2	Fractional(%) 3	34.5 - 45.9 mm Total Wt(%)	Fractional(%) 2	Fractional(%) 3	45.9 - 54.1 mm Total Wt(%)	Fractional(%) 2	Fractional(%) 3
Mn	20.0	99.7	0.3	17.0	96.5	3.5	22.2	97.3	2.7
Fe	23.1	99.7	0.3	19.1	99.1	0.9	10.7	99.4	0.6
Co	0.36	99.7	0.3	0.29	97.6	2.4	0.39	99.7	0.3
Ni	0.28	99.6	0.4	0.33	97.7	2.3	0.91	99.7	0.3
Cu	0.082	99.6	0.4	0.09	98.1	1.9	0.17	99.7	0.3
Zn	0.12	99.6	0.4	0.11	98.4	1.6	0.082	99.7	0.3
Cr*	21.0	95.2	4.8	19.0	96.2	3.8	13.0	89.1	10.9
Pb	0.17	99.7	0.3	0.13	96.7	3.3	0.089	99.6	0.4
Be*	10.0	NM	NM	10.9	NM	NM	3.2	NM	NM
Mg	0.98	98.9	1.1	1.0	96.6	3.6	1.6	99.4	0.6
Ca	2.8	98.4	1.6	5.3	95.7	4.3	1.6	98.7	1.3
Sr	0.24	98.6	1.4	0.21	93.8	6.2	0.098	97.9	2.1
Ba	0.018	31.2	68.8	0.12	4.5	95.5	0.016	39.5	60.5
Al	1.3	70.3	29.7	1.5	78.7	21.3	1.1	79.5	20.5
Residue	13.1	72.4	27.6	32.9	68.1	31.9	10.1	75.1	24.9

RC 14 D4S

Element	0 - 1.0 mm Total Wt(%)	Fractional(%) 2	Fractional(%) 3	1.0 - 2.6 mm Total Wt(%)	Fractional(%) 2	Fractional(%) 3	2.6 - 8.3 mm Total Wt(%)	Fractional(%) 2	Fractional(%) 3
Mn	17.3	100.0	0	14.5	99.7	0.3	11.8	99.5	0.5
Fe	21.3	99.7	0.3	18.4	99.5	0.5	15.9	97.8	2.2
Co	0.62	99.9	0.1	0.41	99.9	0.1	0.32	99.4	0.6
Ni	0.27	NM	NM	0.27	99.4	0.6	0.22	99.8	0.2
Cu	0.086	99.8	0.2	0.10	99.9	0.1	0.097	98.7	1.3
Zn	0.053	99.4	0.6	0.053	99.4	0.6	0.060	98.7	1.3
Cr*	23.0	NM	NM	37.0	80.9	19.1	36.0	67.8	32.2
Pb	0.12	99.9	0.1	0.10	99.8	0.2	0.084	99.1	0.9
Be*	5.8	NM	NM	3.7	NM	NM	4.8	NM	NM
Mg	1.1	97.5	2.5	1.0	98.4	1.6	0.92	97.8	2.2
Ca	2.4	96.3	3.7	2.0	93.1	6.9	1.5	91.0	9.0
Sr	0.15	98.8	1.2	0.13	97.6	2.4	0.10	96.5	3.5
Ba	0.031	84.4	15.6	0.064	85.3	14.7	0.021	40.9	59.1
Al	1.7	82.5	17.5	2.4	81.4	18.6	1.7	39.1	60.9
Residue	15.0	84.6	15.4	26.6	81.7	18.3	33.0	85.0	15.0

RC 14 D4S

Element	8.3 - 9.2 mm Total Wt(%)	Fractional(%) 2	Fractional(%) 3	9.2 - 57.4 mm Total Wt(%)	Fractional(%) 2	Fractional(%) 3
Mn	11.0	99.8	0.2	10.2	98.9	1.1
Fe	16.5	98.8	1.2	16.1	95.8	4.2
Co	0.28	99.8	0.2	0.24	98.3	1.7
Ni	0.19	99.9	0.9	0.14	99.3	0.7
Cu	0.097	99.9	0.1	0.11	96.7	3.3
Zn	0.028	98.9	1.1	0.038	98.2	1.8
Cr*	38.0	69.9	30.0	58.0	50.3	49.7
Pb	0.078	99.5	0.5	0.066	95.0	5.0
Be*	4.0	94.0	6.0	4.0	NM	NM
Mg	0.85	97.8	2.2	0.96	92.5	7.5
Ca	1.5	93.4	6.6	2.0	62.3	37.7
Sr	0.10	95.6	4.4	0.12	73.2	26.8
Ba	0.075	79.2	20.8	0.160	26.0	74.0
Al	2.7	54.3	45.7	6.9	22.9	77.1
Residue	38.2	90.9	9.1	47.1	13.2	86.8

R/V VITIAZ

Element	0-0.4 mm Wt(%) 2	0.4-2.0 mm Wt(%) 2	2.0-6.5 mm Wt(%) 2	6.5-8.2 mm Wt(%) 2	8.2-9.6 mm Wt(%) 2	9.6-11.0 mm Wt(%) 2	11.0-12.8 mm Wt(%) 2	12.8-14.8 mm Wt(%) 2
Mn	23.9	20.8	20.4	17.4	17.9	17.5	15.9	12.3
Fe	27.5	21.2	21.9	17.6	18.0	17.2	17.2	13.5
Co	0.45	0.44	0.44	0.35	0.30	0.29	0.24	0.18
Ni	0.49	0.31	0.34	0.34	0.34	0.34	0.38	0.34
Cu	0.15	0.15	0.14	0.14	0.15	0.15	0.16	0.15
Zn	0.075	0.054	0.051	0.051	0.047	0.053	0.048	0.040
Cr*	24.0	20.0	26.0	24.0	23.0	24.0	24.0	23.0
Pb	0.16	0.16	0.16	0.11	0.095	0.080	0.071	0.052
Be*	4.3	7.8	6.7	4.3	3.2	4.0	3.8	3.1
Mg	1.3	1.2	1.2	1.1	1.1	1.1	1.1	0.99
Ca	2.0	2.1	2.0	1.6	1.5	1.6	1.4	1.1
Sr	0.15	0.13	0.12	0.13	0.11	0.11	0.091	0.067
Ba	0.052	0.113	0.045	0.022	0.017	0.031	0.023	0.020
Al	1.2	1.2	1.4	1.5	1.6	1.8	1.8	1.6
Residue	11.9	14.2	17.1	22.3	25.6	31.6	36.7	43.1

1 = In the $NH_2OH.HCl$ leach of the nodule
2 = In the 6M HCl leach of the nodule or residue of 1
3 = In the remainder
* Concentrations of Be and Cr are in ppm
NM = Not measured

LIST OF PUBLICATIONS OF THE AUTHOR

1. Sharma, P. and Somayajulu, B.L.K., 1979. Growth rates and composition of two ferromanganese nodules from the Central North Pacific. In Sur la Genese des Nodules de Manganese (Ed. C. Lalou) Colloq. Int. C.N.R.S., 289, 281-288.

2. Thomas J., Parker, P., Mangini, A., Cochran, J.K., Turekian, K.K., Krishnaswami, S. and Sharma, P., 1981. ^{10}Be in manganese nodules. To appear in Proc. Symp. on Accelerator Mass Spectrometry held at Argonne National Laboratory, Illinois.

3. Cochran, J.K., Krishnaswami, S. and Sharma, P., 1981. Nuclide mobility in ferromanganese nodules from the North Equatorial Pacific. Paper presented at 182nd ACS National meeting held at New York, Aug.23-28.

4. Sharma, P. and Somayajulu, B.L.K., 1982. ^{10}Be dating of large manganese nodules from world oceans. Earth Planet. Sci. Lett., (in press).

5. Krishnaswami, S., Mangini, A., Thomas, J.H., Sharma,P., Cochran, J.K., Turekian, K.K. and Parker, P.D., 1982. ^{10}Be and Th isotopes in manganese nodules and adjacent sediments : Nodule growth histories and nuclide behaviour. Earth Planet. Sci. Lett., (in press).

6. Somayajulu, B.L.K., Sharma, P. and Berger, W.H., 1982. ^{10}Be and U-Th decay series nuclides in a box core from the Central North Atlantic. (submitted to Nature).

7. Sharma, P., Bhattacharya, S.K. and Somayajulu, B.L.K., 1982. ^{10}Be in deep-sea sediments and Cosmic-Ray intensity variations. (submitted to Science).